

STAR FORMATION RATE DISTRIBUTION IN THE GALAXY NGC 1232

ALEXANDRE ARAÚJO DE SOUZA,^{1,2} LUCIMARA P. MARTINS,¹ ALBERTO RODRÍGUEZ-ARDILA,³ AND LUCIANO FRAGA³

¹*Universidade Cruzeiro do Sul
Rua Galvão Bueno, 868*

São Paulo, SP. CEP 01506-000. BR

²*CRAAM, Mackenzie Presbyterian University
Rua da Consolacao, 896*

Sao Paulo, Brazil

³*Laboratório Nacional de Astrofísica
R. dos Estados Unidos, 154 - Naes*

Itajubá - MG, 37530-000. BR

(Received August 2, 2017; Revised February 19, 2018; Accepted March 12, 2018)

Submitted to AJ

ABSTRACT

NGC 1232 is a face-on spiral galaxy and a great laboratory for the study of star-formation due to its proximity. We obtained high spatial resolution H α images of this galaxy, with adaptive optics, using the SAM instrument at the SOAR telescope, and used these images to study its H II regions. These observations allowed us to produce the most complete H II region catalog for it to date, with a total of 976 sources. This doubles the number of H II regions previously found for this object. We used these data to construct the H II luminosity function, and obtained a power-law index lower than the typical values found for Sc galaxies. This shallower slope is related to the presence of a significant number of high-luminosity H II regions ($\log L > 39$ dex). We also constructed the size distribution function, verifying that, as for most galaxies, NGC 1232 follows an exponential law. We also used the H α luminosity to calculate the star formation rate. An extremely interesting fact about this galaxy is that X-ray diffuse observations suggest that NGC 1232 recently suffered a collision with a dwarf galaxy. We found an absence of star formation around the region where the X-ray emission is more intense, which we interpret as a star formation quenching due to the collision. Along with that, we found an excess of star-forming regions in the northeast part of the galaxy, where the X-ray emission is less intense.

Keywords: NGC 1232 – H II regions – SFR

arXiv:1805.09911v1 [astro-ph.GA] 24 May 2018

1. INTRODUCTION

The distribution of H II regions is an excellent tracer of the star formation in spiral galaxies (e.g. Kennicutt 1992). Catalogs of these regions provide an observational base that can be used to study global star formation across galactic disks. From observational properties of these regions (e.g., recombination lines or dust emission) quantities like the star formation rate (SFR) can be obtained.

The SFR is an important factor in the chemical evolution of a galaxy. Its value gives the total amount of gas converted to stars over a given time interval, which may depend on several environmental properties. It is long known that a large fraction of the star formation in the local universe occurs in gas-rich disk galaxies (Kennicutt 1989). Optical imaging clearly reveals that spiral arms in disk galaxies have a high concentration of young stars, implying that SFR must be higher in the arms regions than anywhere else in the galaxy. However, it is still a matter of debate if the higher SFR in the arms is just an effect of the larger gas densities (e.g. Elmegreen 1986, 1995; Foyle et al. 2010), or if the mass excess in the arms could directly act to trigger the star formation (e.g. Roberts 1975; Gittins 2004; Seigar et al. 2002; ?).

Grand-design and multi-arm spiral galaxies are ideal laboratories to study these effects. However, there are only a few of these galaxies close enough that individual clusters can be analyzed. A high-resolution study of these systems can help to shed some light on the nature of the processes converting gas into stars.

NGC 1232 is technically a grand-design spiral galaxy, practically face-on (inclination=29⁰, de Vaucouleurs et al. 1991; Corwin et al. 1994). Morphologically, it is classified as a SAB(rc)c. It has well-defined spiral arms, despite being a bit uncommon as they do not wind smoothly as expected for a galaxy of this type. Its arms appear to be “bent” in areas rather than gently winding structures seen in undisturbed spiral galaxies, which is probably related to the gravitational distortion caused by its satellite (Arp 1982). It is considered a prototype of multi-arm regular spirals, having hints of a bar in the nuclear region, a small bulge and long arms that disperse to the external regions, producing a number of thin arms. Radio studies suggest that it has a large neutral gas envelope that extends much beyond the optical limits of the galaxy (van Zee 1999). It also has a satellite galaxy, NGC 1232A, with which it is believed it has interacted in complex ways, but due to the large difference in their redshifts and lack of any other sign of physical association, it is likely not currently interacting with (Arp 1982). The estimated distance between NGC 1232 and its satellite is 2.4 Mpc (van Zee 1999), which means that they are not currently physically associated. Both galaxies may be associated with the Eridanus group of galaxies, but at a projected distance of 2.2 Mpc from the center of the low-mass cluster, neither is likely to be bound to the cluster (Willmer et al. 1989).

NGC 1232 covers about 6'.7 × 7'.8 on the sky at a distance of 19.8 Mpc¹. The nuclear region seems dominated by an older population, as evidenced from the spectra in the optical (6df galaxy survey; Jones et al. 2009) and near-infrared (Martins et al. 2013), while the spiral arms are populated by numerous regions of star formation.

In a recent study, Garmire (2013) provides evidence that NGC 1232 suffered a collision with a dwarf galaxy using X-ray images from NASA Chandra Observatory. This result is based on the detection of an unusual pattern of diffuse emission, which is related to a shocked gas region with a temperature of 5.8 MK, covering an impact area of 7.25 kpc in diameter. The image of the collision (Figure 1 of Garmire 2013) reveals a cloud with a cometary appearance sweeping across the galaxy and possibly colliding with the disk. The center of the collision is about 4.3 kpc to the west of the nucleus of NGC 1232. According to the authors the shock wave of this collision may have triggered some star formation, producing bright and massive stars.

Motivated by the observed diffuse X-ray emission by Garmire (2013), we obtained optical high angular resolution imaging of NGC 1232 in g', r', and H α to study its star-formation activity, searching for the connection to the spiral arms and looking for additional evidence of this putative collision. The paper is divided as follows: in §2, we present the observations and data reduction; in §3, we present the H II regions detection; in §4 we present the catalog properties; in §5 we obtain the SFR distribution and discuss the results; and in §6 we present our conclusions.

2. OBSERVATIONS AND DATA REDUCTION

2.1. Observations

NGC 1232 was observed on the night of 2014 January 23 (Program SO2013B-021), with the filters g', r', and H α . The observations were carried out with the SOAR telescope using the SOAR Adaptive Module (SAM), an instrument

¹ Distance obtained from NED (NASA/IPAC Extragalactic Database)

with an installed laser-assisted adaptive optics (AO) system (Fraga et al. 2013). By selectively compensating for low-altitude turbulence, AO improves resolution at visible wavelengths. The instrument contains a $4k \times 4k$ pixels CCD sensor that spans a square field of $3'$. The natural seeing in the V band during the observations was $0.8''$. With AO the V band seeing improved to $0.55''$. In $H\alpha$ the seeing was $0.5''$ and in the g' band, $0.66''$. Three individual on-source integrations were carried out for each filter, of 240 s each for g' and r' and 600 s for $H\alpha$. The standard star Hiltner 600 was also observed in the three filters for flux calibration purposes.

2.2. Reduction and Calibration

The images were reduced in a standard way using the Image Reduction and Analysis Facility (IRAF²; Valdes (1998); Valdes & Tody (1998)). The reduction process includes bias subtraction, flat-field corrections, and cosmic-ray cleaning. Correction for Galactic extinction was applied using the dust maps from Schlegel et al. (1998) and the extinction law from Cardelli (1989). SAM has a substantial optical distortion, typical of two off-axis parabolic mirrors (Fraga et al. 2013). The distortion can reach up to 42 pixels ($1.93''$ in the sky) in the image. The distortion is well described by quadratic terms in x and y (in pixels, described in the instrument manual), and we applied these corrections to our images.

Flux calibration was done using the g', r' and $H\alpha$ images of the standard star. Using these images, the transmission curves of each filter³ and its flux-calibrated spectrum obtained from Hamuy et al. (1992, 1994), we calculated the conversion factor from photon counts to flux units ($\text{erg cm}^{-2} \text{s}^{-1}$). Figure 1 shows the resulting image obtained after combining the final exposures in each filter.

3. $H\alpha$ PHOTOMETRY AND H II REGION IDENTIFICATION

The continuum subtraction was done using the r' image as described in Schmitt et al. (2006). Since this is a broadband filter and encompasses the $H\alpha$ emission-line region, it is contaminated by that emission. This means that besides the scaling for the $H\alpha$ filter width, it has to be corrected for the contribution of the $H\alpha$ flux to the total observed flux. The subtraction then has to be recursive. This is done by first subtracting the scaled continuum image from the line image; then, the resulting line image was subtracted from the continuum image to remove the emission-line contribution to this image, and the corrected continuum image was used to subtract the continuum emission from the original line image. This process was repeated a few times, until the $H\alpha$ and continuum fluxes in regions affected by contamination did not change, indicating that the process had converged. In total, we needed six iterations to reach convergence.

The detection of the H II regions in the NGC 1232 $H\alpha$ image was performed with the aid of SExtractor (Bertin & Arnouts 1996). This software is used to build a catalog of objects from an astronomical image. It first determines the background, and then which pixels of the image are objects, being able to separate close or superimposed objects. For each identified H II regions in the NGC 1232 $H\alpha$ image was performed with the aid of region, its position and size are determined by fitting an ellipse function. It also derives the photometry of each source. There are two important input parameters used in SExtractor for H II region photometry, the minimum number of pixels of a given source and the minimum flux compared to the background. We adopted 10 pixels as the minimum number of pixels for an object to be detected, which roughly correspond to the seeing of the observation. We also required that to be detected the sources should have a minimum flux of 2σ , where σ is the average sky noise around the source. The average sky noise surface brightness in our image was about $2 \times 10^{-18} \text{ erg cm}^2 \text{ s}^{-1} \text{ arcsec}^{-2}$.

We detected 976 sources. The highest number of sources ever detected for this galaxy was 529 sources by Hodge & Kennicutt (1983). It is important to take into account that our result almost doubles the number of sources already detected for this galaxy, even though our image does not encompass the whole galaxy but only the central part.

A direct comparison of individual H II regions properties from our study and Hodge & Kennicutt (1983) is extremely difficult. This is because their study was done using a photographic plate, and no information about sensitivity is given in their paper. Also, they state that the individual separation of the objects is dependent on the properties of the plate, and many times a number of bright knots in a lower-luminosity envelope were given a single object identification number.

² IRAF is distributed by the National Optical Astronomy Observatory, which is operated by the Association of Universities for Research in Astronomy, Inc., under cooperative agreement with the National Science foundation.

³ Obtained at <http://www.ctio.noao.edu/soar/content/filters-available-> Soar

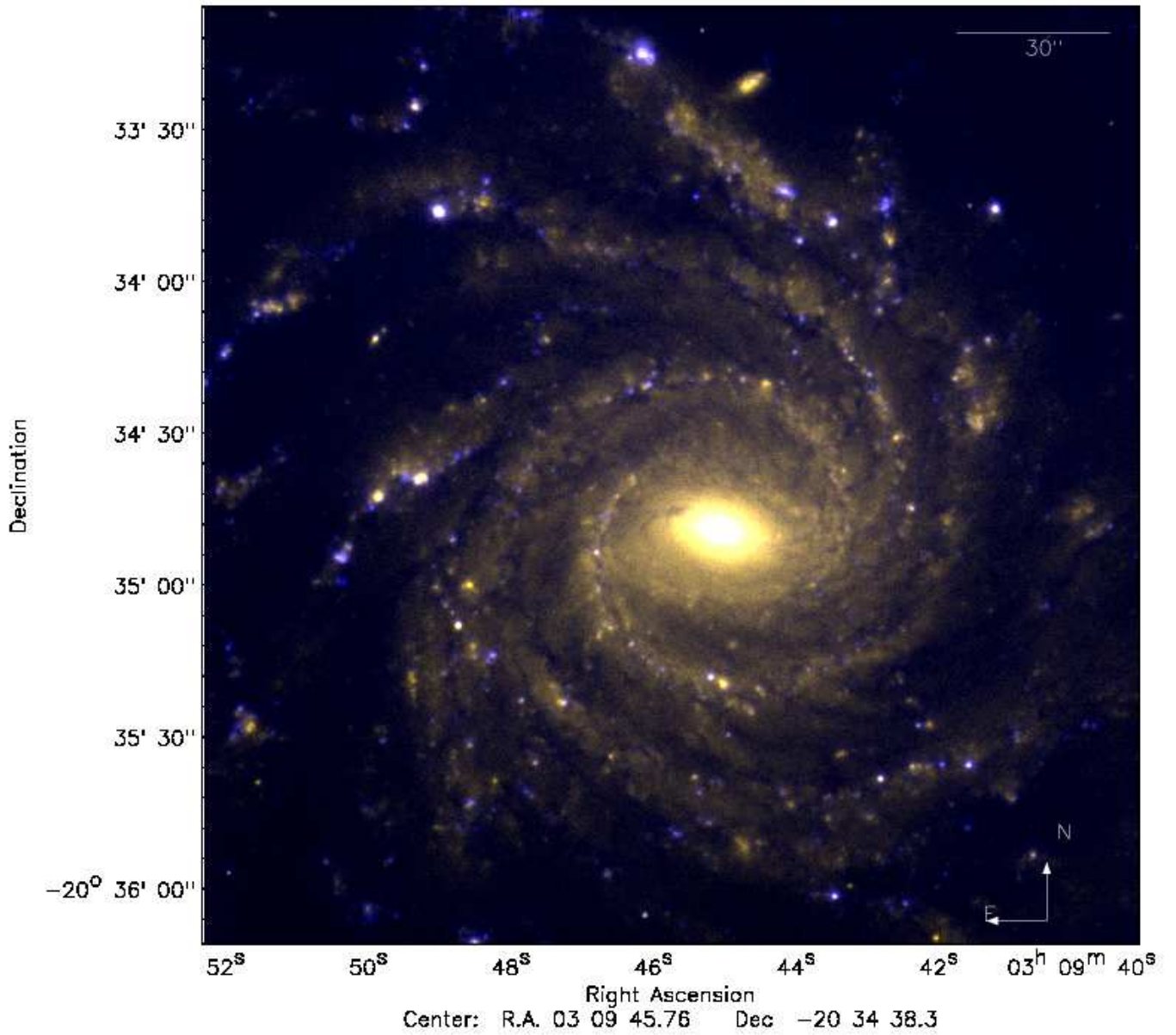


Figure 1. NGC 1232 combined flux-calibrated image of the filters g' (green), r' (red), and $H\alpha$ (blue), obtained with the instrument SAM at SOAR.

In any case, we expect that the higher number of H II regions identified here can help to improve studies such as the nature of the spiral structure and the spatial distribution of star-forming regions, abundance gradients, and the use of H II properties (sizes, luminosities, etc.) for the extragalactic distance scale. Figure 2 shows the sources detected by SExtractor. Table 1 shows, as an example, the ten most luminous H II regions detected. The complete catalog can be found in the online material.

The $H\alpha$ luminosity of each H II region can be obtained from the $H\alpha$ flux measured by SExtractor, after correcting for two effects: internal extinction and the contamination from [N II] lines to the total flux.

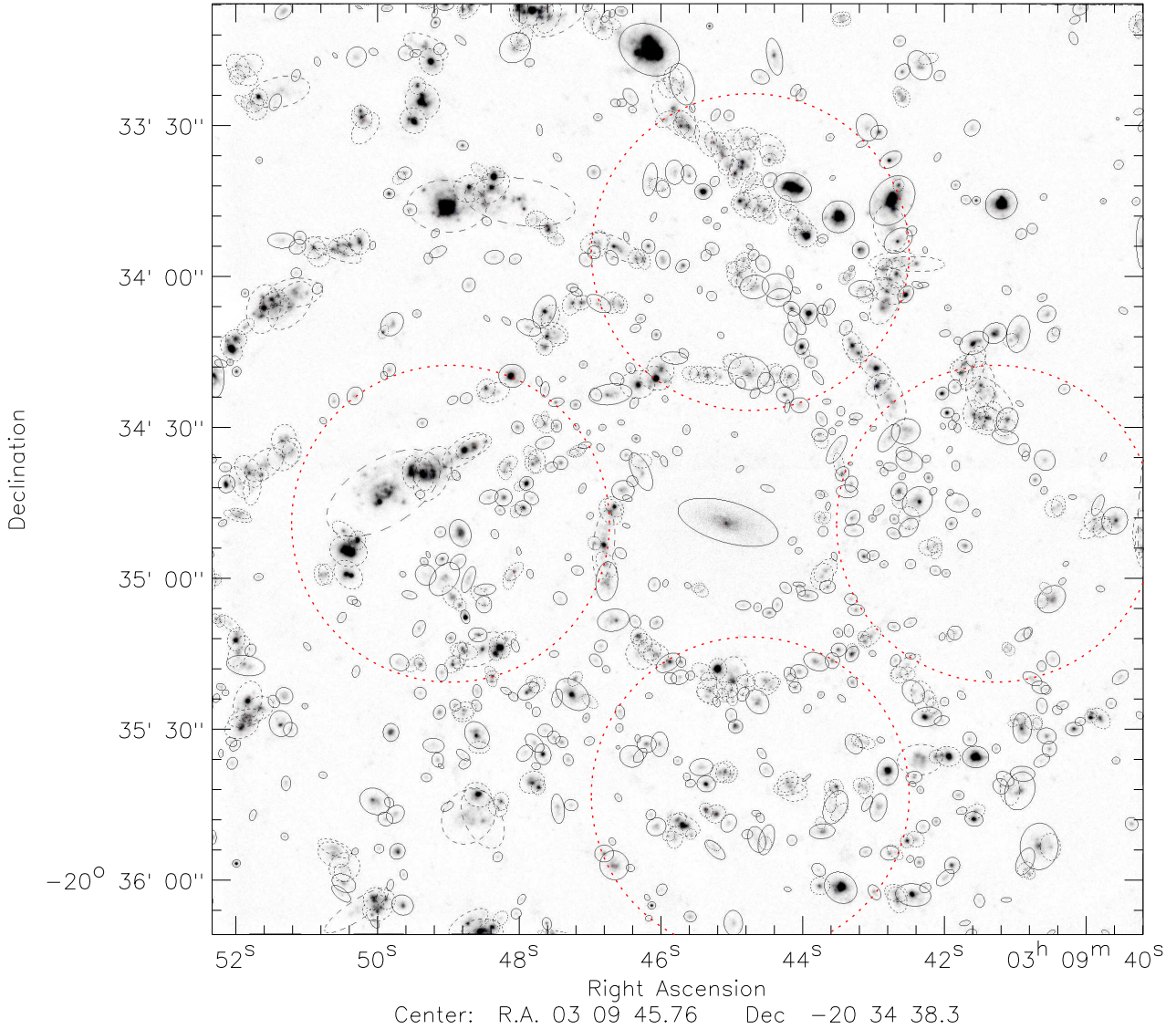


Figure 2. The image shows the H II regions fitted by SExtractor for NGC 1232. As in figure 1, north is up and east is left. Darker H II regions are regions with higher $H\alpha$ emission. Black dashed lines represent fonts marked with the crowded flag, where the Kron radius measured by SExtractor was not determined with confidence. We detected 976, which is the highest number of sources ever detected for this galaxy. The large dotted red circles refer to figure 3

For the internal extinction, we adopt the values of Bresolin et al. (2005), who measured emission lines of 13 H II regions in NGC 1232. They obtained the interstellar extinction using the Balmer decrement measured using the $H\alpha$, $H\beta$, and $H\delta$ lines. From their values of $c(H\beta)$ and using Cardelli (1989) extinction law, we obtain $A_{H\alpha}$, which varies from 0.0 to 0.8, with an average value of 0.52, removing the lowest and the highest values. We then applied this average value to correct the flux of all H II regions in our sample.

Table 1. Data for the 10 most luminous H II regions detected in galaxy NGC 1232. The complete catalog can be found in the on-line material.

Source	Position (RA)	Position (Dec)	F(H α) (10^{-17} erg/cm 2 /s)	SFR (M_{\odot} /yr)	Area (pixel 2)	L(H α) (erg s $^{-1}$)
1.0	03h09m45.70s	-20h33m16.35s	16220.49 \pm 7.99	40.332e-3 \pm 4.840e-3	9670.00	7.61e+39
2.0	03h09m42.93s	-20h33m46.88s	11033.00 \pm 7.91	27.433e-3 \pm 3.292e-3	9366.00	5.18e+39
3.0	03h09m47.64s	-20h33m43.09s	4593.81 \pm 4.58	11.422e-3 \pm 1.371e-3	3051.00	2.16e+39
4.0	03h09m49.00s	-20h33m45.82s	4528.41 \pm 5.67	11.260e-3 \pm 1.351e-3	4841.00	2.12e+39
5.0	03h09m42.06s	-20h34m43.09s	3880.59 \pm 7.12	9.649e-3 \pm 1.158e-3	7131.00	1.82e+39
6.0	03h09m50.50s	-20h33m46.72s	3652.16 \pm 4.41	9.081e-3 \pm 1.090e-3	2902.00	1.71e+39
7.0	03h09m41.58s	-20h34m54.59s	3640.34 \pm 4.34	9.052e-3 \pm 1.086e-3	2848.00	1.71e+39
8.0	03h09m48.26s	-20h33m48.91s	2729.06 \pm 4.11	6.786e-3 \pm 0.814e-3	2503.00	1.28e+39
9.0	03h09m44.12s	-20h33m08.82s	2611.27 \pm 3.74	6.493e-3 \pm 0.779e-3	2147.00	1.23e+39
10.	03h09m42.61s	-20h33m26.54s	2354.45 \pm 4.36	5.854e-3 \pm 0.703e-3	2839.00	1.10e+39

The correction for the contamination of [N II] is necessary because the lines [N II] $\lambda 6548\text{\AA}$ and [N II] $\lambda 6584\text{\AA}$ are very close to the H α line and fall within the bandpass of the H α filter used. To this purpose, we again use the values obtained by [Bresolin et al. \(2005\)](#). Although the study is based only on strong emission-line regions, searching for high-metallicity objects, we believe they give the best estimate for the [N II]/H α ratio we could get for this galaxy, instead of doing actual spectroscopy of each region (which is beyond the scope of this paper). They found a large variation of this ratio, with values between 0.07 and 0.63, with 61% of the objects with a ratio smaller than 0.3. We excluded the highest and lowest values, and from these data we obtained an average [N II] $\lambda 6584\text{\AA}$ /H α ratio of 0.24. To account for the other [N II] line, we used the theoretical ratio between the two, which is 1/3. We then assumed that, on average, 32% of the flux measured by SExtractor for each H II region is a contamination by the [N II] lines, and corrected for this amount. It is important to realize that this is an approximation, since each object might have very different ratios from this average value, and the errors associated with this will propagate to the H α luminosity and SFR measurements. After these corrections the H α fluxes were employed to derive the H α luminosity adopting a galaxy distance of 19.8 Mpc.

4. CATALOG PROPERTIES

The faintest H II region luminosity measured was about 7.6×10^{35} erg s $^{-1}$. These low luminosity regions are probably ionized by single stars or matter bounded regions with significant photon loss ([Youngblood & Hunter 1999](#)). The most luminous H II region we detected in NGC 1232 has a luminosity of 6.6×10^{39} erg s $^{-1}$, comparable with the luminosity of the 30 Doradus nebula in the Large Magellanic Cloud (7×10^{39} erg s $^{-1}$, [Kennicutt 1984](#)). In this section, we will analyze the general properties of the H II regions detected here with respect with their luminosity and sizes.

The H II luminosity function is an important diagnostic of star formation properties in galaxies ([Kennicutt 1989](#)). The differential H II luminosity function is usually parameterized as a power law ([Kennicutt 1989](#); [Banfi et al. 1993](#); [Oey & Clarke 1998](#)):

$$N(L)dL = AL^{-a}dL, \quad (1)$$

where $N(L)dL$ is the number of nebulae with H α luminosities in the range of L to $L+dL$, A is a constant and a is the power-law index. Past studies found that the slope of the H II luminosity function is correlated with the morphological type, in the sense that early-type galaxies show steeper slopes than late types. The power-law index a is ≈ 2.6 for Sa galaxies ([Caldwell et al. 1991](#)), ≈ 2.0 for Sb-Sc galaxies ([Kennicutt 1989](#); [Banfi et al. 1993](#)), and between 1.0 and 1.7 for Im galaxies ([Kennicutt 1989](#); [Youngblood & Hunter 1999](#)). In a study of the H II region luminosity functions of 30 nearby galaxies, [Kennicutt \(1989\)](#) found that late-type spirals and irregulars have shallower slopes often extending

beyond 10^{39} ergs s^{-1} , while among earlier-type spirals the luminosity functions rarely extend beyond this value. These differences have been interpreted as differences in star formation properties, like differences in gas dynamics and molecular cloud mass spectrum (Kennicutt 1989; Thronson et al. 1991; Rand 1992) or related to the evolution of the ionizing clusters, where steeper slopes would be the consequence of aging effects (Oey & Clarke 1998). Steeper slopes in earlier-type galaxies can be explained by a lower maximum number of ionizing stars cutoff found for the parent OB associations (Oey & Clarke 1998). Late-type galaxies would have a large number of what Oey & Clarke (1998) calls "saturated" clusters, which are rich clusters with complete statistics in terms of initial mass function. These clusters would be responsible for the high-luminosity end of the luminosity function.

We built the luminosity function for NGC 1232, following the same criteria used by previous authors (e.g. Kennicutt 1989; Oey & Clarke 1998; Youngblood & Hunter 1999), binning the luminosities in logarithmic intervals of 0.2 dex. The result is shown in figure 3. It can be seen that the luminosity function in NGC 1232 shows a break in slope, with the fainter H II regions showing a shallower slope compared with the high-luminosity objects. This same effect was already observed for a large number of other galaxies (e.g. Kennicutt 1989; Rand 1992; Walterbos & Braun 1992; Rozas et al. 1996). Oey & Clarke (1998) showed that this might be related to the aging of the stellar population, where the slope transition moves to lower L as the population ages and objects grow fainter. Kennicutt (1989) found that for most galaxies in their sample, this turnover point occurred between 10^{36} and 10^{37} ergs s^{-1} . In NGC 1232 the break in slope happens around $\log L = 37.5$ dex. To obtain the power law index, we excluded the points below this value. With that we obtained a $\alpha = 1.14$ for the power law index (left panel of figure 3). This value is lower than typical values found for Sc galaxies, being closer to the values found for Im galaxies. In agreement with what is seen in the literature, where shallower luminosity functions are related with the presence of high-luminosity H II regions, we find that NGC 1232 has a significant number of H II regions with luminosities higher than 10^{39} ergs s^{-1} .

The properties of the H II regions could be affected by dynamical and chemical differences along the disk (e.g. Hodge 1987; Knapen 1998; Cedrés et al. 2013). For this reason, it is important to determine if the luminosity function is affected by the location of the H II regions in the galaxy. This is especially important in the scenario where a possible collision with a dwarf galaxy might have affected different regions of this galaxy in different ways. We then constructed the luminosity function in four different parts of the galaxy, all at the same distance from the center (≈ 2.7 kpc), one in each direction from the nucleus, in a way that the west region of the galaxy that includes the x-ray peak was inside one of them. This is shown in the right panel of figure 3, where for each plot the red circle over the image of the galaxy represents the region considered. From this plot we can see that the western region of the galaxy has no high-luminosity H II regions, which makes the slope of the luminosity function steeper, compared to the other regions. The high-luminosity regions are mostly concentrated in the northern and in the eastern regions of the galaxy.

With respect to sizes, van den Bergh (1981) proposed that the frequency distribution of H II regions in spiral galaxies follows the law

$$N = N_0 e^{-D/D_0}, \quad (2)$$

where N is the number of H II regions observed with a diameter larger than D, and D_0 is the characteristic diameter of the galaxy. N_0 is an (extrapolated) characteristic value for the total number of regions. Most spiral galaxies, independent of the specific morphological type, seem to follow this distribution (Ye 1992). We obtained the diameters of the H II regions of NGC 1232 from the areas measured by SExtractor, defining $D = 2(A/\pi)^{1/2}$, where A is the area, and constructed this cumulative distribution function, as shown in figure 4. From this figure it is possible to see that the largest regions are too big compared to the distribution defined by the rest of the regions. This effect was previously observed for other galaxies as well (Hodge & Kennicutt 1983; Youngblood & Hunter 1999). These points, all located in the upper part of the galaxy, were excluded when determining the slope of the diameter distribution. We then obtained $D_0 = 100.9 \pm 1.5$ pc for NGC 1232, which is a typical value found for spiral galaxies (Hodge 1987; Ye 1992).

Hodge (1987) suggested that there is a variation of the diameter distribution with galactocentric distance, showing a tendency to have a larger D_0 for outer than for inner regions. Their results imply that the slope of the diameter distribution might be related to the environment, probably the gas density and/or the dynamical environment of the gas. In order to verify this for NGC 1232, we divided it in two parts: inner and outer region. The inner region is defined as the region inside half of the maximum H II region distance to the center, which is 11.2 kpc. Indeed, we found $D_0 = 89.7 \pm 1.7$ pc for the inner region and $D_0 = 106.6 \pm 2.6$ pc for the outer region. The different cumulative

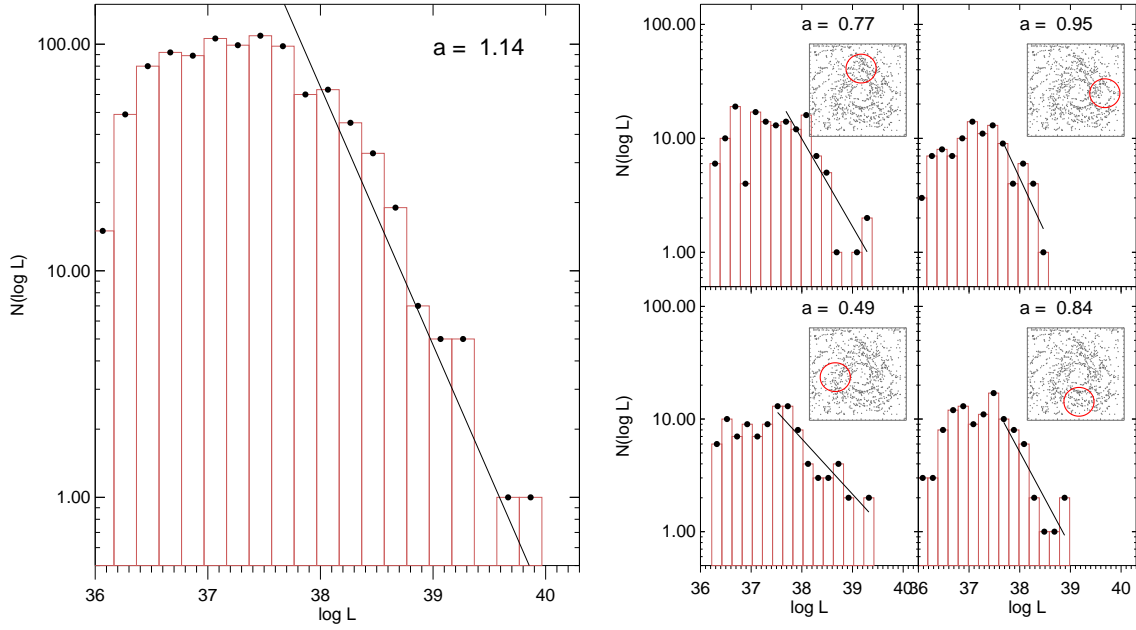


Figure 3. H II luminosity function of NGC 1232. The left panel shows the luminosity function including all H II regions of the galaxy. The solid line represents the power-law fitted for $\log L \geq 37.5$ dex. The four panels in the left side of this figure correspond to the luminosity functions in four different regions of the galaxy, as indicated by the red circle over the galaxy's image of each plot. Slope values a for each of the fits are shown in the top of each plot.

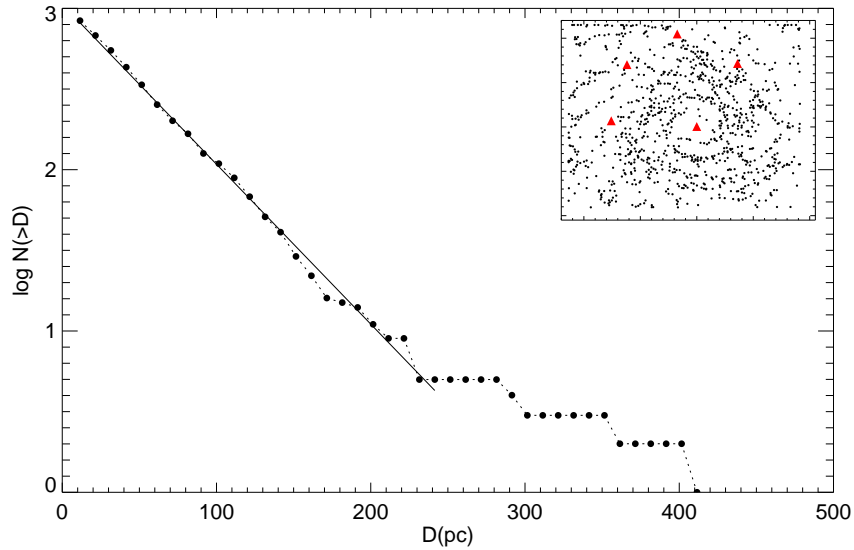


Figure 4. H II regions size cumulative distribution. The inset in the top right of this figure shows the location of the five brightest H II regions detected (red triangles), which were excluded from the fit. The fit to the remaining regions is shown by the solid line. The characteristic diameter of the galaxy obtained by this fit is $D_0 = 100.9 \pm 1.5$ pc.

distributions for the inner and outer regions are shown in figure 5. From this figure we can also see that the five largest H II regions are located in the outer region of NGC 1232.

Another characteristic of the H II regions that can be explored is if they are radiation or matter bounded. If they are radiation bounded and have similar gas densities across the galaxy, then their diameter should scale as the cube root

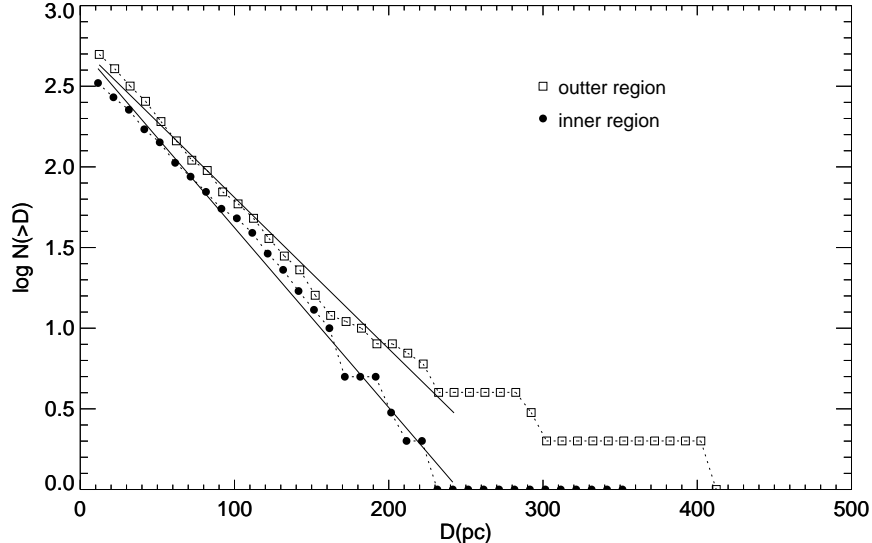


Figure 5. H II regions size cumulative distribution for the inner (filled circle) and outer (open square) region of NGC 1232. The inner region is defined as the region inside half of the maximum H II region distance to the center, which is 11.2 kpc. The solid lines represent the fits for each distribution. We found $D_0 = 89.7 \pm 1.7$ pc for the inner region and $D_0 = 106.6 \pm 2.6$ pc for the outer region, following the trend found in the literature, which shows a tendency to have a larger D_0 for outer than for inner regions.

of the ionizing luminosity (Osterbrock 1989). Previous studies (e.g. Kennicutt 1989; Banfi et al. 1993) found that H II regions in galaxies are essentially radiation bounded. To verify that for the H II regions of NGC 1232 we plotted the luminosities versus their diameters. This is shown in figure 6. In this figure the two dotted lines mark the expected slopes for radiation bounded H II regions. It is important to realize that most of these regions will be ionized by more than one star, which results in a situation physically different from that expected by a Strömgren sphere. However, we can see from figure 6 that, at least the larger regions seem to be indeed radiation bounded. Smaller regions, as previously mentioned, might be matter bounded.

5. STAR FORMATION RATE

The SFR is then obtained adopting the equation from Calzetti et al. (2007):

$$SFR(M_{\odot} \text{ yr}^{-1}) = 5.3 \times 10^{-42} L(H\alpha) \text{ (erg s}^{-1}\text{)}. \quad (3)$$

The $H\alpha$ flux, luminosity, and the SFR for each H II region are presented in table 1. The left side of figure 7 shows the SFR distribution in the galaxy. The uncertainties in the SFR vary from 12% to 17%, with an average value of 13%, taking into account the errors in the fluxes obtained by SExtractor and the error in the distance determination. It does not take into account the approximations for the extinction and [N II] correction, which are much harder to estimate.

As expected, the SFR is higher in the spiral arms, as is commonly accepted in the literature that the H II regions are tracers of these arms. Another quantity that can be studied with our data and which carries more physical meaning, is the SFR density, or SFR per unity area (ΣSFR). The results are shown in the right panel of figure 7. ΣSFR was obtained by dividing the SFR of every H II region by their physical size, given by SExtractor. In can be seen in the right panel of figure 7 that the spiral pattern becomes less obvious, supporting the hypothesis that the spiral arms only show more star formation because they concentrate most of the gas, but not necessarily are they more efficient at forming stars (Scoville et al. 2001; Foyle et al. 2010; Gutiérrez et al. 2011; Kreckel et al. 2016). Of course, a more conclusive result can only be achieved by separating the H II regions of the arms from the inter-arms, which is non-trivial for multi-armed galaxies.

In terms of general behavior, NGC 1232 is a typical spiral galaxy, which have total SFR values around $1 M_{\odot} \text{ yr}^{-1}$ (Lee et al. 2009). We found a value of $0.77 M_{\odot} \text{ yr}^{-1}$ from our data, measuring the total $H\alpha$ flux inside a large aperture

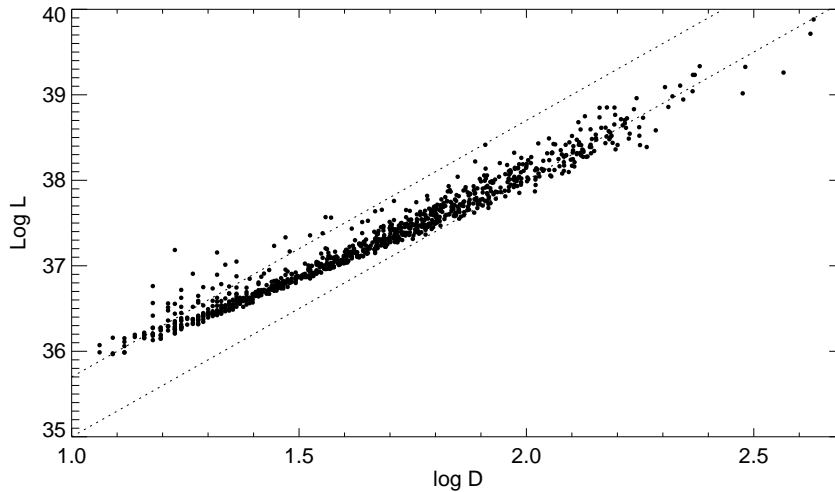


Figure 6. Logarithm of the Luminosity versus the logarithm of the diameter for the H II regions detected in NGC 1232. The dotted lines indicate the trend expected if the H II regions are radiation bounded, which is the cube root of the ionizing luminosity

and performing the same process to obtain the H α luminosity as was done for each H II region. It is important to remember that our data do not encompass the whole galaxy. Flux sensitivity also has to be taken into account for direct comparisons with other authors, in the sense that low sensitivities will result in significant amounts of H α diffuse emission not being detected, leading to a lower SFR measurement. Our sensitivity is just slightly higher than that of Lee et al. (2009).

The Σ SFR values obtained in this work for NGC 1232 can be compared with the values obtained by Grosbol & Dottori (2012). They derived Σ SFR gradients for several spiral galaxies, including NGC 1232, finding an essentially constant Σ SFR along the radius of the galaxy, with values between 10^{-2} - $10^{-3} M_{\odot} yr^{-1} kpc^{-2}$. With our superior image quality, we confirm their results. If we look at the average radial values, we can also see that there is no obvious Σ SFR gradient in the galaxy.

However, the most interesting feature that we found in this distribution is a clear asymmetry in the intensity of the SFR, where the regions of more intense formation (red symbols) appear to be located preferably in the northeast side of the galaxy (figure 7), while we notice an absence of star formation to the west and very likely to the south of the nucleus.

As mentioned previously, Garmire (2013) found a diffuse X-ray emission in NGC 1232 that indicates a possible collision with a dwarf galaxy. The peak of the diffuse X-ray emission is coincident with the zone where the H II regions are smaller and more sparse, while the excess SFR in the northeast of the galaxy is where the emission is weaker. The X-ray contours in the left panel of figure 7 can help to see that. We interpret this result as a suppression of the star formation in the hot gas region and/or as an intensification of the star formation in the post-shock region of the dwarf galaxy's passage.

To make this effect more evident, we picked an annulus including the x-ray peak region, and divided this annulus in six sections of 60° each. For each of these sections we computed average properties related to the H II regions, namely, the number of regions in each section, the average diameter of the regions, and average luminosity. This is shown in figure 8. These numbers will, of course, be affected by the size of the chosen regions (which, if too big will just average out any localized differences) and their placement (inter-arm locations will naturally have less H II regions than in arm locations). By looking at sections at the same distance from the center in all directions we tried to avoid both these effects. It can be seen from Figure 8 that the green section is clearly deficient compared to the other regions, both in terms of number of regions and in average properties (sizes and luminosities). This section is located close to the x-ray

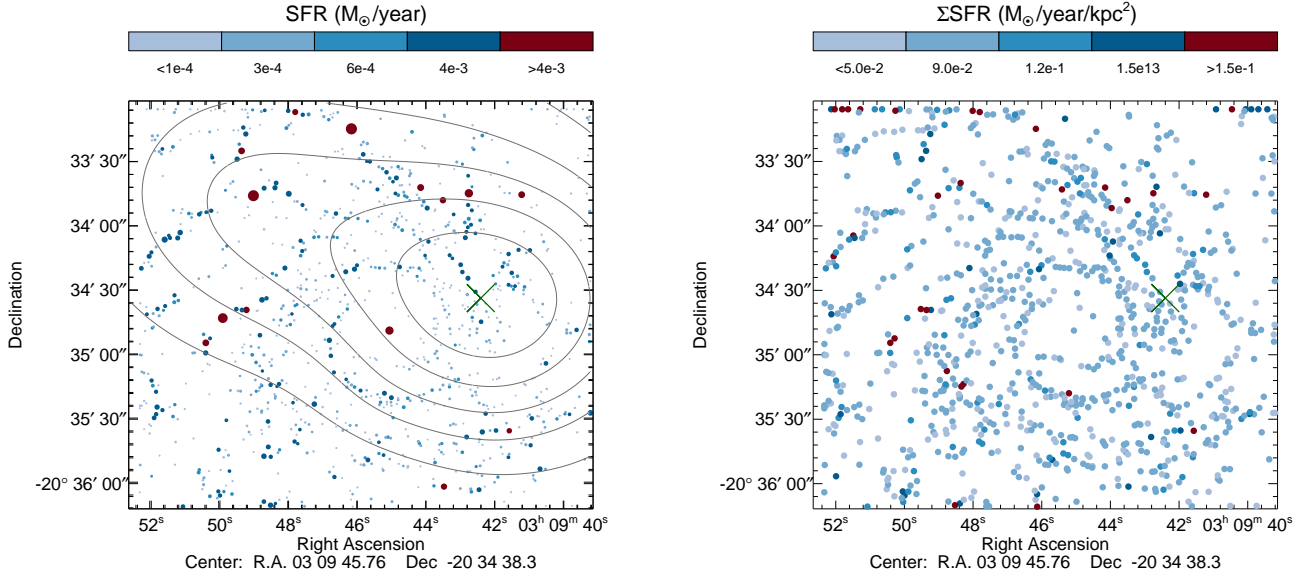


Figure 7. The SFR of NGC 1232, calculated for each H II region. Left: SFR distribution. The size of the dots is proportional to the size of each H II region. The gray contour represents the x-ray contours from [Garmire \(2013\)](#). Right: distribution of the SFR per unity area. The green “x” in both plots marks the peak of the x-ray emission (X-ray data obtained from G. Garmire, private communication.)

peak. This result provides additional evidence on the quenching of the star formation as a result of the collision with the dwarf galaxy. In-depth spectroscopic study will certainly be helpful to reach a definitive conclusion on this issue.

6. CONCLUSIONS

In this work, we study the star formation distribution in the galaxy NGC 1232, a spiral galaxy seen practically face on. It is considered a grand-design spiral, and therefore an excellent laboratory for the study of the relationship between star formation and spiral arms. Besides that, [Garmire \(2013\)](#) reports evidence that a dwarf galaxy might have crossed the disk of NGC 1232, based on the detection of a diffuse, hot X-ray emission cloud observed in this galaxy.

We obtained a high spatial resolution H α image of NGC 1232 using SAM at SOAR telescope, with AO. This resulted in the best spatial resolution image of this galaxy so far. A total of 976 H II regions were detected for the SOAR image field, which encompasses about the 50% central part of optical image of the galaxy. Despite not covering the entire galaxy, the number of sources detected here represent the most complete H α source catalog for this galaxy in the literature, since double the number of H II regions were already detected in this object.

We also constructed the H II regions luminosity function, obtaining a power-law index of $a = 1.14$. This is a value typically lower than what is found for Sc galaxies. In the case of NGC 1232 this is related to the presence of a significant number of high-luminosity H II regions. These are mainly found in the northern and eastern part of the galaxy, while the eastern part of the galaxy clearly shows a lack of these brighter regions. We also constructed the size distribution function of the H II regions, verifying that, as for most galaxies, NGC 1232 follows an exponential law, with a characteristic diameter of $D_0 = 100.9 \pm 1.5$ pc.

We used the H α luminosity to determine the SFR of each H II region, and analyzed their distribution in the galaxy. We also calculated the SFR density Σ SFR for each source. Results show that, as expected, stronger star formation is found along the spiral arms. However, the apparent concentration of H II regions in the spiral arms is diluted when the SFR density is analyzed.

We also found an interesting pattern in the distribution of the SFR, where there seems to be an lower number of H II sources exactly in the region where the diffuse X-ray gas has a peak of emission. This might be due to a quenching of star formation due to the collision with the dwarf galaxy. On the other hand, there seems to be an excess of star formation in the northeast part of the galaxy, where the X-ray emission is weaker. We suggest that this excess might have been induced by a shock wave from the collision.

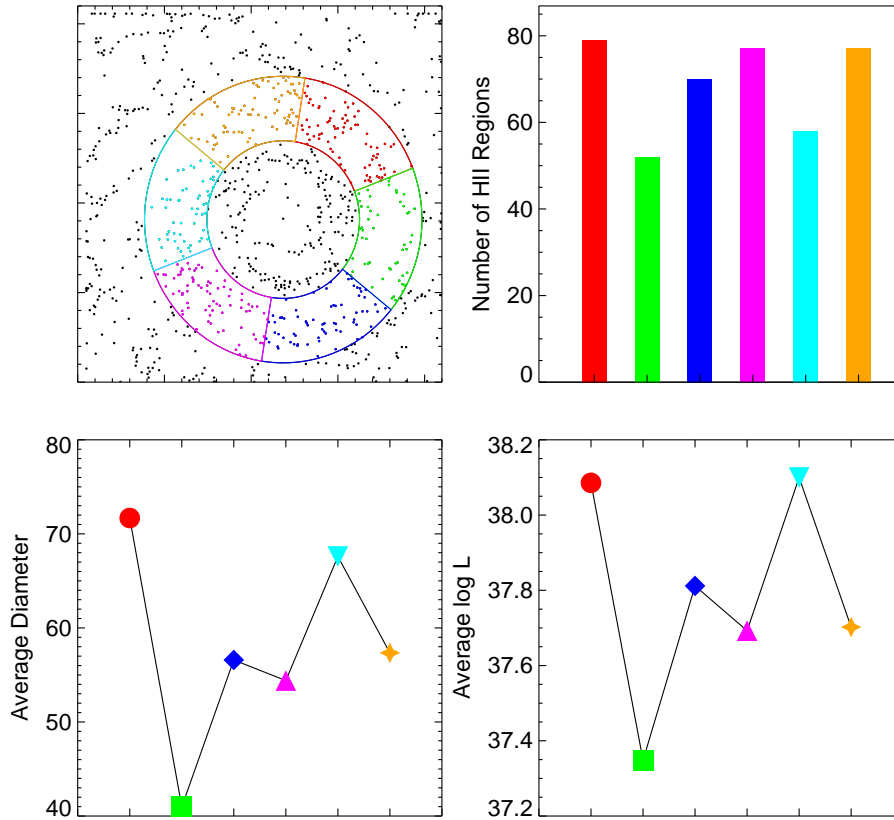


Figure 8. Main properties of the H II regions in six different regions of NGC 1232, at the same distance from the center, color-coded as shown in the top left plot. The top right plot shows the number of H II regions in each section, starting by the one on the top left (red region) and with following in the clockwise direction. The bottom left plot shows the average diameter of the H II regions (in pc) in each section as measured by SEXTRACTOR and the bottom right plot the average luminosity (in Log units), following the same order as the top right plot. It can be clearly seen that the green region (second point in each plot), which is around the region of the X-Ray peak, has a deficiency of large and luminous H II regions.

We thank the referee for invaluable suggestions that greatly improved the paper. Based on observations obtained at the Southern Astrophysical Research (SOAR) telescope, which is a joint project of the Ministério da Ciência, Tecnologia, e Inovação (MCTI) da República Federativa do Brasil, the U.S. National Optical Astronomy Observatory (NOAO), the University of North Carolina at Chapel Hill (UNC), and Michigan State University (MSU). A.A.S. acknowledges CAPES for financial support. L.M. thanks CNPQ for financial support through grant 303697/2015-6 and FAPESP through grant 2015/14575-0. A.R.A. thanks CNPq for partial support to this work. We thank Andrei Tokovinin from the SOAR observatory, for the excellent support during the observations with SAM/SOAR. We also thank G. Garmire for the x-ray data used in this paper.

Facilities: SOAR(SAM)

Software: IRAF (Valdes 1998; Valdes & Tody 1998), SExtractor (Bertin & Arnouts 1996)

APPENDIX
A. SOURCES DATA

Table 2. Data from sources detected in galaxy NGC 1232, in order of luminosity.

Source	Position (RA)	Position (Dec)	F(H α) (10^{-17} erg/cm 2 /s)	SFR (M_{\odot} /yr)	Area (pixel 2)	L(H α) (erg s $^{-1}$)
1.0	03h09m45.70s	-20h33m16.35s	16220.49 \pm 7.99	40.332e-3 \pm 4.840e-3	9670.00	7.61e+39
2.0	03h09m42.93s	-20h33m46.88s	11033.00 \pm 7.91	27.433e-3 \pm 3.292e-3	9366.00	5.18e+39
3.0	03h09m47.64s	-20h33m43.09s	4593.81 \pm 4.58	11.422e-3 \pm 1.371e-3	3051.00	2.16e+39
4.0	03h09m49.00s	-20h33m45.82s	4528.41 \pm 5.67	11.260e-3 \pm 1.351e-3	4841.00	2.12e+39
5.0	03h09m42.06s	-20h34m43.09s	3880.59 \pm 7.12	9.649e-3 \pm 1.158e-3	7131.00	1.82e+39
6.0	03h09m50.50s	-20h33m46.72s	3652.16 \pm 4.41	9.081e-3 \pm 1.090e-3	2902.00	1.71e+39
7.0	03h09m41.58s	-20h34m54.59s	3640.34 \pm 4.34	9.052e-3 \pm 1.086e-3	2848.00	1.71e+39
8.0	03h09m48.26s	-20h33m48.91s	2729.06 \pm 4.11	6.786e-3 \pm 0.814e-3	2503.00	1.28e+39
9.0	03h09m44.12s	-20h33m08.82s	2611.27 \pm 3.74	6.493e-3 \pm 0.779e-3	2147.00	1.23e+39
10.	03h09m42.61s	-20h33m26.54s	2354.45 \pm 4.36	5.854e-3 \pm 0.703e-3	2839.00	1.10e+39
11.	03h09m46.75s	-20h34m48.59s	2220.19 \pm 6.20	5.520e-3 \pm 0.663e-3	4716.00	1.04e+39
12.	03h09m48.31s	-20h36m01.20s	2045.70 \pm 3.96	5.087e-3 \pm 0.610e-3	2315.00	9.60e+38
13.	03h09m50.14s	-20h35m35.40s	1945.00 \pm 3.30	4.836e-3 \pm 0.580e-3	1610.00	9.13e+38
14.	03h09m42.72s	-20h34m39.24s	1877.97 \pm 4.09	4.670e-3 \pm 0.560e-3	2583.00	8.81e+38
15.	03h09m40.44s	-20h34m07.34s	1536.83 \pm 3.81	3.821e-3 \pm 0.459e-3	2221.00	7.21e+38
16.	03h09m46.61s	-20h35m17.58s	1514.98 \pm 2.85	3.767e-3 \pm 0.452e-3	1192.00	7.11e+38
17.	03h09m40.00s	-20h34m15.08s	1511.77 \pm 2.90	3.759e-3 \pm 0.451e-3	1287.00	7.09e+38
18.	03h09m42.60s	-20h34m39.30s	1503.07 \pm 2.64	3.737e-3 \pm 0.449e-3	1107.00	7.05e+38
19.	03h09m43.43s	-20h36m09.90s	1448.23 \pm 3.17	3.601e-3 \pm 0.432e-3	1568.00	6.79e+38
20.	03h09m47.82s	-20h33m52.46s	1242.06 \pm 2.95	3.088e-3 \pm 0.371e-3	1296.00	5.83e+38
21.	03h09m42.44s	-20h34m38.88s	1194.76 \pm 2.50	2.971e-3 \pm 0.357e-3	954.000	5.61e+38
22.	03h09m43.57s	-20h33m41.05s	1161.43 \pm 2.72	2.888e-3 \pm 0.347e-3	1106.00	5.45e+38
23.	03h09m43.16s	-20h34m34.56s	1148.81 \pm 3.39	2.856e-3 \pm 0.343e-3	1719.00	5.39e+38
24.	03h09m42.48s	-20h33m30.31s	1132.09 \pm 3.10	2.815e-3 \pm 0.338e-3	1461.00	5.31e+38
25.	03h09m45.76s	-20h34m20.32s	1103.09 \pm 3.04	2.743e-3 \pm 0.329e-3	1375.00	5.18e+38
26.	03h09m42.73s	-20h33m18.87s	1080.70 \pm 3.08	2.687e-3 \pm 0.323e-3	1430.00	5.07e+38
27.	03h09m43.64s	-20h35m13.41s	1017.89 \pm 2.40	2.531e-3 \pm 0.304e-3	893.000	4.78e+38
28.	03h09m41.58s	-20h34m59.24s	995.96 \pm 3.12	2.476e-3 \pm 0.297e-3	1429.00	4.67e+38
29.	03h09m43.80s	-20h34m19.90s	958.57 \pm 2.92	2.383e-3 \pm 0.286e-3	1285.00	4.50e+38
30.	03h09m43.53s	-20h33m43.22s	936.37 \pm 3.03	2.328e-3 \pm 0.279e-3	1399.00	4.39e+38
31.	03h09m44.64s	-20h35m22.63s	890.94 \pm 3.37	2.215e-3 \pm 0.266e-3	1653.00	4.18e+38

Table 2 continued on next page

Table 2 (continued)

Source	Position (RA)	Position (Dec)	F(H α) (10^{-17} erg/cm 2 /s)	SFR (M_{\odot} /yr)	Area (pixel 2)	L(H α) (erg s $^{-1}$)
32.	03h09m48.94s	-20h35m38.10s	880.89 \pm 2.81	2.190e-3 \pm 0.263e-3	1176.00	4.13e+38
33.	03h09m40.23s	-20h35m24.60s	875.85 \pm 3.11	2.178e-3 \pm 0.261e-3	1446.00	4.11e+38
34.	03h09m46.16s	-20h35m48.63s	875.47 \pm 2.77	2.177e-3 \pm 0.261e-3	1126.00	4.11e+38
35.	03h09m49.77s	-20h35m35.21s	842.55 \pm 2.58	2.095e-3 \pm 0.251e-3	1010.00	3.95e+38
36.	03h09m43.92s	-20h33m08.28s	838.53 \pm 2.46	2.085e-3 \pm 0.250e-3	913.000	3.93e+38
37.	03h09m43.92s	-20h33m45.93s	818.01 \pm 3.67	2.034e-3 \pm 0.244e-3	1955.00	3.84e+38
38.	03h09m43.35s	-20h35m42.66s	801.46 \pm 2.90	1.993e-3 \pm 0.239e-3	1214.00	3.76e+38
39.	03h09m46.95s	-20h33m38.67s	772.49 \pm 2.86	1.921e-3 \pm 0.231e-3	1234.00	3.62e+38
40.	03h09m45.05s	-20h34m53.06s	747.28 \pm 3.24	1.858e-3 \pm 0.223e-3	1502.00	3.51e+38
41.	03h09m40.15s	-20h35m29.65s	728.21 \pm 2.63	1.811e-3 \pm 0.217e-3	1065.00	3.42e+38
42.	03h09m40.87s	-20h34m04.03s	708.13 \pm 3.34	1.761e-3 \pm 0.211e-3	1656.00	3.32e+38
43.	03h09m45.52s	-20h34m21.52s	705.59 \pm 2.94	1.754e-3 \pm 0.211e-3	1250.00	3.31e+38
44.	03h09m47.85s	-20h34m07.76s	704.17 \pm 2.35	1.751e-3 \pm 0.210e-3	837.000	3.30e+38
45.	03h09m49.30s	-20h36m02.76s	693.22 \pm 2.87	1.724e-3 \pm 0.207e-3	1187.00	3.25e+38
46.	03h09m43.23s	-20h33m43.43s	678.29 \pm 2.87	1.687e-3 \pm 0.203e-3	1232.00	3.18e+38
47.	03h09m39.78s	-20h34m20.66s	663.49 \pm 2.65	1.650e-3 \pm 0.198e-3	1067.00	3.11e+38
48.	03h09m46.42s	-20h33m43.88s	659.26 \pm 2.11	1.639e-3 \pm 0.197e-3	663.000	3.09e+38
49.	03h09m49.38s	-20h35m35.82s	653.95 \pm 3.19	1.626e-3 \pm 0.195e-3	1488.00	3.07e+38
50.	03h09m43.10s	-20h34m50.86s	648.67 \pm 2.61	1.613e-3 \pm 0.194e-3	1024.00	3.04e+38
51.	03h09m48.89s	-20h34m06.11s	643.98 \pm 2.91	1.601e-3 \pm 0.192e-3	1222.00	3.02e+38
52.	03h09m40.20s	-20h35m27.91s	635.01 \pm 2.38	1.579e-3 \pm 0.190e-3	879.000	2.98e+38
53.	03h09m48.76s	-20h34m18.47s	634.42 \pm 2.68	1.577e-3 \pm 0.189e-3	1070.00	2.98e+38
54.	03h09m50.12s	-20h34m13.75s	593.80 \pm 2.46	1.476e-3 \pm 0.177e-3	899.000	2.79e+38
55.	03h09m42.01s	-20h36m05.51s	591.83 \pm 2.30	1.472e-3 \pm 0.177e-3	815.000	2.78e+38
56.	03h09m40.80s	-20h34m06.55s	583.83 \pm 2.89	1.452e-3 \pm 0.174e-3	1263.00	2.74e+38
57.	03h09m46.81s	-20h35m19.65s	579.02 \pm 2.90	1.440e-3 \pm 0.173e-3	1174.00	2.72e+38
58.	03h09m41.70s	-20h34m52.50s	574.42 \pm 1.97	1.428e-3 \pm 0.171e-3	595.000	2.70e+38
59.	03h09m40.59s	-20h34m06.55s	567.58 \pm 2.07	1.411e-3 \pm 0.169e-3	694.000	2.66e+38
60.	03h09m41.96s	-20h36m03.61s	561.50 \pm 2.14	1.396e-3 \pm 0.168e-3	706.000	2.63e+38
61.	03h09m40.97s	-20h36m10.90s	556.46 \pm 3.14	1.384e-3 \pm 0.166e-3	1011.00	2.61e+38
62.	03h09m40.07s	-20h35m12.32s	555.19 \pm 2.29	1.380e-3 \pm 0.166e-3	785.000	2.60e+38
63.	03h09m43.17s	-20h35m07.39s	554.97 \pm 1.53	1.380e-3 \pm 0.166e-3	348.000	2.60e+38
64.	03h09m49.47s	-20h35m27.31s	554.76 \pm 2.47	1.379e-3 \pm 0.166e-3	897.000	2.60e+38
65.	03h09m51.02s	-20h35m53.36s	551.74 \pm 3.06	1.372e-3 \pm 0.165e-3	1328.00	2.59e+38
66.	03h09m43.23s	-20h35m47.00s	549.83 \pm 3.43	1.367e-3 \pm 0.164e-3	1667.00	2.58e+38
67.	03h09m48.81s	-20h34m21.80s	549.50 \pm 2.49	1.366e-3 \pm 0.164e-3	919.000	2.58e+38
68.	03h09m43.29s	-20h34m33.84s	534.10 \pm 2.38	1.328e-3 \pm 0.159e-3	849.000	2.51e+38

Table 2 continued on next page

Table 2 (continued)

Source	Position (RA)	Position (Dec)	F(H α) (10^{-17} erg/cm 2 /s)	SFR (M_{\odot} /yr)	Area (pixel 2)	L(H α) (erg s $^{-1}$)
69.	03h09m52.45s	-20h35m27.56s	522.90 \pm 3.37	1.300e-3 \pm 0.156e-3	1784.00	2.45e+38
70.	03h09m43.34s	-20h35m30.80s	522.15 \pm 2.62	1.298e-3 \pm 0.156e-3	1003.00	2.45e+38
71.	03h09m49.34s	-20h34m44.77s	521.21 \pm 2.64	1.296e-3 \pm 0.156e-3	1017.00	2.45e+38
72.	03h09m48.97s	-20h34m24.69s	490.19 \pm 3.02	1.219e-3 \pm 0.146e-3	1301.00	2.30e+38
73.	03h09m41.41s	-20h33m55.59s	487.34 \pm 2.49	1.212e-3 \pm 0.146e-3	929.000	2.29e+38
74.	03h09m50.40s	-20h34m11.90s	478.69 \pm 2.25	1.190e-3 \pm 0.143e-3	747.000	2.25e+38
75.	03h09m50.78s	-20h35m29.73s	478.33 \pm 2.52	1.189e-3 \pm 0.143e-3	938.000	2.24e+38
76.	03h09m44.09s	-20h35m40.09s	477.83 \pm 2.35	1.188e-3 \pm 0.143e-3	846.000	2.24e+38
77.	03h09m46.02s	-20h33m27.92s	469.01 \pm 2.63	1.166e-3 \pm 0.140e-3	1048.00	2.20e+38
78.	03h09m46.68s	-20h33m36.07s	458.59 \pm 2.54	1.140e-3 \pm 0.137e-3	941.000	2.15e+38
79.	03h09m40.06s	-20h34m13.28s	449.85 \pm 2.13	1.119e-3 \pm 0.134e-3	684.000	2.11e+38
80.	03h09m41.74s	-20h33m53.91s	449.46 \pm 2.38	1.118e-3 \pm 0.134e-3	843.000	2.11e+38
81.	03h09m40.55s	-20h34m05.46s	448.50 \pm 1.72	1.115e-3 \pm 0.134e-3	466.000	2.10e+38
82.	03h09m41.78s	-20h33m29.67s	447.64 \pm 2.11	1.113e-3 \pm 0.134e-3	686.000	2.10e+38
83.	03h09m52.04s	-20h34m49.04s	446.01 \pm 2.50	1.109e-3 \pm 0.133e-3	909.000	2.09e+38
84.	03h09m45.25s	-20h33m54.87s	442.98 \pm 2.54	1.101e-3 \pm 0.132e-3	880.000	2.08e+38
85.	03h09m48.45s	-20h34m14.10s	442.25 \pm 2.14	1.100e-3 \pm 0.132e-3	682.000	2.07e+38
86.	03h09m51.18s	-20h35m04.31s	441.54 \pm 2.64	1.098e-3 \pm 0.132e-3	1015.00	2.07e+38
87.	03h09m44.31s	-20h33m51.03s	441.26 \pm 2.10	1.097e-3 \pm 0.132e-3	651.000	2.07e+38
88.	03h09m40.23s	-20h34m39.19s	430.91 \pm 2.46	1.071e-3 \pm 0.129e-3	879.000	2.02e+38
89.	03h09m46.21s	-20h33m31.22s	428.14 \pm 2.25	1.065e-3 \pm 0.128e-3	755.000	2.01e+38
90.	03h09m44.33s	-20h33m10.03s	420.78 \pm 2.28	1.046e-3 \pm 0.126e-3	789.000	1.97e+38
91.	03h09m50.20s	-20h34m22.42s	416.52 \pm 2.70	1.036e-3 \pm 0.124e-3	918.000	1.95e+38
92.	03h09m44.25s	-20h34m07.36s	416.35 \pm 2.33	1.035e-3 \pm 0.124e-3	788.000	1.95e+38
93.	03h09m43.24s	-20h36m08.21s	404.81 \pm 2.59	1.007e-3 \pm 0.121e-3	980.000	1.90e+38
94.	03h09m40.38s	-20h35m25.97s	402.80 \pm 2.25	1.002e-3 \pm 0.120e-3	770.000	1.89e+38
95.	03h09m47.04s	-20h34m19.33s	400.83 \pm 2.59	0.997e-3 \pm 0.120e-3	968.000	1.88e+38
96.	03h09m45.10s	-20h35m00.23s	399.99 \pm 2.54	0.995e-3 \pm 0.120e-3	937.000	1.88e+38
97.	03h09m39.93s	-20h34m41.73s	398.61 \pm 2.01	0.991e-3 \pm 0.119e-3	554.000	1.87e+38
98.	03h09m49.18s	-20h34m04.15s	390.53 \pm 1.82	0.971e-3 \pm 0.117e-3	501.000	1.83e+38
99.	03h09m43.41s	-20h35m13.79s	376.48 \pm 2.42	0.936e-3 \pm 0.112e-3	845.000	1.77e+38
100.	03h09m44.29s	-20h34m12.05s	376.27 \pm 2.22	0.936e-3 \pm 0.112e-3	730.000	1.77e+38
101.	03h09m45.22s	-20h35m56.59s	371.38 \pm 2.37	0.923e-3 \pm 0.111e-3	827.000	1.74e+38
102.	03h09m45.83s	-20h34m18.55s	367.13 \pm 2.10	0.913e-3 \pm 0.110e-3	665.000	1.72e+38
103.	03h09m50.13s	-20h35m47.73s	366.34 \pm 1.89	0.911e-3 \pm 0.109e-3	537.000	1.72e+38
104.	03h09m45.94s	-20h35m16.34s	360.13 \pm 2.08	0.895e-3 \pm 0.108e-3	626.000	1.69e+38
105.	03h09m43.58s	-20h35m14.55s	353.27 \pm 1.42	0.878e-3 \pm 0.105e-3	314.000	1.66e+38

Table 2 continued on next page

Table 2 (continued)

Source	Position (RA)	Position (Dec)	F(H α) (10^{-17} erg/cm 2 /s)	SFR (M_{\odot} /yr)	Area (pixel 2)	L(H α) (erg s $^{-1}$)
106	03h09m42.66s	-20h33m15.95s	347.90 \pm 2.44	0.865e-3 \pm 0.104e-3	859.000	1.63e+38
107	03h09m41.96s	-20h35m44.14s	347.78 \pm 2.28	0.865e-3 \pm 0.104e-3	771.000	1.63e+38
108	03h09m46.92s	-20h33m45.73s	339.88 \pm 1.93	0.845e-3 \pm 0.102e-3	552.000	1.59e+38
109	03h09m44.00s	-20h34m40.98s	339.13 \pm 1.67	0.843e-3 \pm 0.101e-3	403.000	1.59e+38
110	03h09m45.20s	-20h34m45.54s	332.05 \pm 1.91	0.826e-3 \pm 0.099e-3	529.000	1.56e+38
111	03h09m40.39s	-20h33m26.04s	327.93 \pm 1.82	0.815e-3 \pm 0.098e-3	490.000	1.54e+38
112	03h09m48.57s	-20h33m55.43s	327.55 \pm 1.86	0.814e-3 \pm 0.098e-3	509.000	1.54e+38
113	03h09m47.75s	-20h34m14.15s	322.75 \pm 1.71	0.803e-3 \pm 0.096e-3	434.000	1.51e+38
114	03h09m50.75s	-20h35m42.25s	317.81 \pm 2.35	0.790e-3 \pm 0.095e-3	773.000	1.49e+38
115	03h09m50.72s	-20h34m12.12s	316.03 \pm 2.39	0.786e-3 \pm 0.094e-3	837.000	1.48e+38
116	03h09m50.30s	-20h34m28.51s	313.50 \pm 1.89	0.780e-3 \pm 0.094e-3	528.000	1.47e+38
117	03h09m40.71s	-20h34m32.83s	310.72 \pm 2.27	0.773e-3 \pm 0.093e-3	738.000	1.46e+38
118	03h09m49.18s	-20h34m30.96s	309.80 \pm 2.43	0.770e-3 \pm 0.093e-3	857.000	1.45e+38
119	03h09m41.60s	-20h33m54.63s	299.03 \pm 1.87	0.744e-3 \pm 0.089e-3	526.000	1.40e+38
120	03h09m46.46s	-20h35m40.37s	298.41 \pm 1.79	0.742e-3 \pm 0.089e-3	469.000	1.40e+38
121	03h09m42.17s	-20h35m30.40s	297.92 \pm 1.81	0.741e-3 \pm 0.089e-3	485.000	1.40e+38
122	03h09m45.15s	-20h34m46.50s	293.80 \pm 2.01	0.731e-3 \pm 0.088e-3	583.000	1.38e+38
123	03h09m46.60s	-20h35m46.36s	293.79 \pm 1.88	0.730e-3 \pm 0.088e-3	484.000	1.38e+38
124	03h09m43.56s	-20h36m09.06s	291.29 \pm 1.53	0.724e-3 \pm 0.087e-3	349.000	1.37e+38
125	03h09m43.26s	-20h33m08.12s	289.66 \pm 1.78	0.720e-3 \pm 0.087e-3	470.000	1.36e+38
126	03h09m49.06s	-20h34m00.21s	289.08 \pm 2.07	0.719e-3 \pm 0.086e-3	616.000	1.36e+38
127	03h09m50.11s	-20h34m27.87s	286.59 \pm 2.00	0.713e-3 \pm 0.086e-3	589.000	1.34e+38
128	03h09m49.08s	-20h33m53.63s	283.40 \pm 2.09	0.705e-3 \pm 0.085e-3	629.000	1.33e+38
129	03h09m45.15s	-20h34m23.45s	281.17 \pm 2.22	0.699e-3 \pm 0.084e-3	701.000	1.32e+38
130	03h09m45.19s	-20h35m07.91s	281.12 \pm 2.19	0.699e-3 \pm 0.084e-3	664.000	1.32e+38
131	03h09m49.94s	-20h34m19.55s	279.55 \pm 1.99	0.695e-3 \pm 0.084e-3	576.000	1.31e+38
132	03h09m44.23s	-20h35m34.51s	278.19 \pm 1.75	0.692e-3 \pm 0.083e-3	448.000	1.31e+38
133	03h09m48.92s	-20h34m03.42s	275.40 \pm 2.06	0.685e-3 \pm 0.082e-3	625.000	1.29e+38
134	03h09m40.20s	-20h35m17.49s	275.16 \pm 2.35	0.684e-3 \pm 0.082e-3	771.000	1.29e+38
135	03h09m48.98s	-20h33m37.87s	274.55 \pm 1.90	0.683e-3 \pm 0.082e-3	513.000	1.29e+38
136	03h09m42.27s	-20h35m54.06s	272.67 \pm 1.72	0.678e-3 \pm 0.081e-3	442.000	1.28e+38
137	03h09m46.86s	-20h33m40.38s	270.15 \pm 1.76	0.672e-3 \pm 0.081e-3	450.000	1.27e+38
138	03h09m43.42s	-20h35m47.26s	265.59 \pm 2.41	0.660e-3 \pm 0.079e-3	810.000	1.25e+38
139	03h09m51.85s	-20h35m28.09s	264.75 \pm 1.83	0.658e-3 \pm 0.079e-3	499.000	1.24e+38
140	03h09m44.04s	-20h35m22.01s	260.95 \pm 1.73	0.649e-3 \pm 0.078e-3	449.000	1.22e+38
141	03h09m48.98s	-20h33m51.17s	256.72 \pm 2.32	0.638e-3 \pm 0.077e-3	758.000	1.20e+38
142	03h09m48.97s	-20h34m01.36s	256.62 \pm 2.04	0.638e-3 \pm 0.077e-3	596.000	1.20e+38

Table 2 continued on next page

Table 2 (*continued*)

Source	Position (RA)	Position (Dec)	F(H α) (10^{-17} erg/cm 2 /s)	SFR (M_{\odot} /yr)	Area (pixel 2)	L(H α) (erg s $^{-1}$)
143	03h09m45.53s	-20h35m11.13s	251.11 \pm 1.72	0.624e-3 \pm 0.075e-3	426.000	1.18e+38
144	03h09m48.53s	-20h34m15.51s	246.34 \pm 1.73	0.613e-3 \pm 0.074e-3	443.000	1.16e+38
145	03h09m40.45s	-20h34m37.82s	243.71 \pm 2.15	0.606e-3 \pm 0.073e-3	672.000	1.14e+38
146	03h09m46.12s	-20h33m31.11s	243.30 \pm 1.51	0.605e-3 \pm 0.073e-3	344.000	1.14e+38
147	03h09m44.18s	-20h35m41.07s	243.27 \pm 1.52	0.605e-3 \pm 0.073e-3	354.000	1.14e+38
148	03h09m40.70s	-20h34m36.03s	237.42 \pm 2.00	0.590e-3 \pm 0.071e-3	602.000	1.11e+38
149	03h09m48.99s	-20h33m57.47s	236.59 \pm 2.16	0.588e-3 \pm 0.071e-3	679.000	1.11e+38
150	03h09m43.96s	-20h34m45.86s	234.94 \pm 1.64	0.584e-3 \pm 0.070e-3	400.000	1.10e+38
151	03h09m51.72s	-20h35m27.88s	234.88 \pm 1.33	0.584e-3 \pm 0.070e-3	263.000	1.10e+38
152	03h09m47.00s	-20h33m46.52s	234.41 \pm 1.80	0.583e-3 \pm 0.070e-3	490.000	1.10e+38
153	03h09m44.25s	-20h34m14.18s	233.52 \pm 1.81	0.581e-3 \pm 0.070e-3	467.000	1.10e+38
154	03h09m41.40s	-20h35m54.86s	230.99 \pm 1.98	0.574e-3 \pm 0.069e-3	580.000	1.08e+38
155	03h09m47.16s	-20h35m24.09s	230.30 \pm 1.90	0.573e-3 \pm 0.069e-3	533.000	1.08e+38
156	03h09m49.08s	-20h36m03.71s	225.48 \pm 1.73	0.561e-3 \pm 0.067e-3	465.000	1.06e+38
157	03h09m48.88s	-20h33m59.15s	224.74 \pm 1.80	0.559e-3 \pm 0.067e-3	484.000	1.05e+38
158	03h09m46.86s	-20h35m28.96s	223.49 \pm 1.54	0.556e-3 \pm 0.067e-3	350.000	1.05e+38
159	03h09m48.05s	-20h35m49.93s	222.90 \pm 1.93	0.554e-3 \pm 0.067e-3	501.000	1.05e+38
160	03h09m49.68s	-20h34m23.56s	222.12 \pm 1.48	0.552e-3 \pm 0.066e-3	329.000	1.04e+38
161	03h09m42.34s	-20h36m04.76s	220.69 \pm 1.75	0.549e-3 \pm 0.066e-3	440.000	1.04e+38
162	03h09m40.67s	-20h35m28.91s	220.47 \pm 1.80	0.548e-3 \pm 0.066e-3	462.000	1.03e+38
163	03h09m40.10s	-20h35m14.68s	219.15 \pm 1.91	0.545e-3 \pm 0.066e-3	538.000	1.03e+38
164	03h09m42.54s	-20h33m23.52s	217.60 \pm 1.60	0.541e-3 \pm 0.065e-3	384.000	1.02e+38
165	03h09m41.12s	-20h33m55.28s	216.86 \pm 1.81	0.539e-3 \pm 0.065e-3	473.000	1.02e+38
166	03h09m50.57s	-20h34m28.90s	216.83 \pm 1.77	0.539e-3 \pm 0.065e-3	445.000	1.02e+38
167	03h09m43.87s	-20h33m16.07s	216.62 \pm 1.98	0.539e-3 \pm 0.065e-3	578.000	1.02e+38
168	03h09m47.72s	-20h33m49.55s	214.26 \pm 1.79	0.533e-3 \pm 0.064e-3	466.000	1.01e+38
169	03h09m48.45s	-20h35m14.74s	210.46 \pm 1.53	0.523e-3 \pm 0.063e-3	346.000	9.87e+37
170	03h09m44.63s	-20h34m05.73s	209.05 \pm 1.78	0.520e-3 \pm 0.063e-3	478.000	9.81e+37
171	03h09m51.49s	-20h35m30.13s	207.74 \pm 1.56	0.517e-3 \pm 0.062e-3	372.000	9.75e+37
172	03h09m47.11s	-20h34m02.49s	207.56 \pm 1.95	0.516e-3 \pm 0.062e-3	531.000	9.74e+37
173	03h09m46.46s	-20h35m45.60s	206.72 \pm 1.49	0.514e-3 \pm 0.062e-3	333.000	9.70e+37
174	03h09m42.11s	-20h36m03.67s	203.51 \pm 1.56	0.506e-3 \pm 0.061e-3	366.000	9.55e+37
175	03h09m42.99s	-20h35m03.44s	203.09 \pm 1.72	0.505e-3 \pm 0.061e-3	436.000	9.53e+37
176	03h09m47.40s	-20h33m17.77s	202.41 \pm 1.88	0.503e-3 \pm 0.061e-3	499.000	9.50e+37
177	03h09m49.09s	-20h34m42.72s	200.41 \pm 1.60	0.498e-3 \pm 0.060e-3	377.000	9.40e+37
178	03h09m43.45s	-20h34m22.43s	199.60 \pm 1.59	0.496e-3 \pm 0.060e-3	373.000	9.36e+37
179	03h09m49.39s	-20h33m19.64s	199.58 \pm 1.86	0.496e-3 \pm 0.060e-3	500.000	9.36e+37

Table 2 continued on next page

Table 2 (continued)

Source	Position (RA)	Position (Dec)	F(H α) (10^{-17} erg/cm 2 /s)	SFR (M_{\odot} /yr)	Area (pixel 2)	L(H α) (erg s $^{-1}$)
180	03h09m46.91s	-20h33m59.93s	190.55 \pm 1.83	0.474e-3 \pm 0.057e-3	467.000	8.94e+37
181	03h09m45.77s	-20h35m14.70s	189.28 \pm 1.75	0.471e-3 \pm 0.057e-3	450.000	8.88e+37
182	03h09m49.31s	-20h33m58.22s	189.12 \pm 1.87	0.470e-3 \pm 0.057e-3	499.000	8.87e+37
183	03h09m44.50s	-20h33m09.84s	187.72 \pm 2.06	0.467e-3 \pm 0.056e-3	579.000	8.81e+37
184	03h09m44.76s	-20h34m05.53s	183.46 \pm 1.54	0.456e-3 \pm 0.055e-3	355.000	8.61e+37
185	03h09m42.89s	-20h34m59.93s	182.73 \pm 1.88	0.454e-3 \pm 0.055e-3	481.000	8.57e+37
186	03h09m49.75s	-20h34m27.37s	182.03 \pm 1.35	0.453e-3 \pm 0.054e-3	240.000	8.54e+37
187	03h09m49.83s	-20h35m56.95s	181.65 \pm 1.55	0.452e-3 \pm 0.054e-3	309.000	8.52e+37
188	03h09m47.27s	-20h35m19.95s	178.00 \pm 1.78	0.443e-3 \pm 0.053e-3	442.000	8.35e+37
189	03h09m47.25s	-20h33m47.42s	177.72 \pm 1.64	0.442e-3 \pm 0.053e-3	354.000	8.34e+37
190	03h09m46.77s	-20h33m38.79s	177.63 \pm 1.80	0.442e-3 \pm 0.053e-3	464.000	8.33e+37
191	03h09m49.21s	-20h35m51.95s	177.07 \pm 1.40	0.440e-3 \pm 0.053e-3	285.000	8.31e+37
192	03h09m46.72s	-20h35m37.98s	175.46 \pm 1.53	0.436e-3 \pm 0.052e-3	348.000	8.23e+37
193	03h09m47.96s	-20h35m16.22s	174.95 \pm 1.75	0.435e-3 \pm 0.052e-3	406.000	8.21e+37
194	03h09m49.98s	-20h34m17.79s	172.31 \pm 1.58	0.428e-3 \pm 0.052e-3	366.000	8.08e+37
195	03h09m46.47s	-20h34m19.77s	171.50 \pm 1.58	0.426e-3 \pm 0.051e-3	321.000	8.05e+37
196	03h09m48.03s	-20h36m00.83s	170.32 \pm 1.57	0.423e-3 \pm 0.051e-3	339.000	7.99e+37
197	03h09m41.46s	-20h33m54.70s	167.03 \pm 1.36	0.415e-3 \pm 0.050e-3	284.000	7.84e+37
198	03h09m42.92s	-20h33m07.95s	163.77 \pm 1.28	0.407e-3 \pm 0.049e-3	243.000	7.68e+37
199	03h09m43.69s	-20h34m43.78s	163.28 \pm 1.47	0.406e-3 \pm 0.049e-3	311.000	7.66e+37
200	03h09m43.16s	-20h35m14.17s	162.85 \pm 1.47	0.405e-3 \pm 0.049e-3	310.000	7.64e+37
201	03h09m47.62s	-20h34m06.71s	161.97 \pm 1.37	0.403e-3 \pm 0.048e-3	279.000	7.60e+37
202	03h09m41.52s	-20h34m50.69s	160.91 \pm 1.71	0.400e-3 \pm 0.048e-3	424.000	7.55e+37
203	03h09m48.82s	-20h35m45.22s	160.57 \pm 1.76	0.399e-3 \pm 0.048e-3	441.000	7.53e+37
204	03h09m47.19s	-20h33m46.83s	159.17 \pm 1.57	0.396e-3 \pm 0.048e-3	368.000	7.47e+37
205	03h09m41.77s	-20h33m28.58s	157.99 \pm 1.27	0.393e-3 \pm 0.047e-3	238.000	7.41e+37
206	03h09m41.72s	-20h36m05.92s	157.88 \pm 2.06	0.393e-3 \pm 0.047e-3	575.000	7.41e+37
207	03h09m45.32s	-20h34m42.31s	156.87 \pm 1.63	0.390e-3 \pm 0.047e-3	386.000	7.36e+37
208	03h09m46.08s	-20h35m47.55s	156.80 \pm 1.25	0.390e-3 \pm 0.047e-3	245.000	7.36e+37
209	03h09m40.81s	-20h34m35.21s	155.26 \pm 1.63	0.386e-3 \pm 0.047e-3	407.000	7.28e+37
210	03h09m46.50s	-20h35m21.80s	154.69 \pm 1.67	0.385e-3 \pm 0.046e-3	393.000	7.26e+37
211	03h09m48.24s	-20h35m41.07s	154.15 \pm 1.40	0.383e-3 \pm 0.046e-3	291.000	7.23e+37
212	03h09m46.57s	-20h33m34.42s	153.43 \pm 1.50	0.382e-3 \pm 0.046e-3	339.000	7.20e+37
213	03h09m40.68s	-20h33m25.05s	151.69 \pm 1.99	0.377e-3 \pm 0.046e-3	491.000	7.12e+37
214	03h09m43.67s	-20h35m43.95s	151.12 \pm 1.46	0.376e-3 \pm 0.045e-3	314.000	7.09e+37
215	03h09m47.59s	-20h34m19.97s	150.95 \pm 1.57	0.375e-3 \pm 0.045e-3	354.000	7.08e+37
216	03h09m45.06s	-20h33m12.21s	150.37 \pm 1.62	0.374e-3 \pm 0.045e-3	379.000	7.05e+37

Table 2 continued on next page

Table 2 (*continued*)

Source	Position (RA)	Position (Dec)	F(H α) (10^{-17} erg/cm 2 /s)	SFR (M_{\odot} /yr)	Area (pixel 2)	L(H α) (erg s $^{-1}$)
217	03h09m43.00s	-20h35m16.80s	149.06 \pm 1.39	0.371e-3 \pm 0.045e-3	298.000	6.99e+37
218	03h09m49.15s	-20h33m25.94s	148.96 \pm 1.43	0.370e-3 \pm 0.045e-3	312.000	6.99e+37
219	03h09m45.59s	-20h33m57.08s	148.11 \pm 1.40	0.368e-3 \pm 0.044e-3	296.000	6.95e+37
220	03h09m45.17s	-20h34m05.53s	146.26 \pm 1.64	0.364e-3 \pm 0.044e-3	378.000	6.86e+37
221	03h09m44.14s	-20h34m36.66s	145.95 \pm 1.45	0.363e-3 \pm 0.044e-3	298.000	6.85e+37
222	03h09m42.18s	-20h34m09.96s	145.17 \pm 1.65	0.361e-3 \pm 0.044e-3	356.000	6.81e+37
223	03h09m48.82s	-20h33m32.53s	143.03 \pm 1.32	0.356e-3 \pm 0.043e-3	260.000	6.71e+37
224	03h09m45.51s	-20h33m56.95s	141.90 \pm 1.38	0.353e-3 \pm 0.042e-3	294.000	6.66e+37
225	03h09m49.09s	-20h33m42.88s	140.33 \pm 1.09	0.349e-3 \pm 0.042e-3	193.000	6.58e+37
226	03h09m40.40s	-20h34m39.81s	139.24 \pm 1.33	0.346e-3 \pm 0.042e-3	266.000	6.53e+37
227	03h09m50.37s	-20h34m23.98s	138.40 \pm 1.74	0.344e-3 \pm 0.042e-3	426.000	6.49e+37
228	03h09m40.72s	-20h35m23.38s	136.35 \pm 1.56	0.339e-3 \pm 0.041e-3	361.000	6.40e+37
229	03h09m50.19s	-20h34m28.51s	135.47 \pm 1.20	0.337e-3 \pm 0.041e-3	232.000	6.36e+37
230	03h09m47.61s	-20h35m40.93s	132.43 \pm 1.47	0.329e-3 \pm 0.040e-3	318.000	6.21e+37
231	03h09m41.42s	-20h35m53.58s	130.06 \pm 1.54	0.323e-3 \pm 0.039e-3	360.000	6.10e+37
232	03h09m45.56s	-20h34m38.64s	129.60 \pm 1.66	0.322e-3 \pm 0.039e-3	387.000	6.08e+37
233	03h09m48.70s	-20h35m11.26s	128.48 \pm 1.55	0.319e-3 \pm 0.039e-3	338.000	6.03e+37
234	03h09m45.87s	-20h33m57.16s	128.14 \pm 1.46	0.319e-3 \pm 0.038e-3	312.000	6.01e+37
235	03h09m48.61s	-20h34m55.42s	127.53 \pm 1.32	0.317e-3 \pm 0.038e-3	223.000	5.98e+37
236	03h09m42.15s	-20h33m44.54s	127.20 \pm 1.21	0.316e-3 \pm 0.038e-3	194.000	5.97e+37
237	03h09m44.09s	-20h34m37.19s	127.16 \pm 1.33	0.316e-3 \pm 0.038e-3	256.000	5.97e+37
238	03h09m45.28s	-20h34m05.86s	126.90 \pm 1.42	0.316e-3 \pm 0.038e-3	297.000	5.95e+37
239	03h09m40.09s	-20h34m48.02s	126.28 \pm 1.52	0.314e-3 \pm 0.038e-3	331.000	5.92e+37
240	03h09m52.41s	-20h34m54.56s	123.32 \pm 1.47	0.307e-3 \pm 0.037e-3	318.000	5.79e+37
241	03h09m43.56s	-20h34m23.21s	122.95 \pm 1.58	0.306e-3 \pm 0.037e-3	346.000	5.77e+37
242	03h09m47.53s	-20h34m23.68s	122.58 \pm 1.36	0.305e-3 \pm 0.037e-3	259.000	5.75e+37
243	03h09m46.13s	-20h33m58.36s	122.27 \pm 1.26	0.304e-3 \pm 0.037e-3	236.000	5.74e+37
244	03h09m40.09s	-20h35m56.86s	122.24 \pm 0.95	0.304e-3 \pm 0.037e-3	138.000	5.74e+37
245	03h09m47.01s	-20h33m33.55s	121.05 \pm 1.62	0.301e-3 \pm 0.036e-3	354.000	5.68e+37
246	03h09m50.25s	-20h34m30.00s	120.71 \pm 1.37	0.300e-3 \pm 0.036e-3	281.000	5.66e+37
247	03h09m43.34s	-20h35m10.91s	120.60 \pm 1.28	0.300e-3 \pm 0.036e-3	236.000	5.66e+37
248	03h09m51.77s	-20h34m50.36s	119.70 \pm 1.50	0.298e-3 \pm 0.036e-3	327.000	5.62e+37
249	03h09m45.09s	-20h34m56.91s	119.19 \pm 1.44	0.296e-3 \pm 0.036e-3	295.000	5.59e+37
250	03h09m48.31s	-20h34m39.18s	119.11 \pm 1.29	0.296e-3 \pm 0.036e-3	245.000	5.59e+37
251	03h09m44.99s	-20h33m54.09s	119.00 \pm 1.39	0.296e-3 \pm 0.036e-3	279.000	5.58e+37
252	03h09m49.60s	-20h35m35.20s	118.17 \pm 1.04	0.294e-3 \pm 0.035e-3	173.000	5.54e+37
253	03h09m45.65s	-20h35m32.50s	115.95 \pm 1.31	0.288e-3 \pm 0.035e-3	247.000	5.44e+37

Table 2 continued on next page

Table 2 (*continued*)

Source	Position (RA)	Position (Dec)	F(H α) (10^{-17} erg/cm 2 /s)	SFR (M_{\odot} /yr)	Area (pixel 2)	L(H α) (erg s $^{-1}$)
254	03h09m46.14s	-20h33m23.05s	115.24 \pm 1.66	0.287e-3 \pm 0.035e-3	367.000	5.41e+37
255	03h09m42.56s	-20h35m16.83s	115.23 \pm 1.24	0.287e-3 \pm 0.035e-3	228.000	5.41e+37
256	03h09m44.92s	-20h33m10.85s	114.05 \pm 1.64	0.284e-3 \pm 0.034e-3	308.000	5.35e+37
257	03h09m49.07s	-20h36m02.37s	112.77 \pm 1.35	0.280e-3 \pm 0.034e-3	276.000	5.29e+37
258	03h09m50.09s	-20h34m18.67s	112.53 \pm 1.57	0.280e-3 \pm 0.034e-3	322.000	5.28e+37
259	03h09m48.95s	-20h34m32.20s	112.37 \pm 1.63	0.279e-3 \pm 0.034e-3	359.000	5.27e+37
260	03h09m52.42s	-20h33m54.74s	111.92 \pm 1.58	0.278e-3 \pm 0.034e-3	295.000	5.25e+37
261	03h09m43.84s	-20h34m58.35s	111.48 \pm 1.36	0.277e-3 \pm 0.033e-3	269.000	5.23e+37
262	03h09m45.92s	-20h33m29.85s	111.24 \pm 1.52	0.277e-3 \pm 0.033e-3	330.000	5.22e+37
263	03h09m45.67s	-20h33m54.52s	110.41 \pm 1.21	0.275e-3 \pm 0.033e-3	214.000	5.18e+37
264	03h09m47.58s	-20h35m40.05s	109.16 \pm 1.32	0.271e-3 \pm 0.033e-3	255.000	5.12e+37
265	03h09m43.54s	-20h35m19.17s	108.99 \pm 1.23	0.271e-3 \pm 0.033e-3	221.000	5.11e+37
266	03h09m46.04s	-20h35m50.92s	107.86 \pm 1.52	0.268e-3 \pm 0.032e-3	339.000	5.06e+37
267	03h09m44.25s	-20h34m29.35s	107.79 \pm 1.34	0.268e-3 \pm 0.032e-3	253.000	5.06e+37
268	03h09m40.73s	-20h33m09.45s	107.77 \pm 1.40	0.268e-3 \pm 0.032e-3	274.000	5.06e+37
269	03h09m44.67s	-20h35m19.53s	106.73 \pm 1.27	0.265e-3 \pm 0.032e-3	232.000	5.01e+37
270	03h09m45.68s	-20h35m13.71s	106.47 \pm 1.41	0.265e-3 \pm 0.032e-3	279.000	5.00e+37
271	03h09m48.26s	-20h35m13.89s	105.98 \pm 1.21	0.264e-3 \pm 0.032e-3	210.000	4.97e+37
272	03h09m43.76s	-20h34m37.22s	105.08 \pm 1.30	0.261e-3 \pm 0.032e-3	251.000	4.93e+37
273	03h09m44.33s	-20h34m08.37s	104.45 \pm 1.32	0.260e-3 \pm 0.031e-3	263.000	4.90e+37
274	03h09m51.11s	-20h34m08.32s	104.44 \pm 1.44	0.260e-3 \pm 0.031e-3	292.000	4.90e+37
275	03h09m47.32s	-20h33m37.76s	104.40 \pm 1.20	0.260e-3 \pm 0.031e-3	207.000	4.90e+37
276	03h09m49.99s	-20h34m53.60s	104.27 \pm 1.22	0.259e-3 \pm 0.031e-3	227.000	4.89e+37
277	03h09m50.15s	-20h35m46.30s	104.23 \pm 1.28	0.259e-3 \pm 0.031e-3	227.000	4.89e+37
278	03h09m43.16s	-20h35m25.92s	103.72 \pm 1.29	0.258e-3 \pm 0.031e-3	247.000	4.87e+37
279	03h09m47.67s	-20h33m51.31s	102.84 \pm 1.19	0.256e-3 \pm 0.031e-3	212.000	4.83e+37
280	03h09m45.55s	-20h35m14.77s	101.26 \pm 1.62	0.252e-3 \pm 0.030e-3	359.000	4.75e+37
281	03h09m48.58s	-20h34m02.95s	100.90 \pm 1.52	0.251e-3 \pm 0.030e-3	321.000	4.73e+37
282	03h09m51.12s	-20h35m31.41s	99.49 \pm 1.29	0.247e-3 \pm 0.030e-3	222.000	4.67e+37
283	03h09m43.17s	-20h33m08.70s	99.32 \pm 1.15	0.247e-3 \pm 0.030e-3	197.000	4.66e+37
284	03h09m40.30s	-20h33m27.29s	98.52 \pm 1.33	0.245e-3 \pm 0.030e-3	266.000	4.62e+37
285	03h09m41.54s	-20h36m00.52s	98.03 \pm 1.32	0.244e-3 \pm 0.029e-3	252.000	4.60e+37
286	03h09m45.79s	-20h35m48.93s	97.50 \pm 1.31	0.242e-3 \pm 0.029e-3	248.000	4.57e+37
287	03h09m45.08s	-20h35m54.26s	96.77 \pm 1.24	0.241e-3 \pm 0.029e-3	217.000	4.54e+37
288	03h09m44.38s	-20h36m10.31s	96.73 \pm 1.15	0.241e-3 \pm 0.029e-3	202.000	4.54e+37
289	03h09m43.22s	-20h34m60.00s	96.56 \pm 1.47	0.240e-3 \pm 0.029e-3	295.000	4.53e+37
290	03h09m50.79s	-20h33m07.99s	96.39 \pm 1.13	0.240e-3 \pm 0.029e-3	122.000	4.52e+37

Table 2 continued on next page

Table 2 (*continued*)

Source	Position (RA)	Position (Dec)	F(H α) (10^{-17} erg/cm 2 /s)	SFR (M_{\odot} /yr)	Area (pixel 2)	L(H α) (erg s $^{-1}$)
291	03h09m40.07s	-20h34m19.61s	95.61 \pm 1.03	0.238e-3 \pm 0.029e-3	156.000	4.49e+37
292	03h09m41.22s	-20h34m59.36s	95.60 \pm 1.27	0.238e-3 \pm 0.029e-3	220.000	4.49e+37
293	03h09m47.36s	-20h33m36.67s	95.20 \pm 1.43	0.237e-3 \pm 0.029e-3	290.000	4.47e+37
294	03h09m48.62s	-20h35m12.27s	94.32 \pm 1.15	0.235e-3 \pm 0.028e-3	205.000	4.43e+37
295	03h09m44.44s	-20h35m45.36s	94.22 \pm 1.41	0.234e-3 \pm 0.028e-3	265.000	4.42e+37
296	03h09m46.65s	-20h35m38.13s	94.11 \pm 1.17	0.234e-3 \pm 0.028e-3	209.000	4.42e+37
297	03h09m48.18s	-20h35m16.03s	93.85 \pm 1.14	0.233e-3 \pm 0.028e-3	189.000	4.40e+37
298	03h09m51.88s	-20h34m50.44s	93.71 \pm 1.35	0.233e-3 \pm 0.028e-3	221.000	4.40e+37
299	03h09m42.06s	-20h34m11.51s	93.48 \pm 1.09	0.232e-3 \pm 0.028e-3	162.000	4.39e+37
300	03h09m48.58s	-20h35m40.95s	93.00 \pm 1.27	0.231e-3 \pm 0.028e-3	247.000	4.36e+37
301	03h09m45.73s	-20h36m04.61s	92.60 \pm 0.88	0.230e-3 \pm 0.028e-3	114.000	4.34e+37
302	03h09m42.83s	-20h35m26.31s	91.35 \pm 1.17	0.227e-3 \pm 0.027e-3	201.000	4.29e+37
303	03h09m42.85s	-20h34m56.05s	91.15 \pm 1.14	0.227e-3 \pm 0.027e-3	180.000	4.28e+37
304	03h09m43.70s	-20h34m38.54s	91.08 \pm 1.23	0.226e-3 \pm 0.027e-3	225.000	4.27e+37
305	03h09m40.11s	-20h33m20.21s	90.81 \pm 1.40	0.226e-3 \pm 0.027e-3	268.000	4.26e+37
306	03h09m47.16s	-20h33m45.17s	90.45 \pm 1.46	0.225e-3 \pm 0.027e-3	281.000	4.24e+37
307	03h09m52.41s	-20h34m51.26s	89.11 \pm 1.46	0.222e-3 \pm 0.027e-3	311.000	4.18e+37
308	03h09m46.62s	-20h34m19.90s	89.00 \pm 1.35	0.221e-3 \pm 0.027e-3	258.000	4.18e+37
309	03h09m40.12s	-20h34m47.51s	87.71 \pm 1.18	0.218e-3 \pm 0.026e-3	204.000	4.12e+37
310	03h09m46.22s	-20h33m40.57s	87.01 \pm 1.22	0.216e-3 \pm 0.026e-3	209.000	4.08e+37
311	03h09m46.85s	-20h36m08.14s	86.74 \pm 1.38	0.216e-3 \pm 0.026e-3	206.000	4.07e+37
312	03h09m45.82s	-20h35m32.49s	85.78 \pm 1.33	0.213e-3 \pm 0.026e-3	212.000	4.02e+37
313	03h09m47.84s	-20h35m03.17s	85.76 \pm 1.25	0.213e-3 \pm 0.026e-3	208.000	4.02e+37
314	03h09m48.66s	-20h33m31.58s	85.68 \pm 1.40	0.213e-3 \pm 0.026e-3	255.000	4.02e+37
315	03h09m48.08s	-20h34m58.19s	85.56 \pm 1.32	0.213e-3 \pm 0.026e-3	242.000	4.01e+37
316	03h09m49.11s	-20h33m25.13s	85.44 \pm 1.10	0.212e-3 \pm 0.026e-3	186.000	4.01e+37
317	03h09m43.10s	-20h35m05.06s	85.10 \pm 1.10	0.212e-3 \pm 0.026e-3	174.000	3.99e+37
318	03h09m43.73s	-20h35m11.74s	85.00 \pm 1.28	0.211e-3 \pm 0.026e-3	240.000	3.99e+37
319	03h09m43.88s	-20h34m30.02s	84.63 \pm 1.17	0.210e-3 \pm 0.025e-3	200.000	3.97e+37
320	03h09m51.18s	-20h35m53.48s	84.58 \pm 1.32	0.210e-3 \pm 0.025e-3	258.000	3.97e+37
321	03h09m44.03s	-20h34m10.46s	84.03 \pm 1.28	0.209e-3 \pm 0.025e-3	234.000	3.94e+37
322	03h09m46.03s	-20h33m40.12s	83.75 \pm 1.39	0.208e-3 \pm 0.025e-3	259.000	3.93e+37
323	03h09m44.47s	-20h34m36.92s	83.72 \pm 1.11	0.208e-3 \pm 0.025e-3	180.000	3.93e+37
324	03h09m40.19s	-20h34m10.78s	83.70 \pm 1.19	0.208e-3 \pm 0.025e-3	210.000	3.93e+37
325	03h09m49.15s	-20h33m20.82s	83.33 \pm 1.14	0.207e-3 \pm 0.025e-3	190.000	3.91e+37
326	03h09m48.45s	-20h34m47.88s	83.31 \pm 1.21	0.207e-3 \pm 0.025e-3	205.000	3.91e+37
327	03h09m50.62s	-20h35m41.94s	82.81 \pm 1.40	0.206e-3 \pm 0.025e-3	280.000	3.89e+37

Table 2 continued on next page

Table 2 (*continued*)

Source	Position (RA)	Position (Dec)	F(H α) (10^{-17} erg/cm 2 /s)	SFR (M_{\odot} /yr)	Area (pixel 2)	L(H α) (erg s $^{-1}$)
328	03h09m51.76s	-20h34m48.89s	81.88 \pm 1.28	0.204e-3 \pm 0.025e-3	232.000	3.84e+37
329	03h09m46.39s	-20h35m37.05s	81.70 \pm 1.34	0.203e-3 \pm 0.025e-3	253.000	3.83e+37
330	03h09m46.35s	-20h34m19.55s	81.58 \pm 1.19	0.203e-3 \pm 0.025e-3	212.000	3.83e+37
331	03h09m45.70s	-20h33m41.53s	81.44 \pm 1.44	0.203e-3 \pm 0.025e-3	210.000	3.82e+37
332	03h09m41.83s	-20h33m31.91s	81.24 \pm 1.35	0.202e-3 \pm 0.024e-3	256.000	3.81e+37
333	03h09m46.46s	-20h33m33.61s	80.11 \pm 1.40	0.199e-3 \pm 0.024e-3	272.000	3.76e+37
334	03h09m45.59s	-20h35m12.39s	79.70 \pm 1.20	0.198e-3 \pm 0.024e-3	219.000	3.74e+37
335	03h09m51.25s	-20h33m08.09s	79.08 \pm 1.07	0.197e-3 \pm 0.024e-3	69.0000	3.71e+37
336	03h09m43.15s	-20h33m35.06s	78.77 \pm 1.04	0.196e-3 \pm 0.024e-3	156.000	3.70e+37
337	03h09m47.42s	-20h34m02.43s	78.75 \pm 1.49	0.196e-3 \pm 0.024e-3	211.000	3.69e+37
338	03h09m40.77s	-20h33m08.00s	78.07 \pm 0.76	0.194e-3 \pm 0.023e-3	73.0000	3.66e+37
339	03h09m48.65s	-20h35m41.32s	77.32 \pm 1.24	0.192e-3 \pm 0.023e-3	191.000	3.63e+37
340	03h09m44.38s	-20h34m11.45s	77.23 \pm 1.18	0.192e-3 \pm 0.023e-3	218.000	3.62e+37
341	03h09m49.22s	-20h34m48.00s	76.70 \pm 1.36	0.191e-3 \pm 0.023e-3	193.000	3.60e+37
342	03h09m47.72s	-20h35m18.14s	76.15 \pm 1.14	0.189e-3 \pm 0.023e-3	195.000	3.57e+37
343	03h09m41.55s	-20h35m57.33s	75.61 \pm 1.40	0.188e-3 \pm 0.023e-3	267.000	3.55e+37
344	03h09m41.67s	-20h34m24.07s	74.99 \pm 1.27	0.186e-3 \pm 0.023e-3	230.000	3.52e+37
345	03h09m48.50s	-20h35m06.06s	74.78 \pm 1.20	0.186e-3 \pm 0.023e-3	174.000	3.51e+37
346	03h09m48.98s	-20h35m54.36s	74.37 \pm 1.14	0.185e-3 \pm 0.022e-3	182.000	3.49e+37
347	03h09m46.80s	-20h35m21.75s	74.10 \pm 1.09	0.184e-3 \pm 0.022e-3	164.000	3.48e+37
348	03h09m44.41s	-20h34m29.71s	73.92 \pm 1.11	0.184e-3 \pm 0.022e-3	183.000	3.47e+37
349	03h09m49.33s	-20h35m51.64s	73.64 \pm 1.23	0.183e-3 \pm 0.022e-3	213.000	3.45e+37
350	03h09m47.31s	-20h35m06.50s	73.63 \pm 1.06	0.183e-3 \pm 0.022e-3	160.000	3.45e+37
351	03h09m43.94s	-20h33m14.80s	73.25 \pm 1.12	0.182e-3 \pm 0.022e-3	187.000	3.44e+37
352	03h09m47.78s	-20h34m15.48s	73.10 \pm 0.96	0.182e-3 \pm 0.022e-3	138.000	3.43e+37
353	03h09m49.80s	-20h34m49.16s	73.07 \pm 1.07	0.182e-3 \pm 0.022e-3	164.000	3.43e+37
354	03h09m44.93s	-20h33m40.10s	72.92 \pm 1.19	0.181e-3 \pm 0.022e-3	188.000	3.42e+37
355	03h09m48.03s	-20h34m59.36s	72.90 \pm 1.30	0.181e-3 \pm 0.022e-3	203.000	3.42e+37
356	03h09m48.23s	-20h35m45.11s	71.74 \pm 1.39	0.178e-3 \pm 0.022e-3	218.000	3.37e+37
357	03h09m51.74s	-20h35m27.06s	71.60 \pm 0.83	0.178e-3 \pm 0.021e-3	106.000	3.36e+37
358	03h09m40.11s	-20h34m41.37s	70.68 \pm 1.27	0.176e-3 \pm 0.021e-3	219.000	3.32e+37
359	03h09m42.36s	-20h33m40.50s	69.81 \pm 1.11	0.174e-3 \pm 0.021e-3	174.000	3.28e+37
360	03h09m42.79s	-20h33m11.30s	69.52 \pm 0.95	0.173e-3 \pm 0.021e-3	132.000	3.26e+37
361	03h09m50.15s	-20h33m45.98s	69.22 \pm 0.84	0.172e-3 \pm 0.021e-3	100.000	3.25e+37
362	03h09m47.64s	-20h35m41.98s	69.01 \pm 1.22	0.172e-3 \pm 0.021e-3	210.000	3.24e+37
363	03h09m47.73s	-20h34m25.65s	68.75 \pm 1.20	0.171e-3 \pm 0.021e-3	205.000	3.23e+37
364	03h09m40.36s	-20h33m28.35s	68.08 \pm 1.24	0.169e-3 \pm 0.021e-3	213.000	3.19e+37

Table 2 continued on next page

Table 2 (*continued*)

Source	Position (RA)	Position (Dec)	F(H α) (10^{-17} erg/cm 2 /s)	SFR (M_{\odot} /yr)	Area (pixel 2)	L(H α) (erg s $^{-1}$)
365	03h09m46.03s	-20h33m22.35s	68.07 \pm 1.23	0.169e-3 \pm 0.021e-3	205.000	3.19e+37
366	03h09m45.77s	-20h34m11.81s	67.66 \pm 1.01	0.168e-3 \pm 0.020e-3	149.000	3.17e+37
367	03h09m44.93s	-20h34m52.74s	66.61 \pm 1.01	0.166e-3 \pm 0.020e-3	148.000	3.13e+37
368	03h09m47.45s	-20h34m04.59s	66.56 \pm 1.21	0.165e-3 \pm 0.020e-3	197.000	3.12e+37
369	03h09m43.43s	-20h35m04.92s	66.27 \pm 1.16	0.165e-3 \pm 0.020e-3	184.000	3.11e+37
370	03h09m49.38s	-20h35m56.22s	66.09 \pm 1.04	0.164e-3 \pm 0.020e-3	157.000	3.10e+37
371	03h09m50.95s	-20h34m40.76s	66.09 \pm 1.01	0.164e-3 \pm 0.020e-3	148.000	3.10e+37
372	03h09m47.34s	-20h34m19.70s	65.96 \pm 1.21	0.164e-3 \pm 0.020e-3	200.000	3.09e+37
373	03h09m46.79s	-20h35m38.48s	65.79 \pm 1.07	0.164e-3 \pm 0.020e-3	164.000	3.09e+37
374	03h09m49.29s	-20h35m22.33s	65.78 \pm 1.23	0.164e-3 \pm 0.020e-3	209.000	3.09e+37
375	03h09m48.11s	-20h35m01.44s	65.56 \pm 1.06	0.163e-3 \pm 0.020e-3	166.000	3.08e+37
376	03h09m45.32s	-20h33m08.93s	65.34 \pm 1.07	0.162e-3 \pm 0.020e-3	163.000	3.07e+37
377	03h09m48.45s	-20h35m20.33s	65.10 \pm 1.03	0.162e-3 \pm 0.020e-3	156.000	3.05e+37
378	03h09m44.94s	-20h33m53.82s	64.94 \pm 1.10	0.161e-3 \pm 0.020e-3	154.000	3.05e+37
379	03h09m46.47s	-20h35m22.97s	64.87 \pm 1.18	0.161e-3 \pm 0.020e-3	188.000	3.04e+37
380	03h09m52.37s	-20h33m12.23s	64.86 \pm 1.08	0.161e-3 \pm 0.020e-3	173.000	3.04e+37
381	03h09m48.41s	-20h34m00.24s	64.82 \pm 1.09	0.161e-3 \pm 0.020e-3	171.000	3.04e+37
382	03h09m49.49s	-20h34m40.08s	64.81 \pm 0.95	0.161e-3 \pm 0.019e-3	135.000	3.04e+37
383	03h09m41.28s	-20h34m59.21s	64.39 \pm 1.03	0.160e-3 \pm 0.019e-3	155.000	3.02e+37
384	03h09m42.24s	-20h35m46.66s	64.36 \pm 1.17	0.160e-3 \pm 0.019e-3	194.000	3.02e+37
385	03h09m44.49s	-20h35m32.10s	64.09 \pm 1.04	0.159e-3 \pm 0.019e-3	157.000	3.01e+37
386	03h09m48.32s	-20h33m10.19s	63.78 \pm 1.07	0.159e-3 \pm 0.019e-3	172.000	2.99e+37
387	03h09m48.77s	-20h36m02.15s	63.26 \pm 1.07	0.157e-3 \pm 0.019e-3	166.000	2.97e+37
388	03h09m44.99s	-20h34m05.72s	63.20 \pm 1.17	0.157e-3 \pm 0.019e-3	190.000	2.96e+37
389	03h09m46.26s	-20h36m06.84s	63.03 \pm 1.11	0.157e-3 \pm 0.019e-3	178.000	2.96e+37
390	03h09m42.98s	-20h35m11.57s	62.82 \pm 1.01	0.156e-3 \pm 0.019e-3	145.000	2.95e+37
391	03h09m40.28s	-20h34m42.33s	62.80 \pm 1.34	0.156e-3 \pm 0.019e-3	221.000	2.95e+37
392	03h09m50.92s	-20h35m20.03s	62.42 \pm 1.15	0.155e-3 \pm 0.019e-3	197.000	2.93e+37
393	03h09m47.34s	-20h35m21.08s	62.41 \pm 1.10	0.155e-3 \pm 0.019e-3	174.000	2.93e+37
394	03h09m44.41s	-20h34m25.04s	62.28 \pm 1.04	0.155e-3 \pm 0.019e-3	133.000	2.92e+37
395	03h09m41.19s	-20h33m57.09s	62.22 \pm 1.21	0.155e-3 \pm 0.019e-3	193.000	2.92e+37
396	03h09m39.77s	-20h35m51.69s	62.19 \pm 0.90	0.155e-3 \pm 0.019e-3	124.000	2.92e+37
397	03h09m43.76s	-20h34m59.91s	62.17 \pm 1.11	0.155e-3 \pm 0.019e-3	184.000	2.92e+37
398	03h09m49.49s	-20h34m53.86s	61.98 \pm 1.10	0.154e-3 \pm 0.019e-3	173.000	2.91e+37
399	03h09m48.33s	-20h33m10.90s	61.35 \pm 1.01	0.153e-3 \pm 0.018e-3	159.000	2.88e+37
400	03h09m43.10s	-20h35m15.06s	60.94 \pm 1.11	0.152e-3 \pm 0.018e-3	183.000	2.86e+37
401	03h09m49.22s	-20h34m36.82s	60.84 \pm 1.28	0.151e-3 \pm 0.018e-3	194.000	2.85e+37

Table 2 continued on next page

Table 2 (*continued*)

Source	Position (RA)	Position (Dec)	F(H α) (10^{-17} erg/cm 2 /s)	SFR (M_{\odot} /yr)	Area (pixel 2)	L(H α) (erg s $^{-1}$)
402	03h09m48.00s	-20h34m31.46s	60.54 \pm 1.04	0.151e-3 \pm 0.018e-3	154.000	2.84e+37
403	03h09m41.93s	-20h36m06.75s	60.41 \pm 0.88	0.150e-3 \pm 0.018e-3	121.000	2.83e+37
404	03h09m41.71s	-20h33m18.06s	60.19 \pm 1.22	0.150e-3 \pm 0.018e-3	205.000	2.82e+37
405	03h09m44.41s	-20h33m53.07s	60.09 \pm 1.20	0.149e-3 \pm 0.018e-3	192.000	2.82e+37
406	03h09m46.11s	-20h35m16.19s	59.94 \pm 0.94	0.149e-3 \pm 0.018e-3	124.000	2.81e+37
407	03h09m40.18s	-20h33m21.98s	59.56 \pm 1.20	0.148e-3 \pm 0.018e-3	188.000	2.79e+37
408	03h09m47.67s	-20h35m21.29s	59.49 \pm 0.97	0.148e-3 \pm 0.018e-3	135.000	2.79e+37
409	03h09m48.47s	-20h35m32.62s	59.25 \pm 1.20	0.147e-3 \pm 0.018e-3	149.000	2.78e+37
410	03h09m45.77s	-20h35m08.39s	58.93 \pm 1.05	0.147e-3 \pm 0.018e-3	161.000	2.76e+37
411	03h09m49.88s	-20h34m45.06s	58.89 \pm 1.24	0.146e-3 \pm 0.018e-3	175.000	2.76e+37
412	03h09m48.59s	-20h35m11.30s	58.74 \pm 0.94	0.146e-3 \pm 0.018e-3	132.000	2.76e+37
413	03h09m48.56s	-20h35m31.95s	58.36 \pm 1.05	0.145e-3 \pm 0.018e-3	163.000	2.74e+37
414	03h09m46.97s	-20h33m57.22s	58.32 \pm 0.99	0.145e-3 \pm 0.018e-3	145.000	2.74e+37
415	03h09m43.14s	-20h35m13.61s	57.87 \pm 0.76	0.144e-3 \pm 0.017e-3	90.0000	2.72e+37
416	03h09m40.68s	-20h33m53.91s	57.36 \pm 1.21	0.143e-3 \pm 0.017e-3	202.000	2.69e+37
417	03h09m43.54s	-20h35m20.03s	56.96 \pm 0.95	0.142e-3 \pm 0.017e-3	139.000	2.67e+37
418	03h09m51.16s	-20h35m33.99s	56.77 \pm 1.01	0.141e-3 \pm 0.017e-3	141.000	2.66e+37
419	03h09m47.88s	-20h34m17.16s	56.69 \pm 1.12	0.141e-3 \pm 0.017e-3	171.000	2.66e+37
420	03h09m47.01s	-20h34m01.03s	56.07 \pm 1.17	0.139e-3 \pm 0.017e-3	190.000	2.63e+37
421	03h09m50.72s	-20h35m28.02s	55.73 \pm 0.94	0.139e-3 \pm 0.017e-3	134.000	2.61e+37
422	03h09m47.16s	-20h35m51.47s	55.44 \pm 1.27	0.138e-3 \pm 0.017e-3	133.000	2.60e+37
423	03h09m44.31s	-20h36m08.29s	55.06 \pm 0.92	0.137e-3 \pm 0.017e-3	124.000	2.58e+37
424	03h09m49.30s	-20h35m39.29s	54.78 \pm 0.97	0.136e-3 \pm 0.017e-3	138.000	2.57e+37
425	03h09m44.67s	-20h34m25.51s	54.61 \pm 0.93	0.136e-3 \pm 0.016e-3	118.000	2.56e+37
426	03h09m50.10s	-20h33m31.91s	54.26 \pm 1.12	0.135e-3 \pm 0.016e-3	176.000	2.55e+37
427	03h09m48.17s	-20h35m41.56s	53.69 \pm 0.98	0.134e-3 \pm 0.016e-3	140.000	2.52e+37
428	03h09m48.23s	-20h34m34.38s	53.34 \pm 1.22	0.133e-3 \pm 0.016e-3	113.000	2.50e+37
429	03h09m49.01s	-20h34m50.99s	53.14 \pm 1.13	0.132e-3 \pm 0.016e-3	148.000	2.49e+37
430	03h09m42.14s	-20h34m18.91s	52.94 \pm 1.00	0.132e-3 \pm 0.016e-3	143.000	2.48e+37
431	03h09m42.28s	-20h35m16.50s	52.57 \pm 1.18	0.131e-3 \pm 0.016e-3	182.000	2.47e+37
432	03h09m51.08s	-20h34m36.92s	52.45 \pm 1.09	0.130e-3 \pm 0.016e-3	162.000	2.46e+37
433	03h09m46.59s	-20h35m53.53s	52.32 \pm 1.12	0.130e-3 \pm 0.016e-3	171.000	2.45e+37
434	03h09m51.21s	-20h34m46.43s	52.15 \pm 1.09	0.130e-3 \pm 0.016e-3	151.000	2.45e+37
435	03h09m49.57s	-20h34m53.34s	51.88 \pm 1.06	0.129e-3 \pm 0.016e-3	154.000	2.43e+37
436	03h09m44.12s	-20h35m32.34s	51.87 \pm 1.07	0.129e-3 \pm 0.016e-3	157.000	2.43e+37
437	03h09m50.54s	-20h34m30.35s	51.73 \pm 1.03	0.129e-3 \pm 0.016e-3	150.000	2.43e+37
438	03h09m45.49s	-20h34m32.15s	51.32 \pm 0.84	0.128e-3 \pm 0.015e-3	100.000	2.41e+37

Table 2 continued on next page

Table 2 (*continued*)

Source	Position (RA)	Position (Dec)	F(H α) (10^{-17} erg/cm 2 /s)	SFR (M_{\odot} /yr)	Area (pixel 2)	L(H α) (erg s $^{-1}$)
439	03h09m39.79s	-20h35m08.35s	51.30 \pm 0.91	0.128e-3 \pm 0.015e-3	117.000	2.41e+37
440	03h09m46.52s	-20h33m11.81s	51.10 \pm 0.70	0.127e-3 \pm 0.015e-3	67.0000	2.40e+37
441	03h09m49.09s	-20h35m18.94s	50.53 \pm 1.11	0.126e-3 \pm 0.015e-3	178.000	2.37e+37
442	03h09m52.29s	-20h35m49.17s	50.50 \pm 0.95	0.126e-3 \pm 0.015e-3	133.000	2.37e+37
443	03h09m45.97s	-20h33m23.65s	50.28 \pm 1.10	0.125e-3 \pm 0.015e-3	157.000	2.36e+37
444	03h09m50.89s	-20h35m58.79s	49.86 \pm 0.90	0.124e-3 \pm 0.015e-3	117.000	2.34e+37
445	03h09m43.62s	-20h35m45.30s	49.74 \pm 1.02	0.124e-3 \pm 0.015e-3	150.000	2.33e+37
446	03h09m44.86s	-20h33m08.02s	49.62 \pm 0.88	0.123e-3 \pm 0.015e-3	116.000	2.33e+37
447	03h09m52.43s	-20h34m46.79s	49.39 \pm 1.12	0.123e-3 \pm 0.015e-3	190.000	2.32e+37
448	03h09m50.25s	-20h34m24.33s	49.25 \pm 1.03	0.122e-3 \pm 0.015e-3	151.000	2.31e+37
449	03h09m49.74s	-20h35m59.36s	49.10 \pm 1.03	0.122e-3 \pm 0.015e-3	152.000	2.30e+37
450	03h09m39.86s	-20h35m08.83s	48.89 \pm 0.96	0.122e-3 \pm 0.015e-3	139.000	2.29e+37
451	03h09m44.16s	-20h33m49.42s	48.74 \pm 1.07	0.121e-3 \pm 0.015e-3	161.000	2.29e+37
452	03h09m49.91s	-20h35m42.95s	48.68 \pm 1.00	0.121e-3 \pm 0.015e-3	139.000	2.28e+37
453	03h09m42.43s	-20h33m47.62s	48.66 \pm 0.94	0.121e-3 \pm 0.015e-3	125.000	2.28e+37
454	03h09m52.25s	-20h33m08.32s	48.42 \pm 0.80	0.120e-3 \pm 0.015e-3	59.0000	2.27e+37
455	03h09m49.18s	-20h35m17.22s	48.24 \pm 1.13	0.120e-3 \pm 0.015e-3	168.000	2.26e+37
456	03h09m47.59s	-20h33m47.97s	48.15 \pm 1.07	0.120e-3 \pm 0.015e-3	155.000	2.26e+37
457	03h09m49.21s	-20h34m49.86s	47.23 \pm 1.02	0.117e-3 \pm 0.014e-3	144.000	2.22e+37
458	03h09m46.26s	-20h35m50.40s	46.55 \pm 0.97	0.116e-3 \pm 0.014e-3	132.000	2.18e+37
459	03h09m43.49s	-20h34m43.72s	46.28 \pm 1.02	0.115e-3 \pm 0.014e-3	144.000	2.17e+37
460	03h09m51.27s	-20h34m45.92s	45.85 \pm 1.00	0.114e-3 \pm 0.014e-3	137.000	2.15e+37
461	03h09m40.27s	-20h33m08.11s	45.81 \pm 0.62	0.114e-3 \pm 0.014e-3	46.0000	2.15e+37
462	03h09m52.13s	-20h35m20.00s	45.13 \pm 1.02	0.112e-3 \pm 0.014e-3	142.000	2.12e+37
463	03h09m39.74s	-20h35m00.48s	44.98 \pm 0.89	0.112e-3 \pm 0.014e-3	115.000	2.11e+37
464	03h09m43.15s	-20h35m26.66s	44.97 \pm 0.93	0.112e-3 \pm 0.014e-3	125.000	2.11e+37
465	03h09m42.81s	-20h35m35.77s	44.70 \pm 0.93	0.111e-3 \pm 0.014e-3	124.000	2.10e+37
466	03h09m45.87s	-20h33m43.38s	44.45 \pm 0.96	0.111e-3 \pm 0.013e-3	132.000	2.09e+37
467	03h09m47.33s	-20h33m48.85s	44.38 \pm 1.00	0.110e-3 \pm 0.013e-3	138.000	2.08e+37
468	03h09m50.62s	-20h34m13.30s	44.37 \pm 0.91	0.110e-3 \pm 0.013e-3	124.000	2.08e+37
469	03h09m48.43s	-20h34m41.20s	44.17 \pm 0.91	0.110e-3 \pm 0.013e-3	114.000	2.07e+37
470	03h09m43.07s	-20h34m56.57s	44.02 \pm 1.04	0.109e-3 \pm 0.013e-3	146.000	2.07e+37
471	03h09m40.26s	-20h33m20.01s	44.01 \pm 1.16	0.109e-3 \pm 0.013e-3	167.000	2.06e+37
472	03h09m42.86s	-20h35m18.47s	43.73 \pm 0.95	0.109e-3 \pm 0.013e-3	129.000	2.05e+37
473	03h09m45.28s	-20h35m26.09s	43.66 \pm 1.01	0.109e-3 \pm 0.013e-3	126.000	2.05e+37
474	03h09m46.10s	-20h35m19.21s	43.64 \pm 0.98	0.109e-3 \pm 0.013e-3	119.000	2.05e+37
475	03h09m42.55s	-20h35m09.78s	43.20 \pm 0.97	0.107e-3 \pm 0.013e-3	104.000	2.03e+37

Table 2 continued on next page

Table 2 (*continued*)

Source	Position (RA)	Position (Dec)	F(H α) (10^{-17} erg/cm 2 /s)	SFR (M_{\odot} /yr)	Area (pixel 2)	L(H α) (erg s $^{-1}$)
476	03h09m43.34s	-20h35m22.07s	42.82 \pm 1.00	0.106e-3 \pm 0.013e-3	142.000	2.01e+37
477	03h09m49.41s	-20h35m23.24s	42.76 \pm 1.06	0.106e-3 \pm 0.013e-3	145.000	2.01e+37
478	03h09m45.44s	-20h35m34.89s	42.72 \pm 1.07	0.106e-3 \pm 0.013e-3	150.000	2.00e+37
479	03h09m47.00s	-20h35m20.69s	42.69 \pm 1.00	0.106e-3 \pm 0.013e-3	140.000	2.00e+37
480	03h09m50.83s	-20h35m56.33s	42.64 \pm 1.04	0.106e-3 \pm 0.013e-3	144.000	2.00e+37
481	03h09m42.63s	-20h34m59.14s	42.48 \pm 1.11	0.106e-3 \pm 0.013e-3	93.0000	1.99e+37
482	03h09m46.42s	-20h35m18.10s	42.12 \pm 0.98	0.105e-3 \pm 0.013e-3	130.000	1.98e+37
483	03h09m46.23s	-20h34m19.28s	41.92 \pm 0.94	0.104e-3 \pm 0.013e-3	124.000	1.97e+37
484	03h09m47.59s	-20h35m18.63s	41.73 \pm 0.90	0.104e-3 \pm 0.013e-3	114.000	1.96e+37
485	03h09m50.06s	-20h35m31.81s	41.56 \pm 0.94	0.103e-3 \pm 0.013e-3	123.000	1.95e+37
486	03h09m47.26s	-20h34m21.26s	41.53 \pm 1.01	0.103e-3 \pm 0.013e-3	133.000	1.95e+37
487	03h09m41.39s	-20h34m25.07s	41.26 \pm 0.91	0.103e-3 \pm 0.013e-3	117.000	1.94e+37
488	03h09m47.12s	-20h33m34.47s	41.10 \pm 0.97	0.102e-3 \pm 0.012e-3	121.000	1.93e+37
489	03h09m46.77s	-20h35m48.20s	41.04 \pm 0.98	0.102e-3 \pm 0.012e-3	124.000	1.93e+37
490	03h09m43.86s	-20h34m46.50s	41.03 \pm 0.87	0.102e-3 \pm 0.012e-3	102.000	1.92e+37
491	03h09m48.34s	-20h34m00.90s	40.91 \pm 0.88	0.102e-3 \pm 0.012e-3	118.000	1.92e+37
492	03h09m39.78s	-20h35m00.64s	40.59 \pm 0.98	0.101e-3 \pm 0.012e-3	139.000	1.90e+37
493	03h09m46.89s	-20h34m17.67s	40.53 \pm 1.07	0.101e-3 \pm 0.012e-3	141.000	1.90e+37
494	03h09m44.58s	-20h35m35.60s	40.22 \pm 0.91	0.100e-3 \pm 0.012e-3	125.000	1.89e+37
495	03h09m42.75s	-20h35m32.91s	40.21 \pm 1.09	0.100e-3 \pm 0.012e-3	133.000	1.89e+37
496	03h09m46.87s	-20h34m01.35s	40.06 \pm 0.89	0.100e-3 \pm 0.012e-3	102.000	1.88e+37
497	03h09m50.54s	-20h34m32.27s	39.98 \pm 1.05	0.099e-3 \pm 0.012e-3	143.000	1.88e+37
498	03h09m49.85s	-20h34m22.27s	39.89 \pm 0.88	0.099e-3 \pm 0.012e-3	111.000	1.87e+37
499	03h09m42.72s	-20h33m07.86s	39.36 \pm 0.86	0.098e-3 \pm 0.012e-3	101.000	1.85e+37
500	03h09m43.04s	-20h35m24.91s	38.91 \pm 0.83	0.097e-3 \pm 0.012e-3	102.000	1.83e+37
501	03h09m43.44s	-20h35m01.97s	38.84 \pm 0.92	0.097e-3 \pm 0.012e-3	97.0000	1.82e+37
502	03h09m47.42s	-20h34m19.59s	38.63 \pm 0.90	0.096e-3 \pm 0.012e-3	116.000	1.81e+37
503	03h09m48.13s	-20h34m06.51s	38.47 \pm 0.96	0.096e-3 \pm 0.012e-3	126.000	1.80e+37
504	03h09m49.61s	-20h35m48.14s	38.34 \pm 0.81	0.095e-3 \pm 0.012e-3	98.0000	1.80e+37
505	03h09m45.36s	-20h34m35.35s	38.13 \pm 0.82	0.095e-3 \pm 0.012e-3	97.0000	1.79e+37
506	03h09m44.38s	-20h35m31.19s	38.09 \pm 0.83	0.095e-3 \pm 0.012e-3	101.000	1.79e+37
507	03h09m46.82s	-20h33m33.80s	38.00 \pm 1.03	0.094e-3 \pm 0.012e-3	129.000	1.78e+37
508	03h09m52.44s	-20h33m11.72s	37.90 \pm 0.94	0.094e-3 \pm 0.012e-3	127.000	1.78e+37
509	03h09m43.22s	-20h34m02.21s	37.30 \pm 0.94	0.093e-3 \pm 0.011e-3	122.000	1.75e+37
510	03h09m50.79s	-20h35m38.85s	37.19 \pm 1.04	0.092e-3 \pm 0.011e-3	98.0000	1.74e+37
511	03h09m42.49s	-20h35m16.63s	36.85 \pm 0.95	0.092e-3 \pm 0.011e-3	121.000	1.73e+37
512	03h09m49.02s	-20h34m48.18s	36.73 \pm 0.78	0.091e-3 \pm 0.011e-3	91.0000	1.72e+37

Table 2 continued on next page

Table 2 (*continued*)

Source	Position (RA)	Position (Dec)	F(H α) (10^{-17} erg/cm 2 /s)	SFR (M_{\odot} /yr)	Area (pixel 2)	L(H α) (erg s $^{-1}$)
513	03h09m47.00s	-20h35m19.94s	36.71 \pm 0.89	0.091e-3 \pm 0.011e-3	109.000	1.72e+37
514	03h09m50.84s	-20h35m57.99s	36.65 \pm 0.90	0.091e-3 \pm 0.011e-3	117.000	1.72e+37
515	03h09m48.07s	-20h34m47.82s	36.59 \pm 0.88	0.091e-3 \pm 0.011e-3	104.000	1.72e+37
516	03h09m52.00s	-20h33m08.26s	36.50 \pm 0.64	0.091e-3 \pm 0.011e-3	41.0000	1.71e+37
517	03h09m44.15s	-20h35m20.78s	36.22 \pm 0.90	0.090e-3 \pm 0.011e-3	116.000	1.70e+37
518	03h09m40.81s	-20h35m30.08s	36.12 \pm 0.89	0.090e-3 \pm 0.011e-3	115.000	1.69e+37
519	03h09m48.00s	-20h34m47.70s	36.06 \pm 0.87	0.090e-3 \pm 0.011e-3	99.0000	1.69e+37
520	03h09m47.34s	-20h33m35.26s	35.57 \pm 0.98	0.088e-3 \pm 0.011e-3	127.000	1.67e+37
521	03h09m47.29s	-20h35m51.57s	35.52 \pm 0.96	0.088e-3 \pm 0.011e-3	126.000	1.67e+37
522	03h09m49.87s	-20h33m42.93s	35.49 \pm 0.83	0.088e-3 \pm 0.011e-3	88.0000	1.67e+37
523	03h09m45.57s	-20h34m36.54s	35.19 \pm 0.93	0.087e-3 \pm 0.011e-3	107.000	1.65e+37
524	03h09m40.75s	-20h35m40.76s	34.25 \pm 0.89	0.085e-3 \pm 0.010e-3	117.000	1.61e+37
525	03h09m47.53s	-20h33m46.39s	34.13 \pm 0.93	0.085e-3 \pm 0.010e-3	114.000	1.60e+37
526	03h09m48.37s	-20h34m42.64s	34.08 \pm 0.94	0.085e-3 \pm 0.010e-3	69.0000	1.60e+37
527	03h09m47.28s	-20h35m37.65s	34.01 \pm 0.95	0.085e-3 \pm 0.010e-3	115.000	1.60e+37
528	03h09m48.03s	-20h34m28.40s	33.99 \pm 0.89	0.085e-3 \pm 0.010e-3	108.000	1.59e+37
529	03h09m42.59s	-20h34m29.27s	33.87 \pm 0.79	0.084e-3 \pm 0.010e-3	92.0000	1.59e+37
530	03h09m42.28s	-20h33m41.48s	33.64 \pm 0.84	0.084e-3 \pm 0.010e-3	106.000	1.58e+37
531	03h09m49.09s	-20h34m44.53s	33.42 \pm 0.91	0.083e-3 \pm 0.010e-3	70.0000	1.57e+37
532	03h09m45.17s	-20h33m56.76s	33.27 \pm 0.83	0.083e-3 \pm 0.010e-3	92.0000	1.56e+37
533	03h09m49.85s	-20h35m10.74s	33.22 \pm 0.90	0.083e-3 \pm 0.010e-3	113.000	1.56e+37
534	03h09m45.17s	-20h33m11.20s	33.10 \pm 0.85	0.082e-3 \pm 0.010e-3	102.000	1.55e+37
535	03h09m44.82s	-20h35m27.24s	32.92 \pm 0.76	0.082e-3 \pm 0.010e-3	85.0000	1.54e+37
536	03h09m41.75s	-20h33m08.48s	32.66 \pm 0.77	0.081e-3 \pm 0.010e-3	15.0000	1.53e+37
537	03h09m40.93s	-20h33m53.31s	32.65 \pm 0.83	0.081e-3 \pm 0.010e-3	101.000	1.53e+37
538	03h09m45.02s	-20h35m13.08s	32.53 \pm 0.87	0.081e-3 \pm 0.010e-3	104.000	1.53e+37
539	03h09m42.10s	-20h35m47.64s	32.46 \pm 0.84	0.081e-3 \pm 0.010e-3	101.000	1.52e+37
540	03h09m46.54s	-20h33m54.98s	32.38 \pm 0.89	0.081e-3 \pm 0.010e-3	86.0000	1.52e+37
541	03h09m46.81s	-20h35m23.34s	32.22 \pm 0.86	0.080e-3 \pm 0.010e-3	102.000	1.51e+37
542	03h09m43.99s	-20h35m34.33s	31.97 \pm 0.94	0.079e-3 \pm 0.010e-3	114.000	1.50e+37
543	03h09m48.65s	-20h35m54.08s	31.73 \pm 0.87	0.079e-3 \pm 0.010e-3	101.000	1.49e+37
544	03h09m44.06s	-20h34m43.89s	31.35 \pm 0.86	0.078e-3 \pm 0.010e-3	93.0000	1.47e+37
545	03h09m41.18s	-20h33m07.92s	31.29 \pm 0.55	0.078e-3 \pm 0.009e-3	48.0000	1.47e+37
546	03h09m48.72s	-20h34m48.01s	31.20 \pm 0.73	0.078e-3 \pm 0.009e-3	76.0000	1.46e+37
547	03h09m45.95s	-20h35m50.77s	31.06 \pm 0.77	0.077e-3 \pm 0.009e-3	89.0000	1.46e+37
548	03h09m47.10s	-20h33m56.24s	31.04 \pm 0.76	0.077e-3 \pm 0.009e-3	84.0000	1.46e+37
549	03h09m51.60s	-20h33m09.01s	30.75 \pm 0.87	0.076e-3 \pm 0.009e-3	91.0000	1.44e+37

Table 2 continued on next page

Table 2 (*continued*)

Source	Position (RA)	Position (Dec)	F(H α) (10^{-17} erg/cm 2 /s)	SFR (M_{\odot} /yr)	Area (pixel 2)	L(H α) (erg s $^{-1}$)
550	03h09m48.63s	-20h35m32.32s	30.61 \pm 0.81	0.076e-3 \pm 0.009e-3	95.0000	1.44e+37
551	03h09m45.56s	-20h34m08.62s	30.54 \pm 0.78	0.076e-3 \pm 0.009e-3	85.0000	1.43e+37
552	03h09m45.74s	-20h36m10.48s	30.52 \pm 0.68	0.076e-3 \pm 0.009e-3	23.0000	1.43e+37
553	03h09m44.08s	-20h35m20.07s	30.48 \pm 0.81	0.076e-3 \pm 0.009e-3	95.0000	1.43e+37
554	03h09m48.00s	-20h34m43.21s	30.45 \pm 0.81	0.076e-3 \pm 0.009e-3	92.0000	1.43e+37
555	03h09m39.97s	-20h35m09.20s	30.43 \pm 0.92	0.076e-3 \pm 0.009e-3	105.0000	1.43e+37
556	03h09m50.49s	-20h35m41.28s	30.43 \pm 0.80	0.076e-3 \pm 0.009e-3	93.0000	1.43e+37
557	03h09m44.42s	-20h35m23.36s	30.32 \pm 0.90	0.075e-3 \pm 0.009e-3	103.0000	1.42e+37
558	03h09m40.19s	-20h34m04.27s	30.29 \pm 0.70	0.075e-3 \pm 0.009e-3	71.0000	1.42e+37
559	03h09m43.37s	-20h35m33.25s	30.08 \pm 0.93	0.075e-3 \pm 0.009e-3	114.0000	1.41e+37
560	03h09m47.76s	-20h33m25.16s	30.01 \pm 0.78	0.075e-3 \pm 0.009e-3	88.0000	1.41e+37
561	03h09m41.52s	-20h35m58.42s	29.99 \pm 0.88	0.075e-3 \pm 0.009e-3	106.0000	1.41e+37
562	03h09m50.57s	-20h35m13.74s	29.92 \pm 0.77	0.074e-3 \pm 0.009e-3	88.0000	1.40e+37
563	03h09m48.02s	-20h34m32.72s	29.90 \pm 0.86	0.074e-3 \pm 0.009e-3	91.0000	1.40e+37
564	03h09m44.30s	-20h36m10.36s	29.56 \pm 0.65	0.074e-3 \pm 0.009e-3	66.0000	1.39e+37
565	03h09m47.11s	-20h33m42.01s	29.31 \pm 0.89	0.073e-3 \pm 0.009e-3	105.0000	1.38e+37
566	03h09m47.21s	-20h33m21.65s	28.58 \pm 0.81	0.071e-3 \pm 0.009e-3	87.0000	1.34e+37
567	03h09m49.43s	-20h35m49.15s	28.33 \pm 0.85	0.070e-3 \pm 0.009e-3	95.0000	1.33e+37
568	03h09m48.43s	-20h35m03.86s	27.94 \pm 0.78	0.069e-3 \pm 0.009e-3	83.0000	1.31e+37
569	03h09m44.25s	-20h34m22.54s	27.94 \pm 0.80	0.069e-3 \pm 0.009e-3	88.0000	1.31e+37
570	03h09m49.51s	-20h35m23.66s	27.90 \pm 0.78	0.069e-3 \pm 0.009e-3	85.0000	1.31e+37
571	03h09m51.20s	-20h35m16.16s	27.82 \pm 0.86	0.069e-3 \pm 0.009e-3	99.0000	1.31e+37
572	03h09m48.26s	-20h35m10.51s	27.75 \pm 0.70	0.069e-3 \pm 0.008e-3	71.0000	1.30e+37
573	03h09m48.47s	-20h34m50.31s	27.64 \pm 0.82	0.069e-3 \pm 0.008e-3	96.0000	1.30e+37
574	03h09m43.08s	-20h35m16.54s	27.56 \pm 0.72	0.069e-3 \pm 0.008e-3	77.0000	1.29e+37
575	03h09m48.44s	-20h35m13.67s	27.55 \pm 0.69	0.068e-3 \pm 0.008e-3	72.0000	1.29e+37
576	03h09m47.61s	-20h34m11.63s	27.50 \pm 0.88	0.068e-3 \pm 0.008e-3	101.0000	1.29e+37
577	03h09m46.80s	-20h34m17.03s	27.50 \pm 0.82	0.068e-3 \pm 0.008e-3	96.0000	1.29e+37
578	03h09m51.20s	-20h34m12.38s	27.31 \pm 0.82	0.068e-3 \pm 0.008e-3	90.0000	1.28e+37
579	03h09m46.95s	-20h33m58.13s	27.13 \pm 0.76	0.067e-3 \pm 0.008e-3	83.0000	1.27e+37
580	03h09m42.13s	-20h33m08.60s	26.97 \pm 0.81	0.067e-3 \pm 0.008e-3	95.0000	1.27e+37
581	03h09m47.64s	-20h34m21.06s	26.93 \pm 0.82	0.067e-3 \pm 0.008e-3	90.0000	1.26e+37
582	03h09m49.12s	-20h33m14.92s	26.81 \pm 0.78	0.067e-3 \pm 0.008e-3	85.0000	1.26e+37
583	03h09m40.18s	-20h33m27.07s	26.73 \pm 0.83	0.066e-3 \pm 0.008e-3	97.0000	1.25e+37
584	03h09m49.21s	-20h35m18.70s	26.62 \pm 0.81	0.066e-3 \pm 0.008e-3	90.0000	1.25e+37
585	03h09m47.42s	-20h35m04.93s	26.61 \pm 0.75	0.066e-3 \pm 0.008e-3	76.0000	1.25e+37
586	03h09m49.02s	-20h35m09.41s	26.54 \pm 0.74	0.066e-3 \pm 0.008e-3	75.0000	1.25e+37

Table 2 continued on next page

Table 2 (*continued*)

Source	Position (RA)	Position (Dec)	F(H α) (10^{-17} erg/cm 2 /s)	SFR (M_{\odot} /yr)	Area (pixel 2)	L(H α) (erg s $^{-1}$)
587	03h09m45.74s	-20h35m00.87s	26.49 \pm 0.80	0.066e-3 \pm 0.008e-3	73.0000	1.24e+37
588	03h09m49.04s	-20h35m16.11s	26.40 \pm 0.74	0.066e-3 \pm 0.008e-3	78.0000	1.24e+37
589	03h09m42.63s	-20h33m07.78s	26.33 \pm 0.70	0.065e-3 \pm 0.008e-3	67.0000	1.24e+37
590	03h09m39.86s	-20h35m21.81s	26.28 \pm 0.73	0.065e-3 \pm 0.008e-3	76.0000	1.23e+37
591	03h09m46.47s	-20h33m49.42s	26.24 \pm 0.72	0.065e-3 \pm 0.008e-3	72.0000	1.23e+37
592	03h09m49.51s	-20h33m18.38s	26.10 \pm 0.81	0.065e-3 \pm 0.008e-3	84.0000	1.22e+37
593	03h09m47.33s	-20h33m41.70s	26.08 \pm 0.82	0.065e-3 \pm 0.008e-3	75.0000	1.22e+37
594	03h09m44.87s	-20h35m23.99s	26.00 \pm 0.85	0.065e-3 \pm 0.008e-3	90.0000	1.22e+37
595	03h09m44.99s	-20h33m29.44s	25.82 \pm 0.76	0.064e-3 \pm 0.008e-3	76.0000	1.21e+37
596	03h09m47.69s	-20h34m09.51s	25.32 \pm 0.85	0.063e-3 \pm 0.008e-3	70.0000	1.19e+37
597	03h09m48.36s	-20h34m10.56s	25.22 \pm 0.80	0.063e-3 \pm 0.008e-3	77.0000	1.18e+37
598	03h09m52.41s	-20h33m13.17s	24.87 \pm 0.80	0.062e-3 \pm 0.008e-3	81.0000	1.17e+37
599	03h09m44.05s	-20h34m34.96s	24.66 \pm 0.80	0.061e-3 \pm 0.008e-3	86.0000	1.16e+37
600	03h09m44.25s	-20h34m32.99s	24.22 \pm 0.83	0.060e-3 \pm 0.008e-3	87.0000	1.14e+37
601	03h09m44.00s	-20h33m13.87s	24.10 \pm 0.80	0.060e-3 \pm 0.007e-3	82.0000	1.13e+37
602	03h09m51.04s	-20h35m04.65s	24.07 \pm 0.76	0.060e-3 \pm 0.007e-3	79.0000	1.13e+37
603	03h09m47.23s	-20h33m57.94s	24.02 \pm 0.80	0.060e-3 \pm 0.007e-3	84.0000	1.13e+37
604	03h09m51.64s	-20h33m08.17s	23.97 \pm 0.54	0.060e-3 \pm 0.007e-3	28.0000	1.12e+37
605	03h09m50.55s	-20h35m39.82s	23.62 \pm 0.84	0.059e-3 \pm 0.007e-3	63.0000	1.11e+37
606	03h09m42.51s	-20h34m07.88s	23.55 \pm 0.73	0.059e-3 \pm 0.007e-3	75.0000	1.10e+37
607	03h09m39.98s	-20h34m17.81s	23.30 \pm 0.65	0.058e-3 \pm 0.007e-3	64.0000	1.09e+37
608	03h09m44.76s	-20h34m41.94s	23.23 \pm 0.76	0.058e-3 \pm 0.007e-3	86.0000	1.09e+37
609	03h09m43.57s	-20h33m56.73s	23.16 \pm 0.81	0.058e-3 \pm 0.007e-3	84.0000	1.09e+37
610	03h09m51.05s	-20h35m36.30s	23.08 \pm 0.81	0.057e-3 \pm 0.007e-3	63.0000	1.08e+37
611	03h09m44.27s	-20h35m29.81s	23.06 \pm 0.76	0.057e-3 \pm 0.007e-3	83.0000	1.08e+37
612	03h09m47.28s	-20h35m52.22s	23.02 \pm 0.72	0.057e-3 \pm 0.007e-3	73.0000	1.08e+37
613	03h09m47.05s	-20h33m42.06s	23.01 \pm 0.80	0.057e-3 \pm 0.007e-3	82.0000	1.08e+37
614	03h09m43.33s	-20h35m24.89s	22.98 \pm 0.77	0.057e-3 \pm 0.007e-3	84.0000	1.08e+37
615	03h09m45.42s	-20h34m18.35s	22.96 \pm 0.70	0.057e-3 \pm 0.007e-3	70.0000	1.08e+37
616	03h09m48.81s	-20h34m46.41s	22.88 \pm 0.73	0.057e-3 \pm 0.007e-3	73.0000	1.07e+37
617	03h09m44.95s	-20h35m15.88s	22.81 \pm 0.75	0.057e-3 \pm 0.007e-3	78.0000	1.07e+37
618	03h09m43.37s	-20h35m03.25s	22.77 \pm 0.82	0.057e-3 \pm 0.007e-3	83.0000	1.07e+37
619	03h09m51.81s	-20h34m45.97s	22.63 \pm 0.81	0.056e-3 \pm 0.007e-3	56.0000	1.06e+37
620	03h09m43.91s	-20h34m41.55s	22.46 \pm 0.68	0.056e-3 \pm 0.007e-3	66.0000	1.05e+37
621	03h09m44.62s	-20h35m44.63s	22.33 \pm 0.75	0.056e-3 \pm 0.007e-3	79.0000	1.05e+37
622	03h09m50.40s	-20h34m27.19s	22.10 \pm 0.80	0.055e-3 \pm 0.007e-3	80.0000	1.04e+37
623	03h09m51.79s	-20h33m08.21s	21.91 \pm 0.57	0.054e-3 \pm 0.007e-3	25.0000	1.03e+37

Table 2 continued on next page

Table 2 (*continued*)

Source	Position (RA)	Position (Dec)	F(H α) (10^{-17} erg/cm 2 /s)	SFR (M_{\odot} /yr)	Area (pixel 2)	L(H α) (erg s $^{-1}$)
624	03h09m50.60s	-20h35m14.27s	21.86 \pm 0.69	0.054e-3 \pm 0.007e-3	64.0000	1.03e+37
625	03h09m46.02s	-20h34m16.34s	21.86 \pm 0.81	0.054e-3 \pm 0.007e-3	63.0000	1.03e+37
626	03h09m46.68s	-20h35m21.64s	21.85 \pm 0.78	0.054e-3 \pm 0.007e-3	79.0000	1.02e+37
627	03h09m46.78s	-20h33m29.14s	21.79 \pm 0.71	0.054e-3 \pm 0.007e-3	71.0000	1.02e+37
628	03h09m47.98s	-20h34m20.28s	21.63 \pm 0.76	0.054e-3 \pm 0.007e-3	58.0000	1.01e+37
629	03h09m43.64s	-20h34m46.32s	21.55 \pm 0.66	0.054e-3 \pm 0.007e-3	65.0000	1.01e+37
630	03h09m48.73s	-20h34m55.30s	21.46 \pm 0.71	0.053e-3 \pm 0.007e-3	68.0000	1.01e+37
631	03h09m40.02s	-20h35m36.93s	21.33 \pm 0.73	0.053e-3 \pm 0.007e-3	70.0000	1.00e+37
632	03h09m39.75s	-20h34m36.73s	21.29 \pm 0.62	0.053e-3 \pm 0.007e-3	60.0000	9.99e+36
633	03h09m44.08s	-20h33m49.41s	21.27 \pm 0.71	0.053e-3 \pm 0.007e-3	74.0000	9.98e+36
634	03h09m45.71s	-20h35m46.53s	21.26 \pm 0.73	0.053e-3 \pm 0.007e-3	74.0000	9.97e+36
635	03h09m44.78s	-20h34m17.64s	21.21 \pm 0.68	0.053e-3 \pm 0.007e-3	60.0000	9.95e+36
636	03h09m46.38s	-20h35m02.15s	21.02 \pm 0.73	0.052e-3 \pm 0.007e-3	71.0000	9.86e+36
637	03h09m41.51s	-20h36m02.62s	20.94 \pm 0.75	0.052e-3 \pm 0.007e-3	75.0000	9.82e+36
638	03h09m50.43s	-20h35m33.79s	20.92 \pm 0.68	0.052e-3 \pm 0.006e-3	66.0000	9.82e+36
639	03h09m40.09s	-20h33m22.24s	20.78 \pm 0.78	0.052e-3 \pm 0.006e-3	75.0000	9.75e+36
640	03h09m40.90s	-20h33m55.09s	20.68 \pm 0.77	0.051e-3 \pm 0.006e-3	75.0000	9.70e+36
641	03h09m49.05s	-20h35m54.19s	20.65 \pm 0.73	0.051e-3 \pm 0.006e-3	68.0000	9.69e+36
642	03h09m49.73s	-20h34m58.93s	20.60 \pm 0.67	0.051e-3 \pm 0.006e-3	65.0000	9.67e+36
643	03h09m49.58s	-20h34m58.40s	20.53 \pm 0.68	0.051e-3 \pm 0.006e-3	68.0000	9.63e+36
644	03h09m46.80s	-20h35m26.75s	20.43 \pm 0.74	0.051e-3 \pm 0.006e-3	70.0000	9.59e+36
645	03h09m48.62s	-20h34m04.14s	20.41 \pm 0.75	0.051e-3 \pm 0.006e-3	75.0000	9.58e+36
646	03h09m46.18s	-20h34m30.41s	20.39 \pm 0.70	0.051e-3 \pm 0.006e-3	70.0000	9.57e+36
647	03h09m50.94s	-20h35m28.69s	20.38 \pm 0.73	0.051e-3 \pm 0.006e-3	70.0000	9.56e+36
648	03h09m46.96s	-20h35m05.03s	20.29 \pm 0.72	0.050e-3 \pm 0.006e-3	72.0000	9.52e+36
649	03h09m43.37s	-20h33m39.88s	19.99 \pm 0.73	0.050e-3 \pm 0.006e-3	73.0000	9.38e+36
650	03h09m50.14s	-20h34m47.09s	19.98 \pm 0.71	0.050e-3 \pm 0.006e-3	68.0000	9.37e+36
651	03h09m42.38s	-20h33m17.24s	19.76 \pm 0.72	0.049e-3 \pm 0.006e-3	70.0000	9.27e+36
652	03h09m46.34s	-20h35m01.49s	19.71 \pm 0.66	0.049e-3 \pm 0.006e-3	58.0000	9.25e+36
653	03h09m48.27s	-20h34m37.32s	19.70 \pm 0.73	0.049e-3 \pm 0.006e-3	68.0000	9.24e+36
654	03h09m43.67s	-20h36m07.33s	19.65 \pm 0.73	0.049e-3 \pm 0.006e-3	70.0000	9.22e+36
655	03h09m45.44s	-20h33m25.46s	19.61 \pm 0.73	0.049e-3 \pm 0.006e-3	72.0000	9.20e+36
656	03h09m51.03s	-20h35m21.78s	19.49 \pm 0.74	0.048e-3 \pm 0.006e-3	69.0000	9.14e+36
657	03h09m48.02s	-20h35m22.78s	19.27 \pm 0.65	0.048e-3 \pm 0.006e-3	59.0000	9.04e+36
658	03h09m51.90s	-20h33m46.47s	19.21 \pm 0.56	0.048e-3 \pm 0.006e-3	46.0000	9.01e+36
659	03h09m49.13s	-20h34m39.78s	19.19 \pm 0.65	0.048e-3 \pm 0.006e-3	59.0000	9.00e+36

Table 2 continued on next page

Table 2 (*continued*)

Source	Position (RA)	Position (Dec)	F(H α) (10^{-17} erg/cm 2 /s)	SFR (M_{\odot} /yr)	Area (pixel 2)	L(H α) (erg s $^{-1}$)
660	03h09m42.81s	-20h33m55.81s	19.04 \pm 0.73	0.047e-3 \pm 0.006e-3	39.0000	8.93e+36
661	03h09m47.54s	-20h35m01.56s	18.88 \pm 0.70	0.047e-3 \pm 0.006e-3	63.0000	8.86e+36
662	03h09m40.58s	-20h35m24.54s	18.86 \pm 0.66	0.047e-3 \pm 0.006e-3	58.0000	8.85e+36
663	03h09m51.05s	-20h34m05.08s	18.32 \pm 0.63	0.046e-3 \pm 0.006e-3	59.0000	8.60e+36
664	03h09m39.88s	-20h34m49.43s	18.28 \pm 0.67	0.045e-3 \pm 0.006e-3	65.0000	8.58e+36
665	03h09m49.75s	-20h34m06.83s	18.28 \pm 0.56	0.045e-3 \pm 0.006e-3	47.0000	8.58e+36
666	03h09m52.00s	-20h35m25.13s	18.04 \pm 0.65	0.045e-3 \pm 0.006e-3	59.0000	8.47e+36
667	03h09m44.16s	-20h34m28.78s	17.81 \pm 0.68	0.044e-3 \pm 0.006e-3	62.0000	8.36e+36
668	03h09m44.46s	-20h35m03.61s	17.78 \pm 0.73	0.044e-3 \pm 0.006e-3	51.0000	8.34e+36
669	03h09m44.34s	-20h34m37.78s	17.73 \pm 0.66	0.044e-3 \pm 0.006e-3	60.0000	8.32e+36
670	03h09m50.80s	-20h34m34.88s	17.72 \pm 0.68	0.044e-3 \pm 0.006e-3	66.0000	8.31e+36
671	03h09m41.21s	-20h33m55.34s	17.62 \pm 0.65	0.044e-3 \pm 0.006e-3	62.0000	8.27e+36
672	03h09m50.79s	-20h35m11.29s	17.57 \pm 0.68	0.044e-3 \pm 0.006e-3	62.0000	8.24e+36
673	03h09m45.49s	-20h35m08.18s	17.52 \pm 0.68	0.044e-3 \pm 0.005e-3	63.0000	8.22e+36
674	03h09m47.63s	-20h35m19.92s	17.43 \pm 0.68	0.043e-3 \pm 0.005e-3	62.0000	8.18e+36
675	03h09m44.70s	-20h34m58.09s	17.28 \pm 0.70	0.043e-3 \pm 0.005e-3	37.0000	8.11e+36
676	03h09m50.13s	-20h34m16.90s	17.22 \pm 0.70	0.043e-3 \pm 0.005e-3	63.0000	8.08e+36
677	03h09m40.05s	-20h33m08.15s	17.20 \pm 0.33	0.043e-3 \pm 0.005e-3	18.0000	8.07e+36
678	03h09m42.83s	-20h34m50.68s	17.14 \pm 0.62	0.043e-3 \pm 0.005e-3	56.0000	8.04e+36
679	03h09m40.61s	-20h33m27.04s	17.11 \pm 0.71	0.043e-3 \pm 0.005e-3	49.0000	8.03e+36
680	03h09m46.07s	-20h35m35.80s	17.00 \pm 0.62	0.042e-3 \pm 0.005e-3	49.0000	7.98e+36
681	03h09m48.16s	-20h33m33.46s	16.82 \pm 0.60	0.042e-3 \pm 0.005e-3	55.0000	7.89e+36
682	03h09m42.57s	-20h35m22.54s	16.77 \pm 0.63	0.042e-3 \pm 0.005e-3	56.0000	7.87e+36
683	03h09m39.96s	-20h33m08.18s	16.76 \pm 0.38	0.042e-3 \pm 0.005e-3	23.0000	7.86e+36
684	03h09m48.88s	-20h34m57.06s	16.67 \pm 0.59	0.041e-3 \pm 0.005e-3	46.0000	7.82e+36
685	03h09m40.37s	-20h34m59.94s	16.55 \pm 0.63	0.041e-3 \pm 0.005e-3	60.0000	7.77e+36
686	03h09m42.65s	-20h35m39.28s	16.54 \pm 0.64	0.041e-3 \pm 0.005e-3	59.0000	7.76e+36
687	03h09m49.66s	-20h33m21.69s	16.32 \pm 0.66	0.041e-3 \pm 0.005e-3	58.0000	7.66e+36
688	03h09m44.95s	-20h34m23.48s	16.28 \pm 0.63	0.040e-3 \pm 0.005e-3	54.0000	7.64e+36
689	03h09m51.35s	-20h34m23.05s	16.20 \pm 0.63	0.040e-3 \pm 0.005e-3	52.0000	7.60e+36
690	03h09m50.01s	-20h33m45.82s	16.14 \pm 0.64	0.040e-3 \pm 0.005e-3	61.0000	7.57e+36
691	03h09m43.51s	-20h35m18.10s	16.13 \pm 0.66	0.040e-3 \pm 0.005e-3	56.0000	7.57e+36
692	03h09m48.29s	-20h35m46.12s	16.12 \pm 0.70	0.040e-3 \pm 0.005e-3	59.0000	7.57e+36
693	03h09m51.33s	-20h35m25.36s	16.09 \pm 0.64	0.040e-3 \pm 0.005e-3	52.0000	7.55e+36
694	03h09m41.38s	-20h33m07.89s	16.07 \pm 0.42	0.040e-3 \pm 0.005e-3	28.0000	7.54e+36
695	03h09m43.85s	-20h33m57.07s	15.87 \pm 0.66	0.039e-3 \pm 0.005e-3	36.0000	7.44e+36
696	03h09m49.24s	-20h35m08.62s	15.81 \pm 0.62	0.039e-3 \pm 0.005e-3	51.0000	7.42e+36

Table 2 continued on next page

Table 2 (*continued*)

Source	Position (RA)	Position (Dec)	F(H α) (10^{-17} erg/cm 2 /s)	SFR (M_{\odot} /yr)	Area (pixel 2)	L(H α) (erg s $^{-1}$)
697	03h09m48.01s	-20h35m57.59s	15.73 \pm 0.63	0.039e-3 \pm 0.005e-3	59.0000	7.38e+36
698	03h09m49.24s	-20h34m57.09s	15.72 \pm 0.63	0.039e-3 \pm 0.005e-3	57.0000	7.37e+36
699	03h09m44.93s	-20h33m55.75s	15.70 \pm 0.63	0.039e-3 \pm 0.005e-3	56.0000	7.37e+36
700	03h09m45.03s	-20h34m29.95s	15.58 \pm 0.60	0.039e-3 \pm 0.005e-3	52.0000	7.31e+36
701	03h09m46.84s	-20h34m31.36s	15.28 \pm 0.55	0.038e-3 \pm 0.005e-3	44.0000	7.17e+36
702	03h09m49.68s	-20h35m28.13s	15.14 \pm 0.64	0.038e-3 \pm 0.005e-3	59.0000	7.10e+36
703	03h09m44.81s	-20h33m57.15s	15.13 \pm 0.65	0.038e-3 \pm 0.005e-3	54.0000	7.10e+36
704	03h09m46.57s	-20h35m52.68s	15.12 \pm 0.58	0.038e-3 \pm 0.005e-3	49.0000	7.09e+36
705	03h09m45.87s	-20h36m01.46s	15.02 \pm 0.65	0.037e-3 \pm 0.005e-3	32.0000	7.05e+36
706	03h09m42.61s	-20h34m56.54s	14.80 \pm 0.57	0.037e-3 \pm 0.005e-3	47.0000	6.95e+36
707	03h09m40.88s	-20h34m00.19s	14.74 \pm 0.61	0.037e-3 \pm 0.005e-3	51.0000	6.91e+36
708	03h09m51.05s	-20h35m25.42s	14.30 \pm 0.64	0.036e-3 \pm 0.005e-3	42.0000	6.71e+36
709	03h09m48.16s	-20h35m44.02s	14.24 \pm 0.64	0.035e-3 \pm 0.005e-3	51.0000	6.68e+36
710	03h09m52.07s	-20h35m36.51s	14.19 \pm 0.57	0.035e-3 \pm 0.004e-3	47.0000	6.66e+36
711	03h09m40.39s	-20h33m38.37s	14.15 \pm 0.54	0.035e-3 \pm 0.004e-3	41.0000	6.64e+36
712	03h09m47.15s	-20h35m05.39s	14.11 \pm 0.57	0.035e-3 \pm 0.004e-3	45.0000	6.62e+36
713	03h09m46.96s	-20h35m22.59s	13.92 \pm 0.63	0.035e-3 \pm 0.004e-3	46.0000	6.53e+36
714	03h09m42.02s	-20h35m53.55s	13.86 \pm 0.60	0.034e-3 \pm 0.004e-3	48.0000	6.50e+36
715	03h09m45.28s	-20h35m29.23s	13.85 \pm 0.58	0.034e-3 \pm 0.004e-3	47.0000	6.50e+36
716	03h09m49.39s	-20h35m41.83s	13.84 \pm 0.55	0.034e-3 \pm 0.004e-3	40.0000	6.49e+36
717	03h09m40.01s	-20h35m32.71s	13.79 \pm 0.57	0.034e-3 \pm 0.004e-3	49.0000	6.47e+36
718	03h09m47.74s	-20h35m02.12s	13.78 \pm 0.57	0.034e-3 \pm 0.004e-3	45.0000	6.47e+36
719	03h09m44.70s	-20h34m34.38s	13.74 \pm 0.60	0.034e-3 \pm 0.004e-3	43.0000	6.45e+36
720	03h09m51.07s	-20h34m42.86s	13.70 \pm 0.59	0.034e-3 \pm 0.004e-3	47.0000	6.43e+36
721	03h09m46.68s	-20h35m22.72s	13.60 \pm 0.61	0.034e-3 \pm 0.004e-3	45.0000	6.38e+36
722	03h09m44.68s	-20h34m29.81s	13.60 \pm 0.56	0.034e-3 \pm 0.004e-3	42.0000	6.38e+36
723	03h09m47.69s	-20h33m24.26s	13.59 \pm 0.62	0.034e-3 \pm 0.004e-3	35.0000	6.38e+36
724	03h09m47.60s	-20h33m59.65s	13.53 \pm 0.57	0.034e-3 \pm 0.004e-3	48.0000	6.35e+36
725	03h09m48.40s	-20h35m10.11s	13.43 \pm 0.60	0.033e-3 \pm 0.004e-3	51.0000	6.30e+36
726	03h09m47.04s	-20h33m34.72s	13.39 \pm 0.58	0.033e-3 \pm 0.004e-3	48.0000	6.28e+36
727	03h09m43.17s	-20h35m36.53s	13.33 \pm 0.60	0.033e-3 \pm 0.004e-3	46.0000	6.25e+36
728	03h09m50.11s	-20h36m10.59s	13.03 \pm 0.55	0.032e-3 \pm 0.004e-3	35.0000	6.11e+36
729	03h09m47.03s	-20h35m50.45s	13.01 \pm 0.58	0.032e-3 \pm 0.004e-3	42.0000	6.11e+36
730	03h09m45.11s	-20h33m09.93s	13.00 \pm 0.60	0.032e-3 \pm 0.004e-3	24.0000	6.10e+36
731	03h09m51.58s	-20h35m28.64s	12.99 \pm 0.55	0.032e-3 \pm 0.004e-3	42.0000	6.10e+36
732	03h09m42.35s	-20h35m58.71s	12.99 \pm 0.56	0.032e-3 \pm 0.004e-3	43.0000	6.10e+36
733	03h09m39.92s	-20h34m38.43s	12.98 \pm 0.56	0.032e-3 \pm 0.004e-3	42.0000	6.09e+36

Table 2 continued on next page

Table 2 (*continued*)

Source	Position (RA)	Position (Dec)	F(H α) (10^{-17} erg/cm 2 /s)	SFR (M_{\odot} /yr)	Area (pixel 2)	L(H α) (erg s $^{-1}$)
734	03h09m49.60s	-20h34m54.60s	12.94 \pm 0.62	0.032e-3 \pm 0.004e-3	45.0000	6.07e+36
735	03h09m49.79s	-20h34m43.04s	12.90 \pm 0.55	0.032e-3 \pm 0.004e-3	43.0000	6.05e+36
736	03h09m46.81s	-20h33m58.71s	12.89 \pm 0.57	0.032e-3 \pm 0.004e-3	43.0000	6.05e+36
737	03h09m45.97s	-20h35m19.41s	12.71 \pm 0.58	0.032e-3 \pm 0.004e-3	44.0000	5.96e+36
738	03h09m48.10s	-20h34m24.98s	12.67 \pm 0.55	0.032e-3 \pm 0.004e-3	38.0000	5.94e+36
739	03h09m48.44s	-20h33m58.95s	12.57 \pm 0.52	0.031e-3 \pm 0.004e-3	41.0000	5.90e+36
740	03h09m48.49s	-20h34m27.96s	12.54 \pm 0.58	0.031e-3 \pm 0.004e-3	42.0000	5.88e+36
741	03h09m52.35s	-20h33m46.63s	12.40 \pm 0.53	0.031e-3 \pm 0.004e-3	40.0000	5.82e+36
742	03h09m51.11s	-20h35m22.26s	12.33 \pm 0.56	0.031e-3 \pm 0.004e-3	45.0000	5.79e+36
743	03h09m40.43s	-20h33m08.07s	12.33 \pm 0.28	0.031e-3 \pm 0.004e-3	12.0000	5.79e+36
744	03h09m45.23s	-20h34m20.47s	12.32 \pm 0.58	0.031e-3 \pm 0.004e-3	44.0000	5.78e+36
745	03h09m47.12s	-20h34m23.25s	12.22 \pm 0.60	0.030e-3 \pm 0.004e-3	26.0000	5.73e+36
746	03h09m45.81s	-20h33m42.50s	12.18 \pm 0.62	0.030e-3 \pm 0.004e-3	43.0000	5.71e+36
747	03h09m45.09s	-20h35m17.66s	12.15 \pm 0.53	0.030e-3 \pm 0.004e-3	40.0000	5.70e+36
748	03h09m43.88s	-20h36m06.33s	12.15 \pm 0.55	0.030e-3 \pm 0.004e-3	41.0000	5.70e+36
749	03h09m51.10s	-20h35m02.13s	12.07 \pm 0.57	0.030e-3 \pm 0.004e-3	47.0000	5.66e+36
750	03h09m46.58s	-20h33m41.90s	12.01 \pm 0.60	0.030e-3 \pm 0.004e-3	20.0000	5.63e+36
751	03h09m46.71s	-20h33m47.49s	11.92 \pm 0.56	0.030e-3 \pm 0.004e-3	41.0000	5.59e+36
752	03h09m50.86s	-20h35m10.91s	11.89 \pm 0.57	0.030e-3 \pm 0.004e-3	42.0000	5.58e+36
753	03h09m45.56s	-20h35m34.68s	11.88 \pm 0.63	0.030e-3 \pm 0.004e-3	28.0000	5.57e+36
754	03h09m48.73s	-20h35m14.68s	11.81 \pm 0.56	0.029e-3 \pm 0.004e-3	43.0000	5.54e+36
755	03h09m50.56s	-20h34m03.54s	11.80 \pm 0.58	0.029e-3 \pm 0.004e-3	31.0000	5.54e+36
756	03h09m49.26s	-20h33m51.79s	11.59 \pm 0.56	0.029e-3 \pm 0.004e-3	44.0000	5.44e+36
757	03h09m46.59s	-20h33m28.99s	11.58 \pm 0.56	0.029e-3 \pm 0.004e-3	42.0000	5.43e+36
758	03h09m42.41s	-20h35m03.14s	11.58 \pm 0.56	0.029e-3 \pm 0.004e-3	45.0000	5.43e+36
759	03h09m42.94s	-20h35m45.04s	11.57 \pm 0.60	0.029e-3 \pm 0.004e-3	22.0000	5.43e+36
760	03h09m41.17s	-20h34m03.15s	11.40 \pm 0.57	0.028e-3 \pm 0.004e-3	39.0000	5.35e+36
761	03h09m43.63s	-20h35m55.02s	11.38 \pm 0.53	0.028e-3 \pm 0.004e-3	41.0000	5.34e+36
762	03h09m40.06s	-20h35m33.39s	11.37 \pm 0.55	0.028e-3 \pm 0.004e-3	42.0000	5.33e+36
763	03h09m44.87s	-20h35m31.88s	11.33 \pm 0.54	0.028e-3 \pm 0.004e-3	40.0000	5.31e+36
764	03h09m44.25s	-20h34m27.83s	11.25 \pm 0.53	0.028e-3 \pm 0.004e-3	39.0000	5.28e+36
765	03h09m41.64s	-20h35m04.29s	11.24 \pm 0.52	0.028e-3 \pm 0.004e-3	39.0000	5.27e+36
766	03h09m39.86s	-20h34m18.10s	11.19 \pm 0.56	0.028e-3 \pm 0.004e-3	40.0000	5.25e+36
767	03h09m40.74s	-20h35m51.36s	11.15 \pm 0.50	0.028e-3 \pm 0.004e-3	37.0000	5.23e+36
768	03h09m41.97s	-20h36m08.57s	11.13 \pm 0.57	0.028e-3 \pm 0.004e-3	16.0000	5.22e+36
769	03h09m43.73s	-20h35m21.97s	11.09 \pm 0.53	0.028e-3 \pm 0.004e-3	36.0000	5.20e+36
770	03h09m49.15s	-20h34m35.33s	11.05 \pm 0.58	0.027e-3 \pm 0.004e-3	35.0000	5.18e+36

Table 2 continued on next page

Table 2 (*continued*)

Source	Position (RA)	Position (Dec)	F(H α) (10^{-17} erg/cm 2 /s)	SFR (M_{\odot} /yr)	Area (pixel 2)	L(H α) (erg s $^{-1}$)
771	03h09m44.69s	-20h34m34.85s	10.99 \pm 0.54	0.027e-3 \pm 0.004e-3	37.0000	5.16e+36
772	03h09m48.03s	-20h35m48.27s	10.92 \pm 0.57	0.027e-3 \pm 0.004e-3	42.0000	5.12e+36
773	03h09m45.29s	-20h34m28.97s	10.90 \pm 0.54	0.027e-3 \pm 0.004e-3	38.0000	5.11e+36
774	03h09m47.22s	-20h35m34.36s	10.88 \pm 0.55	0.027e-3 \pm 0.004e-3	41.0000	5.10e+36
775	03h09m41.00s	-20h35m25.35s	10.62 \pm 0.50	0.026e-3 \pm 0.003e-3	37.0000	4.98e+36
776	03h09m45.49s	-20h34m10.52s	10.60 \pm 0.53	0.026e-3 \pm 0.003e-3	38.0000	4.97e+36
777	03h09m45.89s	-20h34m24.36s	10.54 \pm 0.50	0.026e-3 \pm 0.003e-3	34.0000	4.94e+36
778	03h09m45.47s	-20h34m25.13s	10.48 \pm 0.52	0.026e-3 \pm 0.003e-3	31.0000	4.92e+36
779	03h09m46.49s	-20h35m19.72s	10.44 \pm 0.57	0.026e-3 \pm 0.003e-3	36.0000	4.90e+36
780	03h09m46.45s	-20h33m56.28s	10.20 \pm 0.52	0.025e-3 \pm 0.003e-3	36.0000	4.79e+36
781	03h09m46.53s	-20h34m04.25s	10.19 \pm 0.56	0.025e-3 \pm 0.003e-3	35.0000	4.78e+36
782	03h09m48.71s	-20h34m03.95s	10.15 \pm 0.54	0.025e-3 \pm 0.003e-3	26.0000	4.76e+36
783	03h09m49.95s	-20h35m23.12s	10.07 \pm 0.53	0.025e-3 \pm 0.003e-3	26.0000	4.72e+36
784	03h09m50.99s	-20h35m28.92s	10.05 \pm 0.52	0.025e-3 \pm 0.003e-3	38.0000	4.71e+36
785	03h09m50.77s	-20h33m52.60s	10.04 \pm 0.55	0.025e-3 \pm 0.003e-3	28.0000	4.71e+36
786	03h09m46.60s	-20h33m50.64s	10.01 \pm 0.53	0.025e-3 \pm 0.003e-3	39.0000	4.70e+36
787	03h09m44.68s	-20h34m03.39s	9.98 \pm 0.52	0.025e-3 \pm 0.003e-3	33.0000	4.68e+36
788	03h09m40.26s	-20h35m14.46s	9.93 \pm 0.53	0.025e-3 \pm 0.003e-3	35.0000	4.66e+36
789	03h09m45.27s	-20h35m43.10s	9.88 \pm 0.51	0.025e-3 \pm 0.003e-3	31.0000	4.63e+36
790	03h09m46.24s	-20h35m18.86s	9.82 \pm 0.50	0.024e-3 \pm 0.003e-3	33.0000	4.61e+36
791	03h09m49.47s	-20h36m01.36s	9.80 \pm 0.51	0.024e-3 \pm 0.003e-3	35.0000	4.60e+36
792	03h09m48.88s	-20h34m38.82s	9.79 \pm 0.49	0.024e-3 \pm 0.003e-3	28.0000	4.60e+36
793	03h09m45.28s	-20h34m54.67s	9.70 \pm 0.53	0.024e-3 \pm 0.003e-3	34.0000	4.55e+36
794	03h09m48.82s	-20h34m37.15s	9.68 \pm 0.49	0.024e-3 \pm 0.003e-3	35.0000	4.54e+36
795	03h09m42.77s	-20h33m52.14s	9.65 \pm 0.51	0.024e-3 \pm 0.003e-3	36.0000	4.53e+36
796	03h09m43.18s	-20h34m24.35s	9.48 \pm 0.53	0.024e-3 \pm 0.003e-3	19.0000	4.45e+36
797	03h09m48.61s	-20h34m08.39s	9.47 \pm 0.50	0.024e-3 \pm 0.003e-3	35.0000	4.44e+36
798	03h09m46.05s	-20h34m34.59s	9.45 \pm 0.50	0.023e-3 \pm 0.003e-3	34.0000	4.43e+36
799	03h09m50.21s	-20h36m04.05s	9.36 \pm 0.53	0.023e-3 \pm 0.003e-3	35.0000	4.39e+36
800	03h09m47.71s	-20h34m54.28s	9.28 \pm 0.49	0.023e-3 \pm 0.003e-3	33.0000	4.35e+36
801	03h09m49.72s	-20h35m24.35s	9.13 \pm 0.49	0.023e-3 \pm 0.003e-3	28.0000	4.28e+36
802	03h09m48.05s	-20h33m53.12s	9.10 \pm 0.50	0.023e-3 \pm 0.003e-3	31.0000	4.27e+36
803	03h09m51.24s	-20h34m11.62s	9.01 \pm 0.49	0.022e-3 \pm 0.003e-3	32.0000	4.23e+36
804	03h09m49.55s	-20h35m25.17s	9.01 \pm 0.53	0.022e-3 \pm 0.003e-3	29.0000	4.23e+36
805	03h09m44.14s	-20h35m26.11s	9.00 \pm 0.53	0.022e-3 \pm 0.003e-3	23.0000	4.22e+36
806	03h09m41.88s	-20h33m07.82s	9.00 \pm 0.36	0.022e-3 \pm 0.003e-3	16.0000	4.22e+36
807	03h09m48.00s	-20h34m02.52s	8.95 \pm 0.47	0.022e-3 \pm 0.003e-3	30.0000	4.20e+36

Table 2 continued on next page

Table 2 (*continued*)

Source	Position (RA)	Position (Dec)	F(H α) (10^{-17} erg/cm 2 /s)	SFR (M_{\odot} /yr)	Area (pixel 2)	L(H α) (erg s $^{-1}$)
808	03h09m46.24s	-20h35m40.27s	8.93 \pm 0.49	0.022e-3 \pm 0.003e-3	32.0000	4.19e+36
809	03h09m42.84s	-20h33m16.36s	8.86 \pm 0.51	0.022e-3 \pm 0.003e-3	32.0000	4.16e+36
810	03h09m47.64s	-20h35m51.65s	8.84 \pm 0.52	0.022e-3 \pm 0.003e-3	25.0000	4.15e+36
811	03h09m41.24s	-20h34m29.03s	8.63 \pm 0.49	0.021e-3 \pm 0.003e-3	31.0000	4.05e+36
812	03h09m49.34s	-20h34m02.32s	8.60 \pm 0.48	0.021e-3 \pm 0.003e-3	33.0000	4.03e+36
813	03h09m44.43s	-20h33m37.23s	8.58 \pm 0.47	0.021e-3 \pm 0.003e-3	32.0000	4.02e+36
814	03h09m45.67s	-20h35m22.88s	8.52 \pm 0.46	0.021e-3 \pm 0.003e-3	29.0000	4.00e+36
815	03h09m46.92s	-20h34m21.26s	8.52 \pm 0.49	0.021e-3 \pm 0.003e-3	27.0000	4.00e+36
816	03h09m45.23s	-20h33m26.68s	8.35 \pm 0.47	0.021e-3 \pm 0.003e-3	27.0000	3.92e+36
817	03h09m50.92s	-20h33m51.59s	8.32 \pm 0.52	0.021e-3 \pm 0.003e-3	22.0000	3.90e+36
818	03h09m43.47s	-20h33m07.66s	8.29 \pm 0.35	0.021e-3 \pm 0.003e-3	19.0000	3.89e+36
819	03h09m48.11s	-20h34m45.53s	8.29 \pm 0.47	0.021e-3 \pm 0.003e-3	29.0000	3.89e+36
820	03h09m43.47s	-20h33m49.74s	8.27 \pm 0.48	0.021e-3 \pm 0.003e-3	31.0000	3.88e+36
821	03h09m52.44s	-20h33m31.95s	8.25 \pm 0.47	0.021e-3 \pm 0.003e-3	30.0000	3.87e+36
822	03h09m47.63s	-20h34m52.35s	8.24 \pm 0.46	0.020e-3 \pm 0.003e-3	24.0000	3.87e+36
823	03h09m49.90s	-20h34m13.28s	8.24 \pm 0.45	0.020e-3 \pm 0.003e-3	28.0000	3.87e+36
824	03h09m46.20s	-20h35m38.98s	8.23 \pm 0.48	0.020e-3 \pm 0.003e-3	29.0000	3.86e+36
825	03h09m48.96s	-20h34m37.86s	8.22 \pm 0.49	0.020e-3 \pm 0.003e-3	28.0000	3.86e+36
826	03h09m41.69s	-20h35m54.16s	8.22 \pm 0.45	0.020e-3 \pm 0.003e-3	28.0000	3.86e+36
827	03h09m43.57s	-20h34m51.03s	8.15 \pm 0.48	0.020e-3 \pm 0.003e-3	29.0000	3.82e+36
828	03h09m49.86s	-20h34m37.77s	8.15 \pm 0.49	0.020e-3 \pm 0.003e-3	26.0000	3.82e+36
829	03h09m43.83s	-20h35m23.11s	8.12 \pm 0.48	0.020e-3 \pm 0.003e-3	23.0000	3.81e+36
830	03h09m45.19s	-20h35m51.83s	8.09 \pm 0.47	0.020e-3 \pm 0.003e-3	29.0000	3.80e+36
831	03h09m52.11s	-20h33m39.42s	7.94 \pm 0.47	0.020e-3 \pm 0.003e-3	33.0000	3.72e+36
832	03h09m48.67s	-20h35m44.50s	7.91 \pm 0.50	0.020e-3 \pm 0.003e-3	19.0000	3.71e+36
833	03h09m48.31s	-20h35m23.54s	7.83 \pm 0.50	0.019e-3 \pm 0.003e-3	12.0000	3.67e+36
834	03h09m43.85s	-20h35m13.01s	7.81 \pm 0.49	0.019e-3 \pm 0.003e-3	32.0000	3.66e+36
835	03h09m43.13s	-20h33m14.66s	7.73 \pm 0.49	0.019e-3 \pm 0.003e-3	14.0000	3.63e+36
836	03h09m48.46s	-20h34m29.02s	7.71 \pm 0.44	0.019e-3 \pm 0.003e-3	26.0000	3.62e+36
837	03h09m48.03s	-20h33m53.81s	7.69 \pm 0.47	0.019e-3 \pm 0.003e-3	28.0000	3.61e+36
838	03h09m49.26s	-20h35m55.56s	7.67 \pm 0.47	0.019e-3 \pm 0.003e-3	29.0000	3.60e+36
839	03h09m50.82s	-20h34m36.05s	7.66 \pm 0.47	0.019e-3 \pm 0.003e-3	29.0000	3.59e+36
840	03h09m45.87s	-20h34m36.56s	7.66 \pm 0.50	0.019e-3 \pm 0.003e-3	15.0000	3.59e+36
841	03h09m43.96s	-20h36m03.46s	7.58 \pm 0.45	0.019e-3 \pm 0.003e-3	28.0000	3.56e+36
842	03h09m42.67s	-20h33m57.04s	7.53 \pm 0.49	0.019e-3 \pm 0.003e-3	27.0000	3.54e+36
843	03h09m48.29s	-20h34m26.89s	7.50 \pm 0.47	0.019e-3 \pm 0.003e-3	31.0000	3.52e+36
844	03h09m49.79s	-20h35m11.31s	7.44 \pm 0.47	0.018e-3 \pm 0.003e-3	27.0000	3.49e+36

Table 2 continued on next page

Table 2 (continued)

Source	Position (RA)	Position (Dec)	F(H α) (10^{-17} erg/cm 2 /s)	SFR (M_{\odot} /yr)	Area (pixel 2)	L(H α) (erg s $^{-1}$)
845	03h09m49.96s	-20h35m46.08s	7.37 \pm 0.45	0.018e-3 \pm 0.002e-3	26.0000	3.46e+36
846	03h09m48.19s	-20h33m41.33s	7.36 \pm 0.45	0.018e-3 \pm 0.002e-3	24.0000	3.45e+36
847	03h09m45.44s	-20h34m40.52s	7.35 \pm 0.46	0.018e-3 \pm 0.002e-3	25.0000	3.45e+36
848	03h09m44.06s	-20h33m18.93s	7.32 \pm 0.45	0.018e-3 \pm 0.002e-3	20.0000	3.44e+36
849	03h09m44.79s	-20h34m33.46s	7.26 \pm 0.45	0.018e-3 \pm 0.002e-3	23.0000	3.41e+36
850	03h09m48.03s	-20h34m09.01s	7.24 \pm 0.47	0.018e-3 \pm 0.002e-3	25.0000	3.40e+36
851	03h09m47.29s	-20h34m42.00s	7.20 \pm 0.47	0.018e-3 \pm 0.002e-3	22.0000	3.38e+36
852	03h09m43.15s	-20h35m34.78s	7.07 \pm 0.47	0.018e-3 \pm 0.002e-3	28.0000	3.32e+36
853	03h09m41.50s	-20h35m07.74s	7.06 \pm 0.46	0.018e-3 \pm 0.002e-3	30.0000	3.31e+36
854	03h09m47.56s	-20h34m25.86s	7.06 \pm 0.47	0.018e-3 \pm 0.002e-3	18.0000	3.31e+36
855	03h09m40.89s	-20h33m21.82s	7.05 \pm 0.47	0.018e-3 \pm 0.002e-3	16.0000	3.31e+36
856	03h09m39.80s	-20h35m24.03s	6.96 \pm 0.45	0.017e-3 \pm 0.002e-3	27.0000	3.27e+36
857	03h09m47.84s	-20h35m25.52s	6.95 \pm 0.45	0.017e-3 \pm 0.002e-3	14.0000	3.26e+36
858	03h09m44.63s	-20h34m02.62s	6.93 \pm 0.45	0.017e-3 \pm 0.002e-3	27.0000	3.25e+36
859	03h09m51.08s	-20h33m45.48s	6.88 \pm 0.43	0.017e-3 \pm 0.002e-3	24.0000	3.23e+36
860	03h09m43.04s	-20h34m39.48s	6.85 \pm 0.45	0.017e-3 \pm 0.002e-3	25.0000	3.21e+36
861	03h09m47.15s	-20h35m46.28s	6.85 \pm 0.43	0.017e-3 \pm 0.002e-3	25.0000	3.21e+36
862	03h09m44.63s	-20h34m34.97s	6.81 \pm 0.42	0.017e-3 \pm 0.002e-3	27.0000	3.20e+36
863	03h09m41.25s	-20h35m39.03s	6.76 \pm 0.41	0.017e-3 \pm 0.002e-3	26.0000	3.17e+36
864	03h09m46.15s	-20h34m15.39s	6.69 \pm 0.45	0.017e-3 \pm 0.002e-3	25.0000	3.14e+36
865	03h09m48.06s	-20h34m43.08s	6.62 \pm 0.43	0.016e-3 \pm 0.002e-3	21.0000	3.11e+36
866	03h09m50.66s	-20h35m28.77s	6.54 \pm 0.43	0.016e-3 \pm 0.002e-3	27.0000	3.07e+36
867	03h09m48.04s	-20h34m06.98s	6.43 \pm 0.43	0.016e-3 \pm 0.002e-3	23.0000	3.02e+36
868	03h09m45.32s	-20h33m26.60s	6.40 \pm 0.42	0.016e-3 \pm 0.002e-3	14.0000	3.00e+36
869	03h09m42.56s	-20h34m43.30s	6.38 \pm 0.44	0.016e-3 \pm 0.002e-3	24.0000	2.99e+36
870	03h09m44.19s	-20h33m31.95s	6.36 \pm 0.42	0.016e-3 \pm 0.002e-3	26.0000	2.99e+36
871	03h09m47.20s	-20h35m47.15s	6.30 \pm 0.42	0.016e-3 \pm 0.002e-3	24.0000	2.95e+36
872	03h09m43.01s	-20h34m39.67s	6.26 \pm 0.41	0.016e-3 \pm 0.002e-3	25.0000	2.94e+36
873	03h09m42.32s	-20h34m59.07s	6.26 \pm 0.41	0.016e-3 \pm 0.002e-3	22.0000	2.94e+36
874	03h09m44.17s	-20h34m20.93s	6.21 \pm 0.42	0.015e-3 \pm 0.002e-3	24.0000	2.92e+36
875	03h09m52.39s	-20h35m27.59s	6.21 \pm 0.41	0.015e-3 \pm 0.002e-3	24.0000	2.91e+36
876	03h09m45.74s	-20h33m48.82s	6.11 \pm 0.42	0.015e-3 \pm 0.002e-3	23.0000	2.87e+36
877	03h09m51.50s	-20h33m14.79s	6.09 \pm 0.45	0.015e-3 \pm 0.002e-3	22.0000	2.86e+36
878	03h09m48.05s	-20h34m50.49s	6.08 \pm 0.42	0.015e-3 \pm 0.002e-3	21.0000	2.85e+36
879	03h09m43.73s	-20h34m09.20s	6.07 \pm 0.42	0.015e-3 \pm 0.002e-3	23.0000	2.85e+36
880	03h09m41.69s	-20h35m18.39s	6.06 \pm 0.45	0.015e-3 \pm 0.002e-3	22.0000	2.84e+36
881	03h09m49.82s	-20h34m29.73s	6.03 \pm 0.42	0.015e-3 \pm 0.002e-3	24.0000	2.83e+36

Table 2 continued on next page

Table 2 (continued)

Source	Position (RA)	Position (Dec)	F(H α) (10^{-17} erg/cm 2 /s)	SFR (M_{\odot} /yr)	Area (pixel 2)	L(H α) (erg s $^{-1}$)
882	03h09m48.42s	-20h34m37.22s	5.99 \pm 0.35	0.015e-3 \pm 0.002e-3	16.0000	2.81e+36
883	03h09m45.67s	-20h34m04.70s	5.95 \pm 0.40	0.015e-3 \pm 0.002e-3	20.0000	2.79e+36
884	03h09m41.18s	-20h33m19.06s	5.94 \pm 0.42	0.015e-3 \pm 0.002e-3	22.0000	2.79e+36
885	03h09m42.15s	-20h35m44.33s	5.87 \pm 0.42	0.015e-3 \pm 0.002e-3	24.0000	2.75e+36
886	03h09m49.68s	-20h35m11.46s	5.86 \pm 0.42	0.015e-3 \pm 0.002e-3	15.0000	2.75e+36
887	03h09m43.00s	-20h34m24.74s	5.86 \pm 0.42	0.015e-3 \pm 0.002e-3	22.0000	2.75e+36
888	03h09m44.14s	-20h35m36.89s	5.84 \pm 0.40	0.015e-3 \pm 0.002e-3	22.0000	2.74e+36
889	03h09m45.19s	-20h33m09.39s	5.82 \pm 0.41	0.014e-3 \pm 0.002e-3	23.0000	2.73e+36
890	03h09m46.60s	-20h35m24.14s	5.82 \pm 0.42	0.014e-3 \pm 0.002e-3	20.0000	2.73e+36
891	03h09m46.65s	-20h34m11.90s	5.79 \pm 0.40	0.014e-3 \pm 0.002e-3	21.0000	2.71e+36
892	03h09m47.05s	-20h33m54.63s	5.77 \pm 0.39	0.014e-3 \pm 0.002e-3	21.0000	2.71e+36
893	03h09m39.93s	-20h35m22.94s	5.73 \pm 0.41	0.014e-3 \pm 0.002e-3	23.0000	2.69e+36
894	03h09m45.26s	-20h35m33.11s	5.73 \pm 0.36	0.014e-3 \pm 0.002e-3	20.0000	2.69e+36
895	03h09m52.16s	-20h34m07.90s	5.64 \pm 0.41	0.014e-3 \pm 0.002e-3	23.0000	2.65e+36
896	03h09m49.46s	-20h34m36.39s	5.63 \pm 0.39	0.014e-3 \pm 0.002e-3	22.0000	2.64e+36
897	03h09m49.55s	-20h34m42.74s	5.57 \pm 0.41	0.014e-3 \pm 0.002e-3	19.0000	2.61e+36
898	03h09m51.85s	-20h35m02.44s	5.55 \pm 0.40	0.014e-3 \pm 0.002e-3	12.0000	2.61e+36
899	03h09m51.26s	-20h35m26.32s	5.49 \pm 0.41	0.014e-3 \pm 0.002e-3	22.0000	2.58e+36
900	03h09m42.07s	-20h34m20.05s	5.48 \pm 0.39	0.014e-3 \pm 0.002e-3	20.0000	2.57e+36
901	03h09m42.51s	-20h33m17.28s	5.47 \pm 0.39	0.014e-3 \pm 0.002e-3	20.0000	2.57e+36
902	03h09m49.62s	-20h33m37.49s	5.43 \pm 0.41	0.013e-3 \pm 0.002e-3	19.0000	2.55e+36
903	03h09m51.04s	-20h35m17.55s	5.29 \pm 0.40	0.013e-3 \pm 0.002e-3	21.0000	2.48e+36
904	03h09m44.87s	-20h34m47.33s	5.28 \pm 0.38	0.013e-3 \pm 0.002e-3	19.0000	2.48e+36
905	03h09m41.03s	-20h35m13.54s	5.26 \pm 0.39	0.013e-3 \pm 0.002e-3	17.0000	2.47e+36
906	03h09m39.74s	-20h35m25.30s	5.19 \pm 0.34	0.013e-3 \pm 0.002e-3	16.0000	2.44e+36
907	03h09m45.38s	-20h34m43.86s	5.10 \pm 0.39	0.013e-3 \pm 0.002e-3	17.0000	2.39e+36
908	03h09m45.43s	-20h35m57.12s	5.08 \pm 0.39	0.013e-3 \pm 0.002e-3	18.0000	2.38e+36
909	03h09m48.73s	-20h34m30.36s	5.07 \pm 0.39	0.013e-3 \pm 0.002e-3	18.0000	2.38e+36
910	03h09m51.52s	-20h33m11.24s	5.05 \pm 0.40	0.013e-3 \pm 0.002e-3	20.0000	2.37e+36
911	03h09m48.59s	-20h33m34.77s	5.02 \pm 0.40	0.012e-3 \pm 0.002e-3	19.0000	2.36e+36
912	03h09m48.20s	-20h34m55.42s	5.01 \pm 0.36	0.012e-3 \pm 0.002e-3	19.0000	2.35e+36
913	03h09m47.58s	-20h36m01.45s	4.95 \pm 0.35	0.012e-3 \pm 0.002e-3	16.0000	2.32e+36
914	03h09m49.89s	-20h34m30.41s	4.88 \pm 0.39	0.012e-3 \pm 0.002e-3	14.0000	2.29e+36
915	03h09m45.46s	-20h33m27.95s	4.88 \pm 0.35	0.012e-3 \pm 0.002e-3	18.0000	2.29e+36
916	03h09m46.28s	-20h33m27.69s	4.86 \pm 0.38	0.012e-3 \pm 0.002e-3	19.0000	2.28e+36
917	03h09m52.39s	-20h33m29.23s	4.84 \pm 0.39	0.012e-3 \pm 0.002e-3	16.0000	2.27e+36
918	03h09m46.37s	-20h34m03.05s	4.80 \pm 0.38	0.012e-3 \pm 0.002e-3	15.0000	2.25e+36

Table 2 continued on next page

Table 2 (*continued*)

Source	Position (RA)	Position (Dec)	F(H α) (10^{-17} erg/cm 2 /s)	SFR (M_{\odot} /yr)	Area (pixel 2)	L(H α) (erg s $^{-1}$)
919	03h09m49.72s	-20h34m11.81s	4.72 \pm 0.38	0.012e-3 \pm 0.002e-3	20.0000	2.21e+36
920	03h09m41.92s	-20h33m54.65s	4.55 \pm 0.35	0.011e-3 \pm 0.002e-3	18.0000	2.14e+36
921	03h09m48.17s	-20h34m30.84s	4.54 \pm 0.35	0.011e-3 \pm 0.002e-3	15.0000	2.13e+36
922	03h09m50.74s	-20h34m25.77s	4.52 \pm 0.35	0.011e-3 \pm 0.002e-3	19.0000	2.12e+36
923	03h09m44.05s	-20h34m58.80s	4.46 \pm 0.36	0.011e-3 \pm 0.002e-3	18.0000	2.09e+36
924	03h09m49.24s	-20h35m15.23s	4.42 \pm 0.36	0.011e-3 \pm 0.002e-3	19.0000	2.07e+36
925	03h09m51.37s	-20h34m57.39s	4.41 \pm 0.35	0.011e-3 \pm 0.002e-3	15.0000	2.07e+36
926	03h09m49.28s	-20h35m40.63s	4.36 \pm 0.36	0.011e-3 \pm 0.002e-3	17.0000	2.05e+36
927	03h09m41.69s	-20h35m04.83s	4.36 \pm 0.36	0.011e-3 \pm 0.002e-3	16.0000	2.05e+36
928	03h09m49.78s	-20h34m34.63s	4.20 \pm 0.34	0.010e-3 \pm 0.002e-3	14.0000	1.97e+36
929	03h09m46.20s	-20h35m01.07s	4.17 \pm 0.33	0.010e-3 \pm 0.001e-3	14.0000	1.96e+36
930	03h09m49.69s	-20h34m30.02s	4.14 \pm 0.32	0.010e-3 \pm 0.001e-3	16.0000	1.94e+36
931	03h09m47.68s	-20h34m03.21s	4.13 \pm 0.35	0.010e-3 \pm 0.002e-3	14.0000	1.94e+36
932	03h09m51.46s	-20h34m44.25s	4.12 \pm 0.32	0.010e-3 \pm 0.001e-3	16.0000	1.93e+36
933	03h09m49.42s	-20h34m02.32s	4.11 \pm 0.34	0.010e-3 \pm 0.001e-3	16.0000	1.93e+36
934	03h09m44.57s	-20h34m55.49s	4.10 \pm 0.35	0.010e-3 \pm 0.002e-3	15.0000	1.93e+36
935	03h09m45.36s	-20h34m49.28s	4.08 \pm 0.32	0.010e-3 \pm 0.001e-3	15.0000	1.92e+36
936	03h09m44.38s	-20h35m14.65s	4.04 \pm 0.35	0.010e-3 \pm 0.001e-3	13.0000	1.90e+36
937	03h09m39.74s	-20h34m55.49s	4.04 \pm 0.31	0.010e-3 \pm 0.001e-3	12.0000	1.89e+36
938	03h09m48.84s	-20h35m31.84s	4.02 \pm 0.33	0.010e-3 \pm 0.001e-3	16.0000	1.89e+36
939	03h09m42.78s	-20h33m09.50s	4.02 \pm 0.34	0.010e-3 \pm 0.001e-3	16.0000	1.89e+36
940	03h09m42.17s	-20h36m00.85s	3.98 \pm 0.36	0.010e-3 \pm 0.001e-3	12.0000	1.87e+36
941	03h09m51.33s	-20h35m00.84s	3.97 \pm 0.34	0.010e-3 \pm 0.001e-3	16.0000	1.86e+36
942	03h09m47.72s	-20h35m00.91s	3.88 \pm 0.34	0.010e-3 \pm 0.001e-3	15.0000	1.82e+36
943	03h09m40.30s	-20h35m47.18s	3.87 \pm 0.34	0.010e-3 \pm 0.001e-3	16.0000	1.81e+36
944	03h09m45.36s	-20h33m52.67s	3.85 \pm 0.34	0.010e-3 \pm 0.001e-3	15.0000	1.81e+36
945	03h09m43.46s	-20h34m08.70s	3.84 \pm 0.33	0.010e-3 \pm 0.001e-3	15.0000	1.80e+36
946	03h09m42.67s	-20h34m55.13s	3.83 \pm 0.32	0.010e-3 \pm 0.001e-3	13.0000	1.80e+36
947	03h09m41.95s	-20h33m17.06s	3.74 \pm 0.34	0.009e-3 \pm 0.001e-3	14.0000	1.75e+36
948	03h09m45.52s	-20h35m31.35s	3.73 \pm 0.33	0.009e-3 \pm 0.001e-3	13.0000	1.75e+36
949	03h09m43.90s	-20h34m54.34s	3.57 \pm 0.33	0.009e-3 \pm 0.001e-3	15.0000	1.67e+36
950	03h09m52.10s	-20h33m30.49s	3.51 \pm 0.27	0.009e-3 \pm 0.001e-3	11.0000	1.65e+36
951	03h09m50.58s	-20h36m03.94s	3.43 \pm 0.32	0.009e-3 \pm 0.001e-3	15.0000	1.61e+36
952	03h09m51.20s	-20h36m10.67s	3.42 \pm 0.29	0.008e-3 \pm 0.001e-3	12.0000	1.60e+36
953	03h09m44.04s	-20h35m24.87s	3.41 \pm 0.32	0.008e-3 \pm 0.001e-3	12.0000	1.60e+36
954	03h09m45.01s	-20h34m33.92s	3.37 \pm 0.32	0.008e-3 \pm 0.001e-3	11.0000	1.58e+36
955	03h09m46.91s	-20h34m38.13s	3.35 \pm 0.32	0.008e-3 \pm 0.001e-3	12.0000	1.57e+36

Table 2 continued on next page

Table 2 (continued)

Source	Position (RA)	Position (Dec)	F(H α) (10^{-17} erg/cm 2 /s)	SFR (M_{\odot} /yr)	Area (pixel 2)	L(H α) (erg s $^{-1}$)
956	03h09m39.76s	-20h36m04.45s	3.33 ± 0.25	$0.008e-3 \pm 0.001e-3$	10.0000	$1.56e+36$
957	03h09m48.26s	-20h34m29.30s	3.30 ± 0.31	$0.008e-3 \pm 0.001e-3$	13.0000	$1.55e+36$
958	03h09m49.45s	-20h33m55.53s	3.29 ± 0.32	$0.008e-3 \pm 0.001e-3$	11.0000	$1.54e+36$
959	03h09m45.69s	-20h36m07.18s	3.26 ± 0.31	$0.008e-3 \pm 0.001e-3$	13.0000	$1.53e+36$
960	03h09m51.94s	-20h36m10.82s	3.23 ± 0.31	$0.008e-3 \pm 0.001e-3$	12.0000	$1.52e+36$
961	03h09m52.44s	-20h34m26.69s	3.13 ± 0.31	$0.008e-3 \pm 0.001e-3$	10.0000	$1.47e+36$
962	03h09m39.87s	-20h35m34.98s	3.10 ± 0.29	$0.008e-3 \pm 0.001e-3$	11.0000	$1.45e+36$
963	03h09m39.74s	-20h35m23.90s	3.06 ± 0.25	$0.008e-3 \pm 0.001e-3$	8.00000	$1.44e+36$
964	03h09m44.49s	-20h34m20.49s	3.03 ± 0.29	$0.008e-3 \pm 0.001e-3$	11.0000	$1.42e+36$
965	03h09m41.42s	-20h33m17.86s	3.03 ± 0.28	$0.008e-3 \pm 0.001e-3$	13.0000	$1.42e+36$
966	03h09m39.74s	-20h35m24.39s	3.02 ± 0.25	$0.008e-3 \pm 0.001e-3$	9.00000	$1.42e+36$
967	03h09m44.84s	-20h34m30.96s	2.99 ± 0.28	$0.007e-3 \pm 0.001e-3$	13.0000	$1.40e+36$
968	03h09m50.01s	-20h36m08.50s	2.87 ± 0.29	$0.007e-3 \pm 0.001e-3$	12.0000	$1.35e+36$
969	03h09m50.32s	-20h35m19.06s	2.76 ± 0.28	$0.007e-3 \pm 0.001e-3$	9.00000	$1.29e+36$
970	03h09m45.90s	-20h35m00.63s	2.52 ± 0.28	$0.006e-3 \pm 0.001e-3$	7.00000	$1.18e+36$
971	03h09m42.85s	-20h35m37.03s	2.44 ± 0.25	$0.006e-3 \pm 0.001e-3$	9.00000	$1.15e+36$
972	03h09m47.84s	-20h35m39.25s	2.07 ± 0.25	$0.005e-3 \pm 0.001e-3$	7.00000	$9.72e+35$
973	03h09m51.89s	-20h34m36.48s	2.07 ± 0.26	$0.005e-3 \pm 0.001e-3$	9.00000	$9.72e+35$
974	03h09m45.67s	-20h36m03.02s	2.06 ± 0.25	$0.005e-3 \pm 0.001e-3$	9.00000	$9.67e+35$
975	03h09m45.76s	-20h34m35.21s	2.01 ± 0.25	$0.005e-3 \pm 0.001e-3$	8.00000	$9.45e+35$
976	03h09m49.86s	-20h34m28.33s	1.97 ± 0.25	$0.005e-3 \pm 0.001e-3$	8.00000	$9.26e+35$

REFERENCES

- Arp, H. 1982, *ApJ*, 263, 54
- Banfi, M., Rampazzo, R., Chincarini, G., & Henry, R. B. C. 1993, *A&A*, 280, 373
- Bertin, E., & Arnouts, S. 1996, *A&AS*, 117, 393
- Bresolin, F., Schaerer, D., González Delgado, R. M., & Stasińska, G. 2005, *A&A*, 441, 981
- Caldwell, N., Kennicutt, R., Phillips, A. C., & Schommer, R. A. 1991, *ApJ*, 370, 526
- Calzetti, D., Kennicutt, R. C., Engelbracht, C. W., et al. 2007, *ApJ*, 666, 870
- Cardelli, J. A. 1989, *AJ*, 98, 324
- Cedr s, B., Cepa, J., Bongiovanni,  ., et al. 2013, *A&A*, 560, A59
- Corwin, Jr., H. G., Buta, R. J., & de Vaucouleurs, G. 1994, *AJ*, 108, 2128
- de Vaucouleurs, G., de Vaucouleurs, A., Corwin, Jr., H. G., et al. 1991, Third Reference Catalogue of Bright Galaxies. Volume I: Explanations and references. Volume II: Data for galaxies between 0^h and 12^h . Volume III: Data for galaxies between 12^h and 24^h .
- Elmegreen, B. G. 1995, *MNRAS*, 275, 944
- Elmegreen, B. G. & Elmegreen, D. M. 1986, *ApJ*, 311, 554
- Foyle, K., Rix, H.-W., Walter, F., & Leroy, A. K. 2010, *ApJ*, 725, 534
- Fraga, L., Kunder, A., & Tokovinin, A. 2013, *AJ*, 145, 165
- Garmire, G. P. 2013, *ApJ*, 770, 17
- Gittins, D. M. e Clarke, C. J. 2004, *MNRAS*, 349, 909
- Grosbol, P., & Dottori, H. 2012, *VizieR Online Data Catalog*, 354, 29039
- Guti rrez, L., Beckman, J. E., & Buenrostro, V. 2011, *AJ*, 141, 113
- Hamuy, M., Suntzeff, N. B., Heathcote, S. R., et al. 1994, *PASP*, 106, 566

- Hamuy, M., Walker, A. R., Suntzeff, N. B., et al. 1992, *PASP*, 104, 533
- Hodge, P. W. 1987, *PASP*, 99, 915
- Hodge, P. W., & Kennicutt, Jr., R. C. 1983, *AJ*, 88, 296
- Jones, D. H., Read, M. A., Saunders, W., & Colless, e. a. 2009, *MNRAS*, 399, 683
- Kennicutt, Jr., R. C. 1984, *ApJ*, 287, 116
- . 1989, *ApJ*, 344, 685
- . 1992, *ApJ*, 388, 310
- Knapen, J. H. 1998, *MNRAS*, 297, 255
- Kreckel, K., Blanc, G. A., Schinnerer, E., et al. 2016, *ApJ*, 827, 103
- Lee, J. C., Gil de Paz, A., Tremonti, C., et al. 2009, *ApJ*, 706, 599
- Martins, L. P., Rodríguez-Ardila, A., Diniz, S., Gruenwald, R., & de Souza, R. 2013, *MNRAS*, 431, 1823
- Oey, M. S., & Clarke, C. J. 1998, *AJ*, 115, 1543
- Osterbrock, D. E. 1989, *Annals of the New York Academy of Sciences*, 571, 99
- Rand, R. J. 1992, *AJ*, 103, 815
- Roberts, M. S. e Whitehurst, R. N. 1975, *ApJ*, 201, 327
- Rozas, M., Beckman, J. E., & Knapen, J. H. 1996, *A&A*, 307, 735
- Schlegel, D. J., Finkbeiner, D. P., & Davis, M. 1998, *ApJ*, 500, 525
- Schmitt, H. R., Calzetti, D., Armus, L., et al. 2006, *ApJS*, 164, 52
- Scoville, N. Z., Polletta, M., Ewald, S., et al. 2001, *AJ*, 122, 3017
- Seigar, M., Carollo, C. M., Stiavelli, M., de Zeeuw, P. T., & Dejonghe, H. 2002, *AJ*, 123, 184
- Thronson, Jr., H. A., Rubin, H., & Ksir, A. 1991, *MNRAS*, 252, 550
- Valdes, F. G. 1998, in *Astronomical Society of the Pacific Conference Series*, Vol. 145, *Astronomical Data Analysis Software and Systems VII*, ed. R. Albrecht, R. N. Hook, & H. A. Bushouse, 53
- Valdes, F. G., & Tody, D. 1998, in *Society of Photo-Optical Instrumentation Engineers (SPIE) Conference Series*, Vol. 3355, *Optical Astronomical Instrumentation*, ed. S. D’Odorico, 497–506
- van den Bergh, S. 1981, *AJ*, 86, 1464
- van Zee, L. & Bryant, J. 1999, *AJ*, 118, 2172
- Walterbos, R. A. M., & Braun, R. 1992, *A&AS*, 92, 625
- Willmer, C. N. A., Focardi, P., da Costa, L. N., & Pellegrini, P. S. 1989, *AJ*, 98, 1531
- Ye, T. 1992, *MNRAS*, 255, 32
- Youngblood, A. J., & Hunter, D. A. 1999, *ApJ*, 519, 55